

**EXPERIMENTAL AND NUMERICAL  
INVESTIGATIONS OF EFFECT OF A HEAT PIPE  
IN THE METAL HYDRIDE TANK FOR THE  
HYDRIDING PROCESS**

**2019  
Ph.D. THESIS  
ENERGY SYSTEMS ENGINEERING**

**FAWZI ALI MOHAMED ELHAMSHRI**

**EXPERIMENTAL AND NUMERICAL INVESTIGATIONS OF EFFECT OF  
A HEAT PIPE IN THE METAL HYDRIDE TANK FOR THE HYDRIDING  
PROCESS**

**A THESIS SUBMITTED TO  
THE INSTITUTE OF GRADUATE PROGRAMS OF  
KARABUK UNIVERSITY**

**BY**

**FAWZI ALI MOHAMED ELHAMSHRI**

**IN PARTIAL FULFILLMENT OF THE REQUIREMENTS FOR  
THE DEGREE OF DOCTOR OF PHILOSOPHY OF SCIENCE IN  
DEPARTMENT OF  
ENERGY SYSTEMS ENGINEERING**

**November 2019**

I certify that in my opinion the thesis submitted by Fawzi Ali Mohamed ELHAMSHRI titled “EXPERIMENTAL AND NUMERICAL INVESTIGATION OF EFFECT OF A HEAT PIPE IN THE METAL HYDRIDE TANK FOR THE HYDRIDING PROCESS” is fully adequate in scope and in quality as a thesis for the degree of Doctor of Philosophy.

Assoc. Prof. Dr. Muhammet KAYFECİ  
Thesis Advisor, Department of Energy Systems Engineering



This thesis is accepted by the examining committee with a unanimous vote in the Department of Energy Systems Engineering as a Ph.D. thesis. Nov 28, 2019

Examining Committee Members (Institutions)

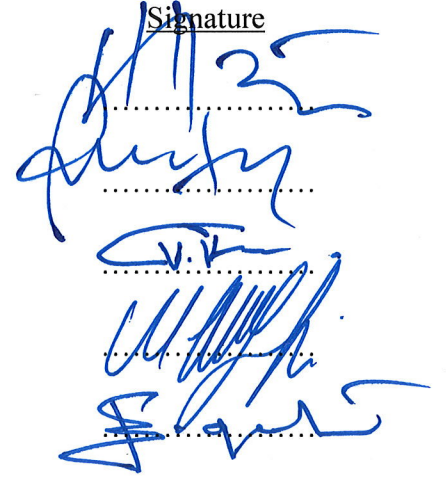
Chairman: Prof. Dr. Mehmet ÖZKAYMAK (KBU)

Member : Prof. Dr. Fevzi BEDİR (GTU)

Member : Assoc. Prof. Dr. Volkan KIRMACI (BU)

Member : Assoc. Prof. Dr. Muhammet KAYFECİ (KBU)

Member : Assoc. Prof. Dr. Engin GEDİK (KBU)

Signature  


..... / ..... / 2019

The degree of Doctor of Philosophy of Science by the thesis submitted is approved by the Administrative Board of the Institute of Graduate Programs, Karabük University.

Prof. Dr. Hasan SOLMAZ  
Head of Institute of Graduate Programs



*“I sincerely declare that the information presented in this thesis has been collected and presented according to ethical principles and academic regulations. I have met all the requirements, principles and regulations, and cited the references of those, which did not originate in this work.”*

Fawzi Ali Mohamed ELHAMSHRI

## **ABSTRACT**

**Ph. D. Thesis**

### **EXPERIMENTAL AND NUMERICAL INVESTIGATIONS OF EFFECT OF A HEAT PIPE IN THE METAL HYDRIDE TANK FOR THE HYDRIDING PROCESS**

**FAWZI ALI MOHAMED ELHAMSHRI**

**Karabük University**

**Institute of Graduate Programs**

**Department of Energy Systems Engineering**

**Thesis Advisor:**

**Assoc. Prof. Dr. Muhammet KAYFECİ**

**November 2019, 110 pages**

The excessive energy demands and depleting fossil fuels created the need to develop energy storing techniques and methodologies. Hydrogen provides an opportunity because in the future, it is expected to become a reasonable alternative to fossil fuels. Hydrogen has the potential to become a reliable energy resource because it can be stored. Several methodologies have been tried to store hydrogen; however, it can be stored as a compressed gas or as a liquid at low temperature. Physically, hydrogen storage is possible in carbon nano-tubes. Chemically, hydrogen could be stored in the solid form using metal hydride (MH) materials. Experts agree that among all the hydrogen storage options, the hydride form is the best and the most effective storage method because it allows appropriate operational conditions, maximum storage capacity, and low pressure operations. Heat transfer in MH bed significantly affects the performance of metal hydride tanks (MHTs). Enhancing heat transfer within the

reaction bed improves the hydriding rate. The current thesis analyzes the performance of three different cylindrical MHT configurations in terms of time and storage capacity applying the  $\text{LaNi}_5$  storage media; I) a tank cooled using the natural convection process, II) a tank equipped with a heat pipe along its central axis, and III) tanks equipped with finned heat pipe. This research examined hydrogen storage capacity theoretically as well as experimentally for demonstrating the impact of using a heat pipe and fins for enhancing heat transfer in MHTs at varying hydrogen supply pressures (experimentally 5-15 bars and numerically 5-35 bars). The mentioned investigation includes a hydrogen absorption test that has certain operating conditions (inlet pressure of hydrogen, coolant surrounding temperature, convective heat transfer coefficient), and tank design parameters (fins, heat pipe, vessel wall thickness, and inlet vessel radius), and MH particle size. The hydrogen storage system has certain design parameters; so, we applied COMSOL Multiphysics software 5.2a to understand the large-scale approaches. The results showed that as the hydrogen charge pressure increases, exothermic reaction increases as well; therefore, it increases the mass of hydrogen. Finned heat pipe showed a significant effect on hydrogen charging time. Consequently, the usage of heat pipe with fins could be a good choice to increase hydrogen storage reactor performance. It was noticed that the charging time decreased almost 75% at gas pressure 10 bars, whereas 60% reduced when a simple heat pipe was used in comparison with the reactor without any heat pipe. A model of 3D metal hydride storage was practically used that could simulate absorption of hydrogen. A metal hydride of the rare alloy  $\text{LaNi}_5$  was used to analyze parameters. Parameters such as hydrogen mass to be stored, internal temperature distribution of the tank, and their duration have been optimized. The model has been validated with experimental result. The obtained results show that the simulation and experimental results reasonably match, which proves that the model has efficiently captured the key experimental trends. Therefore, the model can be used as a helpful tool in the optimization of the MHT designs and performance.

**Keywords** : Heat transfer, hydrogen storage, heat pipe, finned heat pipe, modelling,  $\text{LaNi}_5$ .

**Science Code** : 91441

## **ÖZET**

**Doktora Tezi**

### **METAL HİDRİT TANKINDA ISI BORUSUNUN HİDRÜRLEME İŞLEMİNE ETKİSİNİN DENEYSEL VE SAYISAL OLARAK İNCELENMESİ**

**FAWZI ALI MOHAMED ELHAMSHRI**

**Karabük Üniversitesi**

**Lisansüstü Eğitim Enstitüsü**

**Enerji Sistemleri Mühendisliği Anabilim Dalı**

**Danışman:**

**Doç. Dr. Muhammet KAYFECİ**

**Kasım 2019, 110 sayfa**

Enerji taleplerindeki hızlı artış ve fosil yakıtların tükeniyor olması enerji depolama tekniklerine ve metotlarının geliştirilmesi ihtiyacını yaratmıştır. Hidrojen yakın gelecekte fosil yakıtlara uygun bir alternatif sağlaması beklendiğinden, önemli fırsatlar sağlayacak ve depolanabildiği için güvenilir bir enerji kaynağı olma potansiyeline sahiptir. Hidrojenin depolanması için çeşitli yöntemler denenmiştir; bunlarla birlikte, yaygın olarak sıkıştırılmış gaz veya düşük sıcaklıklarda sıvı olarak ta depolanabilmektedir. Hidrojen fiziksel olarak karbon nano tüplerde depolanabilirken, kimyasal olarak, metal hidrür (MH) malzemeler kullanılarak katı form içinde depolanabilir. Araştırmacılar, tüm hidrojen depolama seçeneklerinde, uygun çalışma koşullarına, maksimum depolama kapasitesine ve düşük basınçlı çalışmalara izin vermesinden dolayı hidrür formunun en iyi ve en etkili depolama yöntemi olduğu konusunda hemfikirlere. MH yatağındaki ısı transferi, metal hidrür

tanklarının (MHT) performansını önemli ölçüde etkiler. Reaksiyon yatağı içindeki ısı transferinin artması hidrürleme hızını da arttırmaktadır. Bu tez çalışmasında, LaNi<sub>5</sub> depolama ortamında, üç farklı metal hidrür tank (MHT) konfigürasyonu kullanılarak, I) doğal taşınım yoluyla soğutulmuş tank, II) merkez eksenini boyunca yerleştirilmiş bir ısı borulu hidrür tank ve III) kanatçıklı ısı borulu hidrür tanklar şarj süresi ve depolama kapasitesi bakımından performansın analizleri yapılmıştır. Çalışmada MHT içerisinde ısı transferini için, ısı borusu ve kanatçıklı ısı borusu kullanımının hidrojen depolama kapasitesine etkisini belirlemek için; deneysel (5-15 bar şarj basıncı) ve teorik analizleri (5-35 şarj basıncı) içermektedir. Çalışma belirli çalışma koşullarına (hidrojen giriş basıncı, çevre sıcaklığı, taşınım ısı transfer katsayısı) ve tank tasarım parametreleri (kanatçıklar, ısı borusu, tank duvarı kalınlığı ve tank giriş yarıçapı) ve MH parçacık büyüklüğü gibi parametreleri inceleyen absorpsiyon deneylerini içermektedir.

Hidrojen depolama sistemi bazı tasarım parametrelerinden dolayı büyük ölçekli yaklaşımları anlamak için, hidrojen absorpsiyonunu simüle eden üç boyutlu metal hidrür reaktör modeli COMSOL Multi-physics yazılım 5.2a'yı kullanılarak analiz edilmiştir. Sonuçlar hidrojenin şarj basıncı arttıkça ekzotermik reaksiyonun da arttığı; bu nedenle depolama miktarının da arttığını göstermiştir. Ayrıca hidrür reaktörde kanatçıklı ısı borusu kullanımı, depolama performansını arttırmak için iyi bir seçenek olduğunu ve şarj süresini önemli oranda etkilediğini göstermiştir. Örneğin 10 bar basınçta, şarj süresinin yaklaşık %75 azaldığı, ısı borusu olmayan reaktöre kıyasla kanatçiksız ısı borusu kullanıldığında ise %60 azaldığı görülmüştür. Parametreleri analiz etmek için nadir bulunan alaşım LaNi<sub>5</sub> hidrür yatak kullanılarak; depolanan hidrojen kütlesi, tankın iç sıcaklık dağılımı ve şarj süresi gibi parametreler optimize edilmiş ve model, deneysel sonuçlar ile doğrulanmıştır. Elde edilen sonuçlar, simülasyon ve deneysel sonuçların birbiriyle uyum içinde olduğunu göstermiş ve modelin MHT tasarımlarının ve performansının, farklı parametrelere bağlı olarak optimizasyonunda kullanılabileceğini göstermiştir.

**Anahtar kelimeler:** Isı transferi, hidrojen depolama, ısı borusu, kanatlı ısı borusu, modelleme, LaNi<sub>5</sub>.

**Bilim kodu** : 91441



## ACKNOWLEDGMENT

First, all praise is for Allah, who has given me the strength, patience, and ability to overcome the difficulties and complete this thesis.

I sincerely thank and acknowledge the great support, encouragement and guidance of my advisor, Assoc.Prof.Dr. Muhammet KAYFECİ, who inspired me as a mentor to perform creatively, rigorously, and logically.

My earnest thanks and respect to Prof.Dr. Mehmet ÖZKAYMAK for his valuable cooperation throughout the academic research process. Also, I am thankful to my professors who are in the thesis review committee and I believe that I have learned a lot from their professional knowledge and research experience during my doctoral education. I would like to mention the names of Prof.Dr. Fevzi BEDİR and Prof.Dr. Mehmet ÖZKAYMAK, because they have significantly contributed to my learning.

I highly praise the faculty members and staff of Karabuk University, Faculty of Technology, for their help, material and moral support, and letting me use the laboratory infrastructure and materials available in the university during my experimental studies. Also, I am really grateful to the Unit of Scientific Research Projects Coordination at Karabuk University for the funding awarded under the number of KBÜ-BAP-13-2-YL-033.

I value the authors of the sources, which I have used in my thesis, and extend sincere gratitude to them.

I dedicate this thesis to my parents, siblings, wife, and children for their endless motivation and support.

## CONTENT

	<u>Page</u>
APPROVAL.....	ii
ABSTRACT.....	iv
ÖZET.....	vi
ACKNOWLEDGMENT.....	viii
CONTENT.....	ix
LIST OF FIGURES.....	xii
LIST OF TABLES.....	xv
SYMBOLS AND ABBREVIATIONS INDEX.....	xvi
CHAPTER 1.....	1
INTRODUCTION.....	1
1.1. BACKGROUND.....	1
1.2. HYDROGEN STORAGE METHODS.....	1
1.3. CHALLENGES WITH METAL HYDRIDE HYDROGEN STORAGE....	2
1.4. OBJECTIVES.....	4
1.5. DISSERTATION OUTLINE.....	4
CHAPTER 2.....	6
LITERATURE REVIEW.....	6
2.1. PREVIOUS WORK ON METAL HYDRIDE HYDROGEN STORAGE ..	6
2.1.1. Geometries used for Experimental Study.....	8
2.1.2. Geometries used for numerical simulation study.....	13
2.1.3. MHT Design for Effective Heat Management.....	26
2.1.3.1. Influence of MHTs geometry and configuration.....	28
2.1.3.2. Influence of cooling rates with operating conditions.....	30

	<u>Page</u>
2.1.3.3. Influence of hydrogen inlet pressure .....	31
2.1.3.4. Influence of permeability and thermal conductivity .....	32
 CHAPTER 3 .....	 33
HYDROGEN STORAGE WITHIN HYDRIDE IN SOLID FORM.....	33
3.1. HYDRIDES ALLOYS FOR HYDROGEN STORAGE .....	33
3.2. METAL HYDRIDES STORAGE OF HYDROGEN.....	34
3.3. METAL HYDRIDE MATERIAL SELECTION.....	36
3.3.1. AB Inter-metallic Compounds .....	36
3.3.2. AB <sub>2</sub> Inter-metallic Compounds.....	37
3.3.3. AB <sub>5</sub> Inter-metallic Compounds.....	37
3.4. HYDRIDING REACTION AND IMPORTANT PARAMETERS .....	38
3.4.1. Equilibrium Pressure.....	39
3.4.2. Particle Distribution of Metal Hydride and Activation.....	41
 CHAPTER 4 .....	 44
EXPERIMENTAL WORK.....	44
4.1. EXPERIMENTAL SETUP, DESIGN, AND PROCEDURE.....	44
4.1.1. Metal Hydride Tank Design.....	45
4.1.2. Machinery and Equipment Used in Experimental Study.....	47
4.1.3. Experimental Set-up.....	53
4.1.4. Experimental procedure .....	54
4.1.5. Uncertainty analysis .....	55
 CHAPTER 5 .....	 57
SIMULATION OF THE HYDRIDING PROCESS .....	57
5.1. DEVELOPMENT OF MATHEMATICAL MODEL .....	57
5.2. CHEMICAL REACTIONS FOR METAL HYDRIDE POWDER .....	58
5.3. GOVERNING EQUATIONS FOR FLOW AND HEAT TRANSFER ....	60
5.3.1. Initial and Boundary Conditions .....	63
5.3.2. Creating a Finite Element Solver Model.....	64
5.3.3. Modeling of MHTs Design for Effective Heat Management .....	68

	<u>Page</u>
5.3.3.1. Modeling of Circular Fins on MHT Outer Surface .....	68
5.3.3.2. The Model Equation for Cooling Fluid [31]: .....	68
CHAPTER 6 .....	72
RESULTS AND DISCUSSION .....	72
6.1. EXPERIMENTAL RESULTS AND DISCUSSION .....	72
6.2. SIMULATION RESULTS AND DISCUSSION .....	84
6.2.1. Model Validation .....	84
6.2.2. Effect of the Tank Configuration (Fin Parameter).....	89
6.2.3. Effect of the Hydrogen Inlet Pressure .....	90
6.2.4. Effect of the Particle Size.....	92
6.2.5. Effect of General Convective Heat Transfer Coefficient.....	93
6.2.6. Effect of Temperature of Cooling Fluid.....	94
6.2.7. Effect of the Wall Thickness of the Storage Tank .....	96
6.2.8. Effect of Inlet Radius of Storage Tank .....	97
CHAPTER 7 .....	99
CONCLUSION.....	99
7.1 SUMMARY AND CONCLUSIONS .....	99
7.2 FUTURE WORK.....	100
REFERENCES.....	102
RESUME .....	110

## LIST OF FIGURES

	<u>Page</u>
Figure 2.1. Typical experimental set-up [29,33,36,54–56] .....	7
Figure 2. 2. Geometry of MHTs: (a) MHST-1 (b) MHT-2 [6]. .....	8
Figure 2.3. Geometrical configurations of MHT [29,30].....	9
Figure 2.4. Geometrical configurations of MHT [69,70].....	9
Figure 2.5. Geometrical configurations of MHT [53,71].....	9
Figure 2.6. Geometry of MHTs: (a) MHT-1 (b) MHT-2 and (c) MHT-3 [72].....	10
Figure 2.7. Cross-sections of two different MHTs: (a) Un-finned (b) Finned [54].	11
Figure 2.8. Photo and schematic view of metal hydride tank [36].....	11
Figure 2.9. MHTs Configurations: a) MHT-1, b) MHST-2, c) MHT-3, d) MHT-4 [12].....	14
Figure 2.10. MHTs Configurations: a) MHT-1, b) MHT-2, c) MHT-3, d) MHT-4 [31].....	15
Figure 2.11. a) Geometry of MHT used in simulations[26], and b) Geometry of MHT used in simulations [15].....	15
Figure 2.12. Geometry of MHTs used in simulations [28].....	16
Figure 2.13. (a) schematic of the cutaway view of MHT and (b) Ax symmetric model used in Ansys Fluent software [66]. .....	17
Figure 2. 14. MHT portion geometry implemented in Comsol Multiphysics software [57].....	18
Figure 2.15. Geometry of three MHT configurations: a) 7 inner tubes; b) 12 inner tubes; c) 12 inner tubes with a cooling jacket and d) geometry of MHTs used in COMSOL Multiphysics [67] .....	18
Figure 2.16. a) Geometry of MHT, b) Geometry of MHT used in the simulation [65] .....	19
Figure 2-17. Geometry of MHT used in simulations [73], and [63].....	20
Figure 2-18. Schematic diagram of cylindrical MHT [40] .....	21
Figure 2. 19. MHT modelling's [74] and [62]. (a) Geometry used in modeling MHT-1 and (b) MHT-2.....	22
Figure 2.20. MHT geometry used in simulation [61] .....	23
Figure 2.21. Computational domain and geometric details of MHT [58] .....	24
Figure 3.1. Amount of hydrogen stored in different storage methods.....	34

	<u>Page</u>
Figure 3.2. Metal Hydride.....	35
Figure 3.3. Schematic isothermal pressure-composition hysteresis loop [77].....	40
Figure 4.1. Schematic diagram of MHTs a) w/o heat pipe b) with heat pipe c) with finned heat pipe [85]......	46
Figure 4.2. Photograph of three metal hydride tank configurations.....	47
Figure 4.3. Laboratory Manufactured Heat Pipe.....	48
Figure 4.4. Characteristics of the heat pipe.....	48
Figure 4.5. Data Collection System (Pico thermocouple data logger TC-08). .....	49
Figure 4.6. K-type thermocouples.....	49
Figure 4.7. Photo of the Mechanical Grinder Machine.....	50
Figure 4.8. LaNi <sub>5</sub> alloy.....	50
Figure 4.9. Hydrogen charge pressure (10 Bar) where the absorption process takes place.....	51
Figure 4.10. Vacuum pump.....	51
Figure 4.11. Ceramic resistance heater. ....	52
Figure 4.12. Analytical weight balance machine. ....	52
Figure 4.13. Schematic diagram of the experimental setup.....	53
Figure 5.1. Geometries of the MHTs used in modeling and simulation: a) MHT using natural convection, b) MHT equipped with a heat pipe in the center, c) MHT with finned heat pipe.....	57
Figure 5.2. Software and revision information used in simulation study. ....	65
Figure 5.3. Modeling work - Mesh screen. ....	65
Figure 5.4. Mesh Structure.....	66
Figure 5.5. Temperature change graph obtained during the absorption process - Three thermocouples placed in different locations.....	67
Figure 5.6. H <sub>2</sub> absorbed mass over time.....	67
Figure 6.1. Hydrogen storage in the metal hydride at the pressure 10 bar by wt% 73	
Figure 6.2. Hydrogen storage in the metal hydride (absorption/g alloy) at the pressure 10 bar .....	73
Figure 6.3. Storage tank weights after absorption process is complete .....	74
Figure 6.4. Temperature of metal hydride during MHT hydriding at 4 bar pressure in the first 500s: a) without heat pipe b) with a heat pipe c) equipped with a finned heat pipe.....	75
Figure 6.5. Comparison between the heat pipe temperature profiles under several hydrogen supply pressures in the MHTs: a) heat pipe, b) finned heat pipe configuration.....	77

Figure 6.6. Initial hydrogen supply pressure and its effect on the hydrogen storage for MHT that is equipped with a finned heat pipe.....	78
Figure 6.7. The impact of the pressure of the initial hydrogen supply on the hydride temperature, a) without the heat pipe, b) with a heat pipe, c) with a finned heat pipe.....	80
Figure 6.8. Comparison between the temperatures of a metal hydride in the MHT hydriding process without the heat pipe, with a heat pipe and with a finned heat pipe: a) supply pressure 4 bars, b) supply pressure 10 bars, c) supply pressure 15 bars.....	81
Figure 6.9. Thermal images of three MHTs at 15 bars charging pressure: a) without heat pipe, b) with a simple heat pipe, c) with a finned heat pipe.....	83
Figure 6.10. Schematic view of the mesh sizes. ....	85
Figure 6.11. Time evolutions of the absorbed hydrogen amount in heat pipe tank configuration under 10 bar hydrogen pressure supply by both experimental and simulation studies.....	86
Figure 6.12. The temperature histories at 35.8mm from the bottom. a) with no heat pipe, b) with a heat pipe, and c) with a finned heat pipe.....	87
Figure 6.13. 3D-temperature distribution inside the MHR configurations; with and without heat pipe, and with a finned heat pipe; P= 10 bar, and h=1500 W/m <sup>2</sup> K. ....	88
Figure 6.14. a) Temperature-time relationship for MHTs where the storage tank having fins or not as variable. b) Hydrogen mass against time where the storage tank having fins or not as variable. ....	89
Figure 6.15. a) Temperature history where hydrogen inlet pressure as variable. b) Hydrogen mass vs. time where hydrogen inlet pressure as variable. ...	91
Figure 6.16. a) Temperature history with respect to time where metal hydride powder's particle size is variable, b) Hydrogen mass against time where metal hydride powder's particle size as variable.....	92
Figure 6.17. a) Temperature history where the convective heat transfer coefficient as variable. b) Hydrogen mass against time where the convective heat transfer coefficient as variable.....	93
Figure 6.18. a) The temperature histories where cooling temperature as variable, b) Hydrogen mass storage against time where cooling temperature as variable.....	95
Figure 6.19. a) The temperature histories where the wall thickness as variable. b) Hydrogen storage mass against time where the wall thickness as variable.....	96
Figure 6.20. a) The temperature histories where the inlet radius of storage tank as variable. b) Hydrogen storage mass against time where the inlet radius of storage tank as variable.....	98

## LIST OF TABLES

	<u>Page</u>
Table 2.1. Summary of experimental studies on MHTs. ....	12
Table 2.2. Parametric values used in modeling[31].....	14
Table 2.3. The physical properties of the components of the MHTs used in modeling [28].....	16
Table 2.4. The parametric values used in modeling [57].....	17
Table 2.5. The input data for simulation [67] .....	19
Table 2.6. The thermal-physical properties of metal hydride and hydrogen [65].....	20
Table 2.7. The thermal-physical properties of metal hydride and hydrogen [73].....	21
Table 2.8. The thermal-physical properties of metal hydride and hydrogen [40].....	22
Table 2.9. The parametric values used in modeling [62].....	23
Table 2.10. The parametric values used in modeling [61].....	24
Table 2.11. The thermal-physical properties and operating conditions used in computations [58].....	25
Table 2. 12. Summary of numerical studies on MHTs. ....	25
Table 3.1. Physical properties of hydrogen.....	33
Table 3.2. Hydrogen storage characteristics of some metal hydride materials [78]..	38
Table 4.1. Uncertainty analysis of absorbed hydrogen and temperature with/without heat pipe at varying charging pressures [85] .....	56
Table 5.1. Hydrogen storage tank geometry and parametric dimension changes used in analyzes. ....	69
Table 5.2. Constantly used parameter values in analyzes.....	70
Table 5.3. Different parameter changes affecting the hydration process.....	70
Table 6.1. Comparison between the present results with the results of other similar investigations [85].....	82
Table 6.2. Mesh size on the domains, the number of elements, minimum and average qualities of them.....	85



## SYMBOLS AND ABBREVIATIONS INDEX

### LATIN SYMBOLS

$A_f$	: Fin surface area, $m^2$
$A_{tot}$	: Total surface area, $m^2$
$A_w$	: Wall surface area, $m^2$
$C_a$	: Kinetic parameter, 1/s
$C_p$	: Specific heat, J/kgK
$d_p$	: Particle diameter, m
$d_i$	: Inside diameter of reactor, m
$E_a$	: Activation energy of the absorption reaction, J/Mole
$E_b$	: Activation energy of the adsorption reaction, J/Mole
$E$	: Thickness of the spiral coil, m
$h$	: Overall heat transfer coefficient, $W/m^2K$
$K$	: Permeability, $m^2$
$L$	: Total bed length, m
$m$	: Amount of hydrogen stored in MH, $kg/m^3$
$\dot{m}_f$	: Mass flow rate of the cooling fluid, kg/s
$M_w$	: Molecular weight of hydrogen, kg/kmol
$n_f$	: Fin efficiency
$N_f$	: Number of fins
$P$	: Pressure, Pa
$P_{eq}$	: Equilibrium pressure of MH, Pa
$Q$	: Heat, J
$r$	: Radius of the reaction bed, m
$R_u$	: Ideal gas constant, J/molH <sub>2</sub> K
$t$	: Time, s

T : Temperature, K  
u : Superficial gas velocity vector, m/s  
u<sub>f</sub> : Cooling fluid velocity, m/s

### GREEK SYMBOLS

$\lambda$  : Thermal conductivity, W/mK  
 $\mu_g$  : Dynamic viscosity, kg/m s  
 $\sigma$  : Reaction rate constant, s<sup>-1</sup>  
 $\rho$  : Density, kg/m<sup>3</sup>  
 $\varepsilon$  : Porosity  
 $\Delta H$  : Enthalpy of desorption, J/molH<sub>2</sub>  
 $\Delta S$  : Entropy of desorption, J/molH<sub>2</sub>K  
 $\Phi$  : Hysteresis factor, J/molH<sub>2</sub>  
 $\Phi, \Phi_0$  : Slope factors  
 $\Delta\rho$  : Fictitious decrease of the hydride density, kg/m<sup>3</sup>

### Subscripts

d : Desorption  
e : Effective, element  
eq : Equilibrium  
f : Final, cooling fluid  
g : Gas phase (H<sub>2</sub>)  
i : Inlet, inner, initial  
m : Metal, alloy  
o : Outlet, outer  
s : Solid phase (MH)  
r : Radial  
X : Hydrogen concentration, H/M  
z : Axial distance, m  
Z : Length of the reactor, m

## **Abbreviations**

MH : Metal hydride

MHT's : Metal hydride tanks

## **CHAPTER 1**

### **INTRODUCTION**

#### **1.1. BACKGROUND**

Interest in metal hydrides began in 1970 with the discovery of hydrogen absorption/desorption in alloys such as FeTi, LaNi<sub>5</sub>, and MgNi [1,2]. After that, new energy sources have been sought to meet the world's growing fuel requirements. Reduced fuel sources and pollution due to consumption of fuels have necessitated alternative resources of clean energy [3]. Hydrogen has great potential to become the most significant alternative fuel because of its great thermal value and environment-friendliness. Moreover, it offers more energy per unit weight in addition to highest gravimetric energy density [4].

#### **1.2. HYDROGEN STORAGE METHODS**

Effective and safe storage of hydrogen is quite challenging. It is a light gas; therefore, it provides maximum energy in terms of energy and also because its mass is low. Moreover, it might leak out of containers; therefore, storing hydrogen is very difficult. In the nutshell, hydrogen storage is a major impediment in the way of getting real benefit out of it, which creates a problem in its commercial use as a fuel.

Almost all the studies in the field of hydrogen energy have shown that the problem of storing hydrogen reduces its use and marketing. Low hydrogen density leads to many storage issues including large volume requirements, weight, and high pressure in addition to posing a safety threat.

Recently, hydrogen can either be stored in the form of compressed gas or it can be stored in liquid form by cooling at low temperatures. These storage methods such as

liquefaction and compression are not ideal because these methods not only require a lot of energy and are very expensive, but also there are safety problems. Hydrogen can actually be stored inside carbon nanotubes and can be chemically stored inside hydrides as a solid. It was noted that storage as a hydride the most effective storage method because of its proper operating conditions, low pressure operations, and high storage capacity, which lead to operational safety and unparalleled density of hydrogen storage. These systems provide greater capacity to store hydrogen.

### **1.3. CHALLENGES WITH METAL HYDRIDE HYDROGEN STORAGE**

Such storage of hydrogen in the MH family is a complex, multi-physics problem involving the flow of compressible gas in a porous medium, along with heat transfer and reaction kinetics. During hydriding process, hydrogen gas is compressed into the porous metal layer as it is absorbed to release heat during an exothermic reaction.

Nowadays, storage of hydrogen in metals or complex compounds is getting attention because of its safety, maximum energy density and reliability [5]. Metal-hydride storage tanks store large hydrogen quantities in small volumes during a short charging period and operate at high pressures; so they have great importance. For this reason, the researchers focused their studies on rare metal alloys. Some inter-metallic compounds, have been observed to charge and discharge very large amounts of hydrogen under very low pressure conditions; so they are under application as a reasonable method of storing hydrogen [6]. Researchers have considered the chemical deposition of hydrogen in MHT metals such as Mg, La, Na and Li [7–11]. Almost 50 metal elements showed tendency to reasonably absorb hydrogen [12].

Tests were conducted on hydrogen storage properties in a several materials. Among these,  $AB_5$  is considered as  $LaNi_5$  because it has excellent hydrogen storage properties such as high volume storage density, easy activation, good kinetic properties, etc. [13]. However, the  $LaNi_5$  alloy has unsatisfactory properties, such as storage capacity that is significantly less than the periodic charging/discharging process, easy crushing, ease of combustion after crushing, plateau pressure is very high and so [14]. Even then, most hydrides' thermal conductivities are extremely

poor, such as, the powder of  $\text{LaNi}_5$  that has porosity factor  $\varepsilon = 0.5$  and thermal conductivity  $1.32 \text{ W/mK}$  [15]. Lower thermal conductivities make it challenging to extract the hydride heat that leads to increasing hydride temperature. During charging, the hydride reaction is rapid at low temperature that decreases with the temperature rise. It stops at a certain point; therefore, for maintaining the high charge rate, removal of heat is needed for metal hydrogen/hydride storage. Several researches have been conducted on heat transfer and the kinetics of the hydrides. The 1D mathematical modeling [16–19] and 2D modeling [6,20–24] were applied for predicting the mass and heat transfer through a porous medium. This type of investigations shows that the main issue is heat transfer rate, which determines the hydrogen storage rate or the rate, at which, it is extracted out of a hydride tank.

In hydrogen storage process, heat exchangers are used to increase the MH heat transfer rate [12,15, 19,25–35]; however, the heat exchange pipes can get leaked, and water might come out that can spoil metal hydrides, therefore, heat pipes can be used to minimize this type of damage [36,37]. Heat pipes generally have extreme thermal conductivity; so they are used in many industries for different purposes including thermal storage, microprocessor cooling, and different types of reactors [38].

Hydrogen storage is a major technical difficulty to develop and use fuel cell energy technologies in transport and portable applications. It is possible to convert hydrogen into electricity in case of application as a direct fuel cell reactant, and it will be the only emission. Thus, hydrogen doesn't emit any greenhouse gas that ultimately mitigates pollution. Fuel cell applications need a hydrogen fuel tank with mobile power source, such as a portable source or a vehicle. The only problem in the way of using hydrogen as an automobile fuel is its storage [39], however, the main problem for storage facilities of metal hydrides is managing their heat transfers. Thus, hydrogen charging to/discharging through metal hydrides is based on kinetic reactions and transfer of heat and mass.

## 1.4. OBJECTIVES

This thesis is aimed at designing a storage system for storing hydrogen using the hydride material, which can instantly eliminate heat that is generated when the reaction takes place; so fundamentally, our aim is to reduce the system temperature. In the nutshell, we want to design a specific type of MHT that has very high efficiency to remove heat despite the hydride storage. We chose  $\text{LaNi}_5$  medium to store hydrogen, since it is an easily available commercial alloy that reacts with hydrogen at low pressure at room temperature. Additionally, the MHT doesn't require heat for charging. Moreover it doesn't need high inlet pressure that decreases both cost and complexity.

The current research aims at methods to increase heat removal out of MHT so as to preserve a high percentage of charge. To achieve this goal, the following have been done:

- This study focused on an MHT pilot design that has fins and a heat pipe to test this concept.
- Experiments were conducted to showcase the effectiveness of the heat pipe, and later, the absorption rate was compared for an MHTs with or without the heat pipe.
- In order to validate the experimental results, a mathematical model has been developed to predict certain parameters, including internal temperature distribution of MHT, and storage quantity of hydrogen gas.
- This model consists of energy, mass and momentum balance. These differential equations are numerically solved by means of the finite element method using the software COMSOL Multyphysics™.

## 1.5. DISSERTATION OUTLINE

The hydrogen storage complexity in several metal hydrides involves reaction kinetics, hydrogen flow, cooling systems, system engineering geometry, and heat

transfer rates, which make the system design difficult without a thorough analysis. In this research, we want to test the hydrogen gas charging rate in the MHT because it depends on the rate of heat removal from the hydrogen storage facility. In this case, we'll explore the following approaches:

- Accelerate the heat transfer rate in the base MHT by using heat pipe and fins.
- Optimization of hydriding process using a heat pipe with fins in a cylindrical MHT.

For investigating various factors and their effectiveness in the proposed approach, we have developed a numerical model, which incorporates heat transfer and reaction kinetics in the software COMSOL Multiphysics™ Version 5.2a. Various storage tank design strategies were explored using simulations, and many hydrides and cooling methods were used for finding optimal designs that accelerate the hydrogen charging rate. We designed an experimental setup for charging hydrogen in a storage tank, and its charging capacity and temperature were monitored to test the numerical model validity.

Chapter 1 discusses the importance of hydrogen, economy, storage methods, and challenges pertaining to hydrogen storage systems and metal hydrides. In Chapter 2, we reviewed literature on hydrogen storage. In Chapter 3, we classified the metal hydride materials, which were used as storage media in the hydrogen storage systems. In Chapter 4, we designed different tank configurations for experimental work. In Chapter 5, we developed a mathematical model pertaining to a hydrogen storage system (hydride-based) in COMSOL Multiphysics™ to validate the experimental results. In Chapter 6, both experimental and simulation results were discussed and highlighted. Chapter 7 includes conclusion and recommendations.



## CHAPTER 2

### LITERATURE REVIEW

#### 2.1. PREVIOUS WORK ON METAL HYDRIDE HYDROGEN STORAGE

Studies have reported that heat transfer from/to hydrogen absorption/desorption processes is a key factor in the MHT design. It is seriously affected by the storage tank geometry and its design configurations; therefore, many researchers have extended methods to develop the rates of heat transfer in MHTs. Hence, the hydrogen storage in MHTs is reliant on the heat removal rate during the absorption process and the heat rate during the desorption process. Improvement in the metal hydride conductivity influenced the heat transfer mechanism by the addition of copper wire net structure [40,41], compressing copper encapsulated powders into compacts [42,43], graphite addition [44,45], and using aluminum foam [19,27,46]. Heat exchangers set with inner concentric tube [47], equipped with plate fin [48], and a spiral-type [29,49] that greatly increases the rate of hydrogen storage in the MHTs. The structure of most of the MHTs is like tube-type heat exchanger [6,50–52]. The addition of fins to the spiral type and tubular heat exchangers were also considered [53]. It showed a significant solution that improves hydriding.

Most of the work in the literature concentrates on the MHTs to be used for hydrogen storage. Each researcher has his individual method to achieve his target. In general, the hydrogen storage methodology has been classified as an experimental and numerical simulation study.

All the experimental studies conducted on hydrogen storage system have the same procedure, which is considered to be a typical procedure used for the MHT design. Activation is required to start with any hydriding process and it is very important, specifically in case of real-time MHT application.

The oxide usually covers the surface of metals and act as a passive film [54] . A typical experimental setup is shown in Figure 2.1 [29,33,36,54–56]. Experimental studies have been summarized in Table 2.1. They were found on MHTs in literature which included the geometry used, the parameters studied and the obtained results.

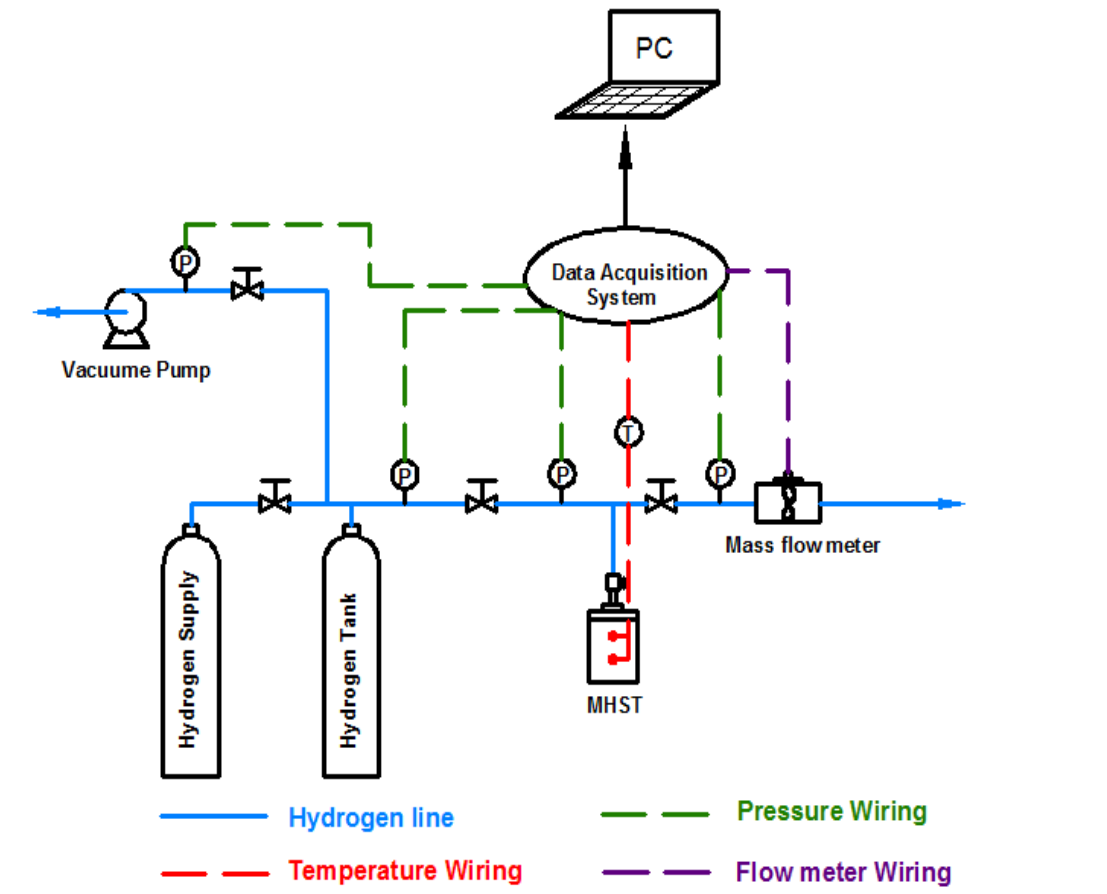


Figure 2.1. Typical experimental set-up [29,33,36,54–56].

Scientists have been succeeded to describe both physical and chemical phenomena in the MH formation by employing mathematical models for obtaining the MHTs' optimal design. Several relevant mathematical models have been developed [6,12, 15,26,28,30,31,40,56–67]. The mathematical model is usually derived from combination of interstitial fluid, energy, momentum, and mass balance to explain the chemical reaction, pressure-temperature ratio, kinetic rate and concentration [15,20,23,26]. The basic assumptions through a macroscopic scale for the hydriding process are decided to achieve the model governing equations [12,15,26, 28,31,40, 56–59,61,62,64,66,68]. Table 2.12 shows the summary of numerical studies on

MHTs in literature, which include the geometry, simulation methods, studied parameters, and the obtained results.

### 2.1.1. Geometries used for Experimental Study

Demircan et al. [6] used 2-D MHTs for metal hydride formation. Two different tanks were chosen for experiments; MHST-1 has the cylindrical shape (Figure 2.2a). MHT-2 has two built-in co-eccentric cylinders and a metal hydride (Figure 2.2b).

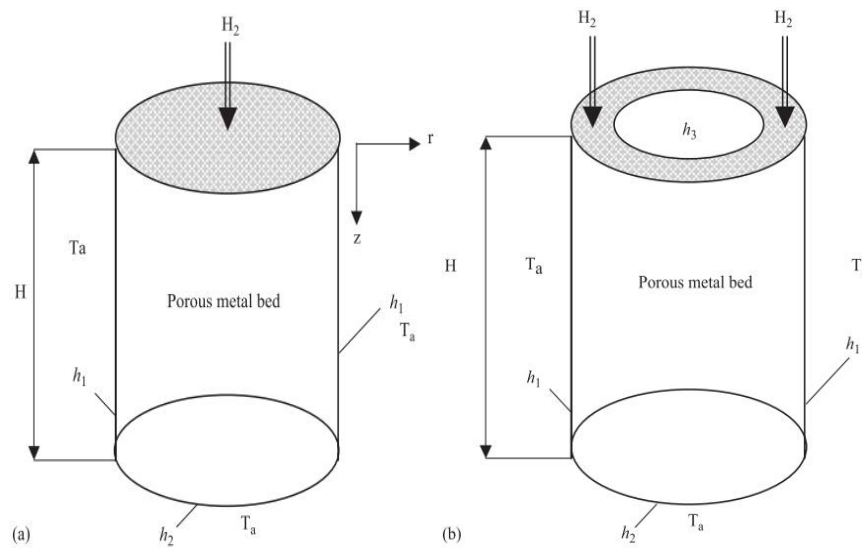


Figure 2. 2. Geometry of MHTs: (a) MHST-1 (b) MHT-2 [6].

Typical base 316-L stainless steel MHTs were cooled by water flow into the shell heat exchanger and/or using spiral coiled stainless steel tube units. Different configurations were tested by the researchers like Mellouli et al. [29,30] (Figure 2.3), Dhaou et al. [69,70] (Figure 2.4), and Souahlia et al. [53,71] (Figure 2.5). In this experiment, a copper fin was inserted inside the metal hydride in order to increase the heat transfer area in MHTs (Figure 2.4b and c, and Figure 2.5c). Another heat exchanger design was based on steel cylindrical tube, which was mounted over the MHT that creates space for the liquid to pass through (Figure 2.5b).

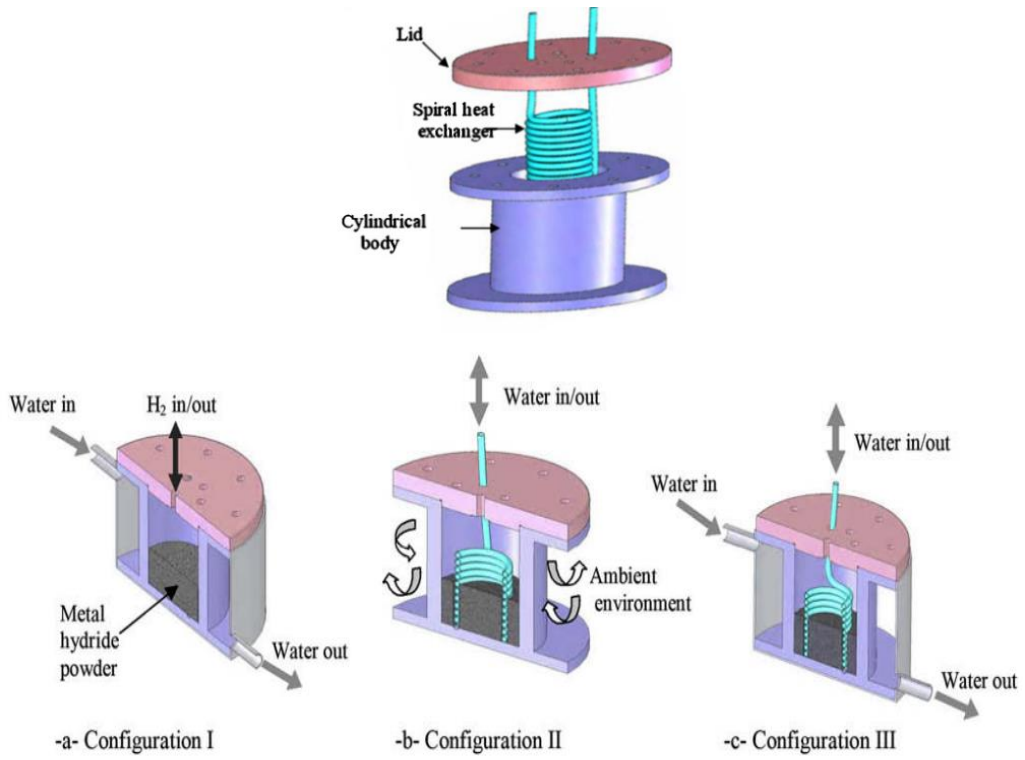


Figure 2.3. Geometrical configurations of MHT [29,30].

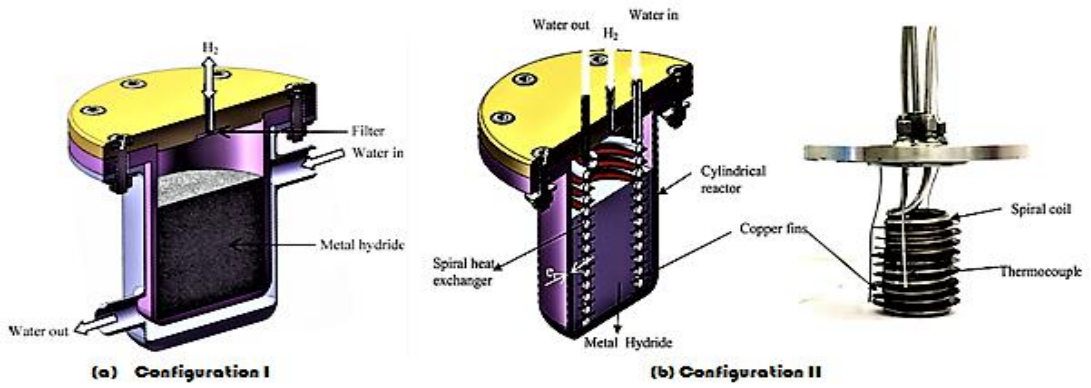


Figure 2.4. Geometrical configurations of MHT [69,70].

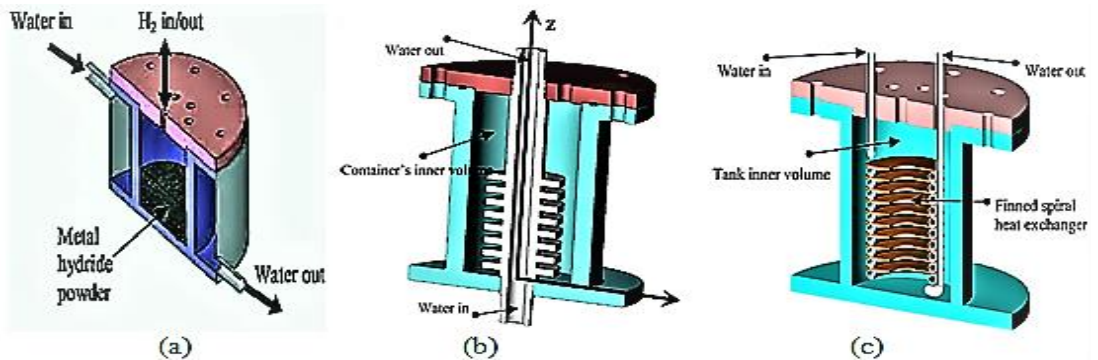


Figure 2.5. Geometrical configurations of MHT [53,71].

Kaplan et al. [72] used three different MHT configurations manufactured using St.42 steel, as shown in Figure 2.6. MHT-1 is used as a base case. It is a cylindrical shaped MHT (Figure 2.6a). MHT-2 has the same dimensions as MHT-1 with additional circular fins at specific geometric dimensions (Figure 2.6b). MHT-3 is designed to investigate the effect of forced convection. Water is utilized for cooling and circulating around metal hydride formation (Figure 2.6c).

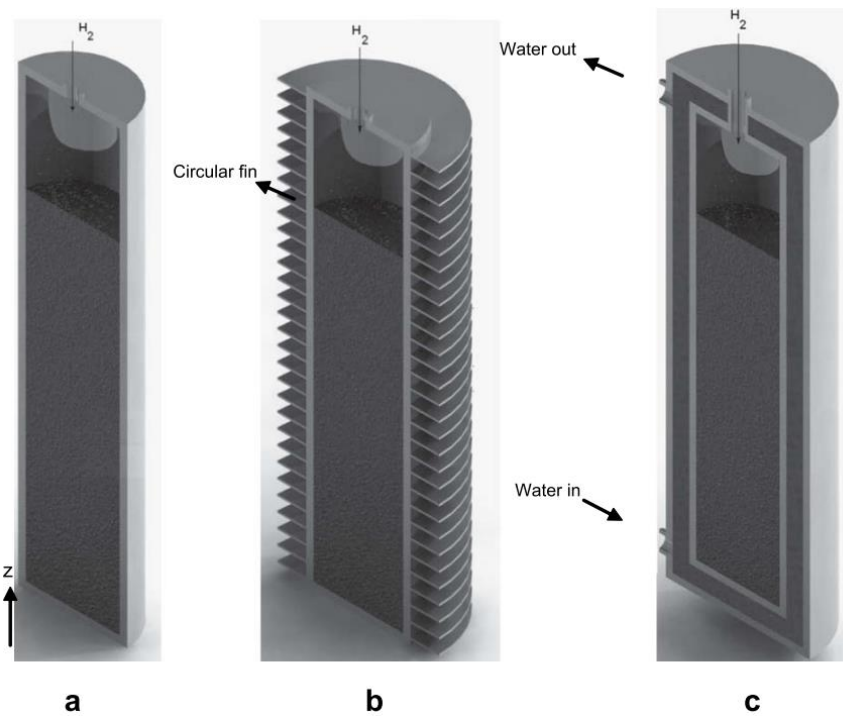


Figure 2.6. Geometry of MHTs: (a) MHT-1 (b) MHT-2 and (c) MHT-3 [72].

Kayfeci et al. [54] use two MHT configurations manufactured using St.42 steel, as shown in Figure 2.7. Un-finned tank was the base case, which has a cylindrical shape (Figure 2.7a). Finned tank has the same dimensions as un-finned tank with additional 23 circular fins at specific geometric dimensions (Figure 2.7b) in order to get a better heat removal from the tank.

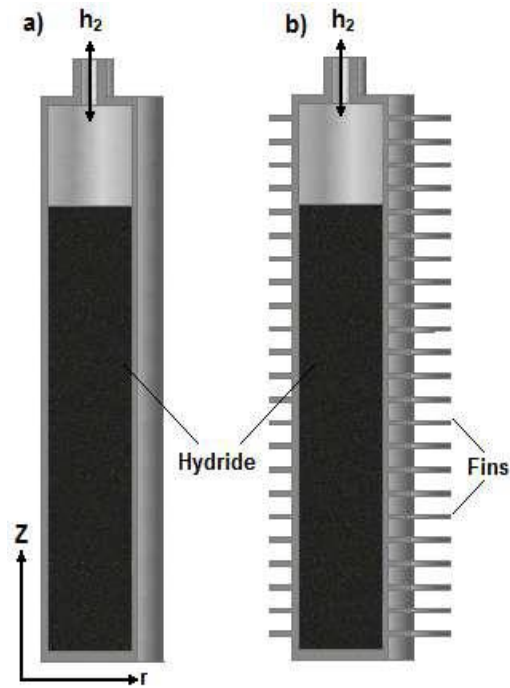


Figure 2.7. Cross-sections of two different MHTs: (a) Un-finned (b) Finned [54].

Chung et al. [36] used two MHT configurations manufactured using 316-L stainless steel, as shown in Figure 2.8. Both MHTs are cylindrical, and have the same dimensions. Heat pipe is immersed in MHT-1 inside the stainless steel sleeve with specific dimensions. It is located on the tank axis (Figure 2.8a). Ten fins with specific dimensions were attached to a sleeve rod in order to increase the heat transfer area.

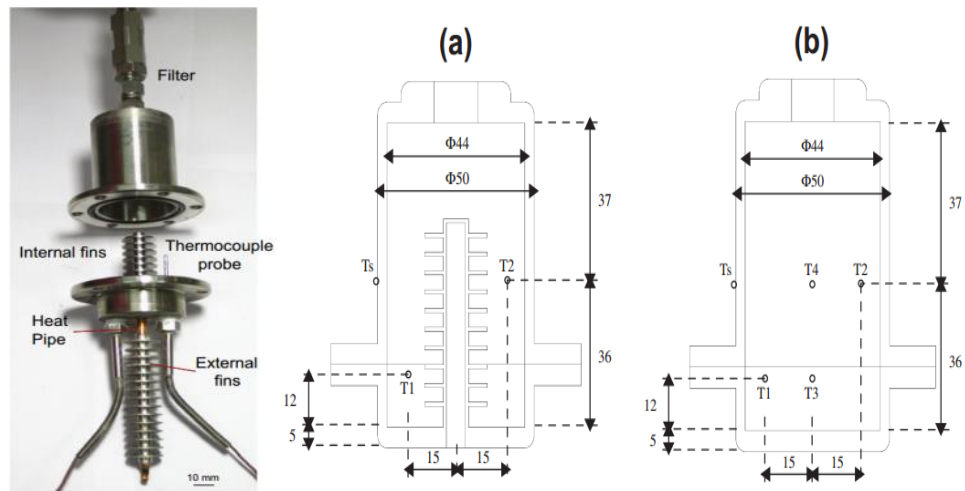


Figure 2.8. Photo and schematic view of metal hydride tank [36].

Table 2.1. Summary of experimental studies on MHTs.

Investigator/ Date	Geometry Used	Parameters Study	Observations
Demircan [6] 2005	Two MHTs shown in Figure 2.2.	2D theoretical model and experimental study was conducted to test kinetic and thermal properties of hydriding by different charged hydrogen pressures in a range: 6–10 bars.	Heat transfer from/to hydrogen absorption/desorption process is a key factor for the MHTs design. It is seriously influenced by the tank geometry. Successful heat removal reduces the hydrogen storing time.
Mellouli [29,30] 2007 & 2009 respectively	Three MHTs shown in Figure 2.3.	1-Experimental work and 2D mathematical equations were used for investigating performances of various MHT designs. 2-The influence of several parameters; e.g., input pressure, tank volume, cooling, and coefficient of heat transfer.	1- Hydrogen storing time is reduced by a spiral coiled tube heat exchanger with a good choice of design study parameters. 2- The experimental-numerical verification is done, and the effectiveness of the proposed model was assured for the MHT design.
Dhaou [69,70] 2010 & 2011 respectively	Figure 2.4 shows the MHTs	The influence of several parameters; e.g. input pressure, mass flow, and fluid cooling temperature.	They clearly reduced the storage time using a spiraled, coiled, and finned heat exchange mechanism with a good choice of design study parameters.
Souahlia [53,71] 2011	Figure 2.5 shows the MHTs	The influence of several parameters e.g. input pressure, cooling/heating fluid, and temperature on effectiveness of MHT.	The successful heat removal design reduces hydrogen storing time with a good choice of design study parameters.
Kaplan [72] 2009	Three MHTs were designed as shown in Figure 2.6.	Heat transfers in MHTs when hydrogen pressure changes between 1–10 bars.	Using the tank design of water circulating around the hydride bed confirms less temperature during the fastest charging time under all specific values of hydrogen pressure.
Kayfeci [54] 2014	Two MHTs shown in Figure 2.7.	Heat transfer during charged hydrogen pressure in MHTs in the range 2–8 bars.	1- Using the MHT design with fins confirms the less charging time under all specific values of hydrogen pressure.

Table 2.1. (continued)

Investigator/ Date	Geometry Used	Parameters Study	Observations
			2- Addition of Aluminum element to the AB <sub>5</sub> alloy enhances the heat transfer and results in reducing the charge time and decreasing the stored mass.
Chung [36] 2013	Two MHTs shown in Figure 2.8.	Heat transfer mechanism in MHTs with and without a heat pipe.	<ol style="list-style-type: none"> <li>1. Heat pipe is a useful way to improve hydrogen storage capacity.</li> <li>2. More than half time reduced during the absorption process, and 44% of the time increased at 1L/min hydrogen flow rate for the desorption process.</li> </ol>

### 2.1.2. Geometries used for numerical simulation study

Mellouli et al. [12] used the MHTs, which are shown in Figure 2.9. 2-D metal hydride formation is numerically simulated in Fortran 90. The typical base 316-L stainless steel MHTs are made using four configurations: MHT-1 is built of two co-concentric cylinders (Figure 2.9a). The outer walls swap heat with cooling fluid and the inner cylinder is attached with spiral-coiled stainless steel tube units. MHT-2 is the same as MHT-1, with additional copper fins between each pair of turns inside the metal hydride formation (Figure 2.9b). MHT-3 is the same as MHT-1, with two additional layers of spirally coiled tubes (Figure 2.9c). MHT-4 is the same as MHT-3, with the additional fins between the turns (Figure 2.9d).



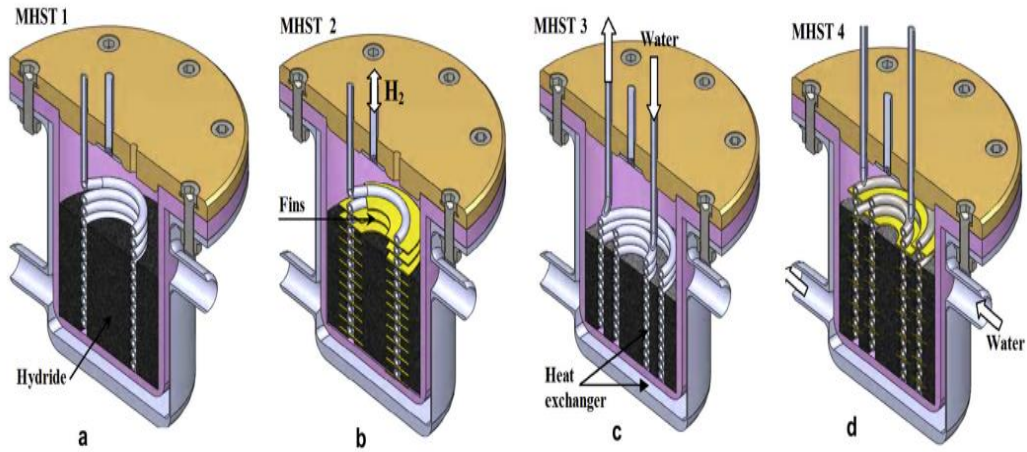


Figure 2.9. MHT Configurations: a) MHT-1, b) MHST-2, c) MHT-3, d) MHT-4 [12].

Askri et al. [31] used the MHT configurations (Figure 2.10), which are simulated as 2D metal hydride formation in control volume finite element method (CVFEM). Four configurations are used: MHT-1 is a cylindrical shape swap heat through its external walls (Figure 2.10a). MHT-2 is a similar to MHT-1 with additional fins on the external surface (Figure 2.10b). MHT-3 is similar to MHT-1 with additional centric heat exchanger tube filled with cooling fluid (Figure 2.10c). MHT-4 is similar to MHT-3 with additional fins around the heat exchanger tube (Figure 2.10d). Table 2.2 shows the simulated parameters.

Table 2.2. Parametric values used in modeling [31].

Parameter	LaNi <sub>5</sub>
Density-Steel (kg/m <sup>3</sup> )	7850
Density-Copper (kg/m <sup>3</sup> )	8400
Conductivity-Steel (W/mK)	26
Conductivity-Copper (W/mK)	121
Pore formation/porosity	0.5
Temperature of starting tank (K)	294
Temperature of the refrigerant (K)	294
Hydrogen inlet pressure (bars)	8
Coefficient of thermal conductivity (W/mK)	1.32
Density of LaNi <sub>5</sub> (kg/m <sup>3</sup> )	8200
Specific heat coefficient of LaNi <sub>5</sub> (J/(kgK))	530
Hydrogen specific heat coefficient (J/(kgK))	14,500

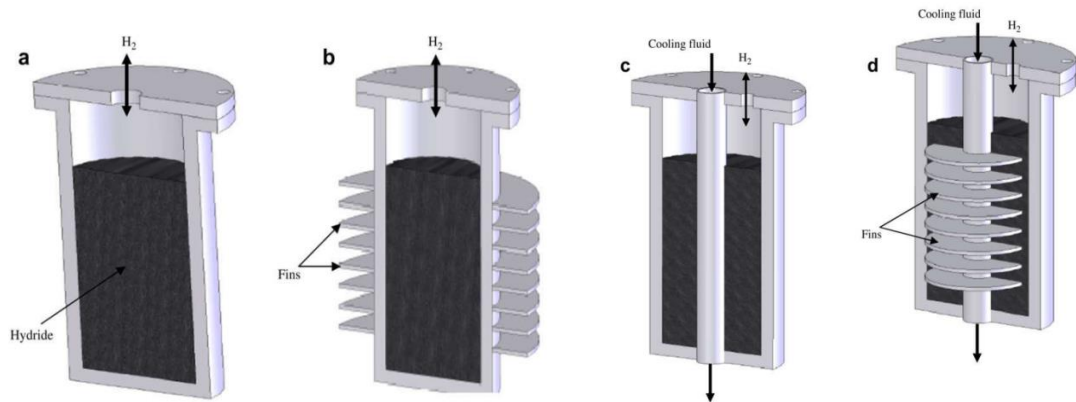


Figure 2.10. MHTs Configurations: a)MHT-1, b)MHT-2, c)MHT-3, d) MHT-4 [31].

2D asymmetric MHTs are modeled as shown in Figure 2.11. At a constant temperature and flow rate heating fluid, the cylindrical tank exchanges heat from base and lateral areas (Figure 2.11a) Jemni et al. [26]. Furthermore, the cylindrical tank exchanged heat through lateral and base areas at a constant temperature and a constant flow rate cooling fluid (Figure 2.11b) Jemni et al. [15]. The tanks have a gaseous phase ( $H_2$ ) and a solid porous phase (MH); so it is an irregular medium.

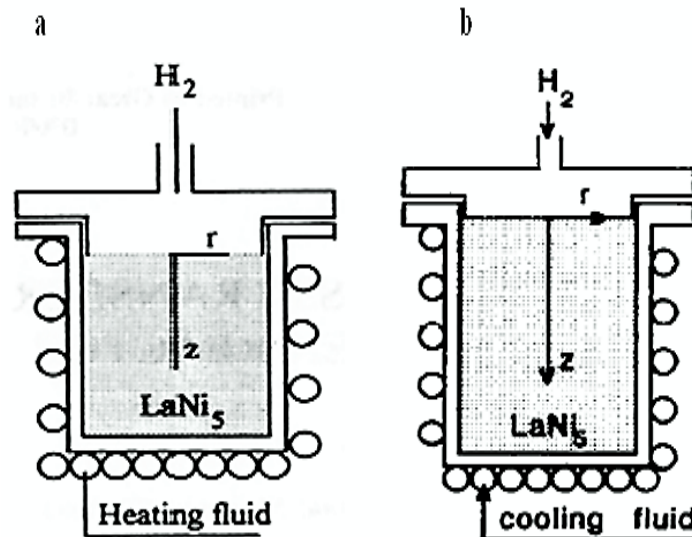


Figure 2.11. a) Geometry of MHT used in simulations [26], and b) Geometry of MHT used in simulations [15].

Mellouli et al. [28] used the MHTs (as shown in Figure 2.12), which were displayed in 2D asymmetric modeling. Two design configurations were considered: MHT-1 is a cylindrical tank (40 mm diameter and 50 mm height), which have metal foam for constant heat exchange from its bottom and lateral surfaces (Figure 2.12a). MHT-2 is

similar to MHT-1 but at 60 mm height, adding a tube is useful for concentric heat exchange with 6 mm diameter that contains a cooling fluid and metal foam (Figure 2.12b). Physical properties of the MHT components after simulation are presented in Table 2.3.

Table 2.3. The physical properties of the components used in modeling [28].

Parameter	LaNi <sub>5</sub>	Al foam	Hydrogen
Density (kg/m <sup>3</sup> )	8300	2700	0.0838
Specific heat, C <sub>p</sub> (J/kgK)	419	963	14.89
Thermal conductivity, $\lambda$ (W/mK)	2.4	10.9	0.24
Porosity	0.55	0.91	–

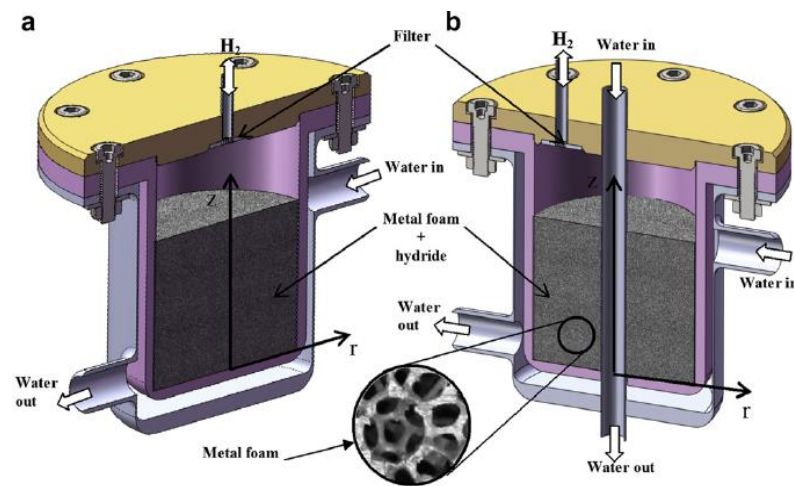


Figure 2.12. Geometry of MHTs used in simulations [28].

Wang et al. [66] used the MHT as shown in Figure 2.13, which is modeled as a two-dimensional axi-symmetric system. MHT has flanges, a cylindrical shell, two cover plates, O-rings, filters, and cylindrical spacers. Aluminum alloy 6061 was used to fabricate the cover plates, the shell, and the spacers. The bottom and top spacers perform by holding the metal hydride powder. A filter paper and nylon mesh are in place to sustain the metal hydride, which exists between the two spacers, and they are appropriate for the internal part of the tank. The tank was 203.2 mm high, had 15.5 mm wall thickness, and 106.7 mm distance between the Delrin spacers that was for the metal powder expansion during hydriding.

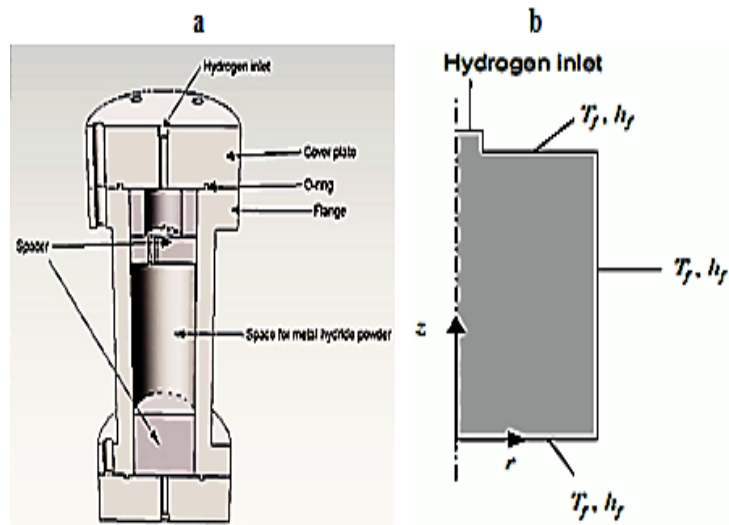


Figure 2.13. (a) Schematic of the cutaway view of MHT and (b) Ax symmetric model used in Ansys Fluent software [66].

Freni et al. [57] used the MHT, as shown in Figure 2.14, which is modeled as a three-dimensional system. It is a cylinder that has some tubes consisting of heating/cooling fluid. The direction of hydrogen entry is axial. MHT has external radius 100 mm and length 500 mm. Total eight heat exchange tubes are used. The external radius of tubes is 100 mm. The parameters considered in the simulation have been given (Table 2.4).

Table 2.4. The parametric values used in modeling [57].

Parameter	LaNi <sub>5</sub>
Hydrides beds' external radius ( $R_e$ )	0.1 m
Hydrides bed length ( $L$ )	0.5 m
Metal tubes' external radius ( $r_m$ )	0.005 m
Number of heat exchange tubes ( $N$ )	8
Heating/cooling fluid velocity ( $v$ )	0.5 m/s
Initial temperature ( $T_0$ )	20 °C
Initial pressure ( $P_0$ )	1.5 bar
Density of initial hydride ( $\rho_0$ )	3200 kg/m <sup>3</sup>
Saturation hydride density ( $\rho_{ss}$ )	3240 kg/m <sup>3</sup>
Hydride bed porosity ( $\epsilon$ )	0.5
LaNi <sub>5</sub> specific heat ( $C_{ps}$ )	419 J/kgK
Hydride thermal conductivity ( $k_s$ )	1.2 W/m <sup>2</sup> K
Sorption enthalpy ( $\Delta H$ )	30800 J/mol
Interface heat exchanger – hydride wall heat transfer coefficient ( $h_w$ )	1650 W/m <sup>2</sup> K
Pressure of hydrogen charge ( $P_{ext}$ )	8 bar
Cooling fluid temperature ( $T_{cool}$ )	20 °C

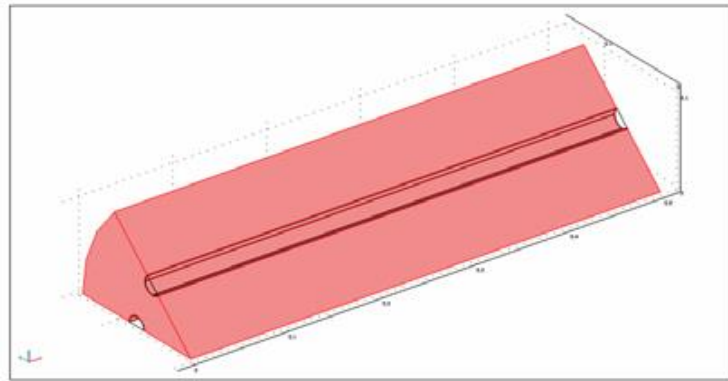


Figure 2.14. MHT portion geometry implemented in Comsol Multiphysics software [57].

Freni et al. [67] used the MHTs, as shown in Figure 2.15, which are modeled as a three-dimensional system. That MHT has a cylindrical shape with 100 mm external radius and 500 mm length. Three cooling system design configurations were simulated (Figure 2.15d). MHT-1 is considered as a basic design. It consists of seven tubes containing cooling water, which flows and displaces in a symmetrical situation in a metal hydride bed (Figure 2.15a). MHT-2 has twelve symmetric tubes, which provided a wider surface for heat transfer (Figure 2.15b). Another tank had the same configuration, and a cooling jacket was surrounding it (Figure 2.15c).

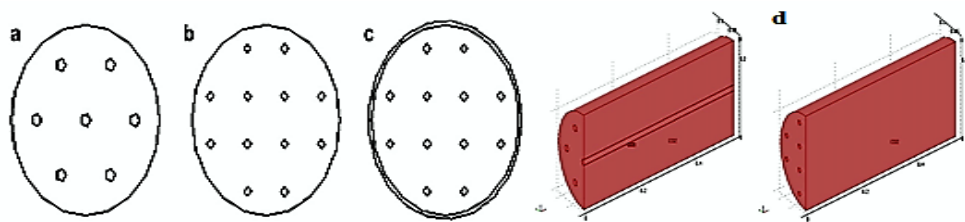


Figure 2.15. Geometry of three MHTs configurations: a) 7 inner tubes; b) 12 inner tubes; c) 12 inner tubes with a cooling jacket and d) geometry of MHTs used in COMSOL Multiphysics [67].

In all the types of configuration, the entry of hydrogen gas to the reactor was in axial direction. The input data for simulation study are given in Table 2.5.

Table 2.5. The input data for simulation [67].

Parameter	LaNi <sub>5</sub>
Hydrides bed external radius, $R_e$ (m)	0.1
Hydrides bed length, $L$ (m)	0.5
Metal tubes' external radius, $r_m$ (m)	0.005
Total heat exchange tubes, $N$	8
External cooling fluid velocity, $v$ (m/s)	0.5
Initial temperature $T_0$ (°C)	20
Initial pressure $P_0$ (bar)	1.5
Initial density of hydride, $\rho_0$ (kg/m <sup>3</sup> )	3200
Saturation hydride density, $\rho_{ss}$ (kg/m <sup>3</sup> )	3240
Hydride bed porosity, $\varepsilon$	0.5
LaNi <sub>5</sub> specific heat, $C_{ps}$ (J/kgK)	419
Thermal conductivity of hydride, $k_s$ , (W/m <sup>2</sup> K)	1.2
Sorption enthalpy ( $\Delta H$ ) (J/mol)	30800
Interface heat exchanger–hydride wall heat transfer coefficient ( $h_w$ ) (W/m <sup>2</sup> K)	1650
Hydride powder particle size, $d_p$ ( $\mu\text{m}$ )	28.3
Pressure of hydrogen charge, $P_{ext}$ (bar)	8
Cooling fluid temperature, $T_{cool}$ (°C)	20

Chung et al. [65] used the MHT as shown in Figure 2.16, which is modeled as a two-dimensional symmetrical system. MHT is cylindrical in shape, and consists of 25 mm internal radius, 20 mm height, and 60 mm length. The tank has a lid with a 10 mm filter diameter for hydrogen gas inflow or outflow to the canister. It has a constant-temperature water bath containing heating/cooling fluid.

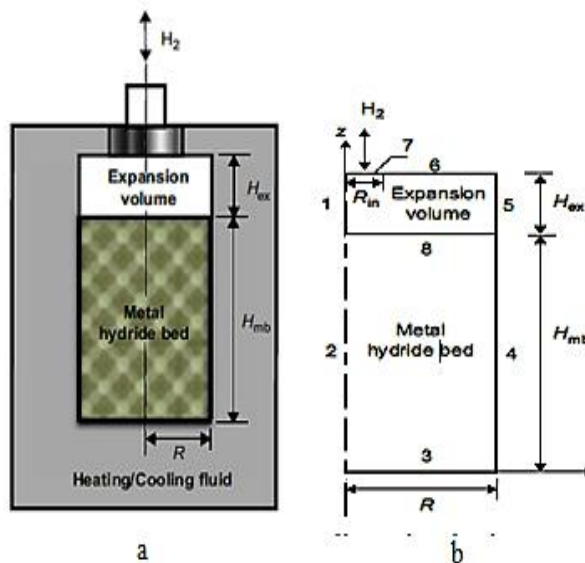


Figure 2.16. a) Geometry of MHT, b) Geometry of MHT used in the simulation [65].

Table 2.6 shows the properties of hydrogen and metal hydride, which are presented in a simulation study.

Table 2.6. The thermal-physical properties of metal hydride and hydrogen gas [65].

Parameter	LaNi <sub>5</sub>
Constant of absorption rate, Ca (1/s)	59.19
Constant of desorption rate, Cd (1/s)	9.57
Hydrogen gas specific heat, Cp <sub>g</sub> (J/molK)	14890
MH specific heat, Cp <sub>s</sub> (J/kgK)	419
Absorption activation energy, Ea (J/mol)	21179.6
Desorption activation energy, Ed (J/mol)	16473
Effective heat convection coefficient, h (W/m <sup>2</sup> K)	1652
MH Permeability, K (m <sup>2</sup> )	10 <sup>-8</sup>
Hydrogen gas heat conductivity, λ <sub>g</sub> (W/mK)	0.1815
MH conductivity, λ <sub>s</sub> (W/mK)	1.087
Hydrogen molecular mass, Mg (kg/kmol)	2.01588
Porosity (ε)	0.5
Hydrogen-free MH density, ρ <sub>emp</sub> (kg/m <sup>3</sup> )	7164
Saturated MH density, ρ <sub>sat</sub> (kg/m <sup>3</sup> )	7259

Kaplan et al. [73] is modeled a 2-D metal hydride cylindrical tank through the control volume finite element method (CVFEM) as shown in (Figure 2.17), and Sakti et al. [63] is modeled the same geometry with finite element lab (FEMLAB). The system represents the experimental configuration of Kaplan et al. [73]. The MHT is a cylindrical-shaped tank that swaps heat through its external walls with the surrounding cooling fluid. The materials' thermo-physical properties, concerned data, and computations have been exhibited in Table 2.7.

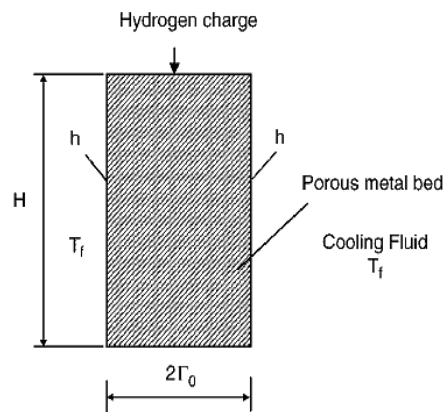


Figure 2.17. Geometry of MHT used in simulations [73] and [63].

Table 2.7. The thermal-physical properties of metal hydride and hydrogen gas [73].

Parameter	LaNi <sub>5</sub>
Density of LaNi <sub>5</sub> ( $\rho_s$ )	4200 (kg/m <sup>3</sup> )
Hydrogen Density ( $\rho_g$ )	0.0838 (kg/m <sup>3</sup> )
LaNi <sub>5</sub> Specific heat (Cps)	419(J/kgK)
Hydrogen - Specific heat (Cpg)	14,890 (J/kgK)
Thermal conductivity of LaNi <sub>5</sub> ( $\lambda_s$ )	1.2 (W/mK)
Hydrogen - Thermal conductivity ( $\lambda_g$ )	0.12(W/mK)
Porosity	0.55
Gas inlet temperature ( $T_0$ )	293 K
Bed and wall - Initial temperature ( $T_f$ )	293 K
Coefficient of Heat transfer (h)	1652 (W/m <sup>2</sup> K)

Mohan et al. [40] used the MHT, as shown in Figure 2.18, which simulated the 2-D metal hydride formation in COMSOL Multiphysics. MHT is built in a cylindrical shape with many tubes and filters distributed inside the metal hydride. The cooling tubes are arranged in a triangular configuration inside the MHT and the filters are located at the center of each triangular arrangement. The center-to-center distance between the tubes ( $s$ ) is called pitch distance. The LaNi<sub>5</sub> alloy and hydrogen have good thermo-physical properties, which are part of the simulation study (Table 2.8).

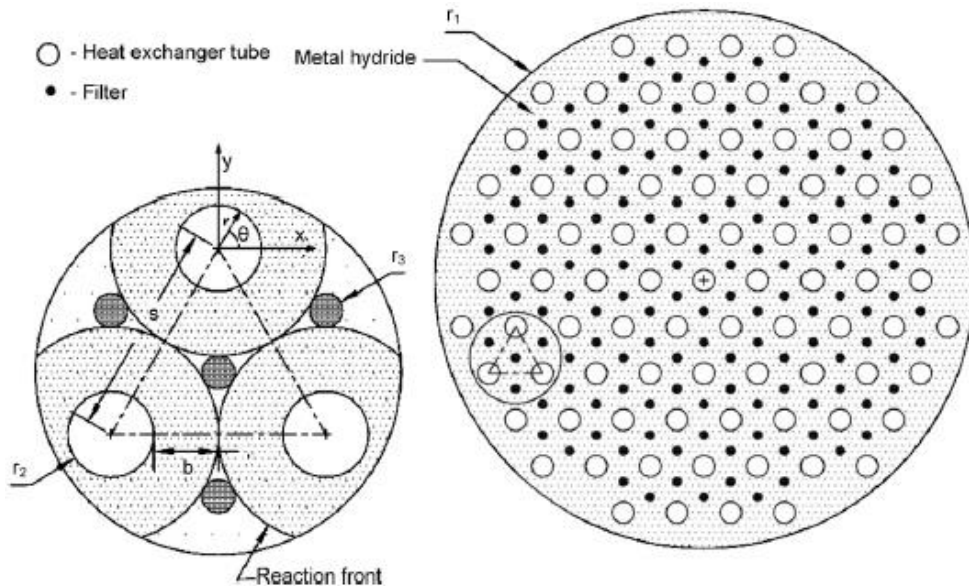


Figure 2.18. Schematic diagram of cylindrical MHT [40].



Table 2.8. The thermal-physical properties of metal hydride and hydrogen gas [40].

Parameter	LaNi <sub>5</sub>
Density of LaNi <sub>5</sub> , $\rho_s$ (kg/m <sup>3</sup> )	8200
Hydrogen Density, $\rho_g$ (kg/m <sup>3</sup> )	0.0838
LaNi <sub>5</sub> specific heat, Cps (J/kgK)	419
Hydrogen - Specific heat, Cp <sub>g</sub> (J/kgK)	14,890
Thermal conductivity of LaNi <sub>5</sub> , $\lambda_s$ (W/mK)	1.2
Hydrogen - Thermal conductivity, $\lambda_g$ (W/mK)	0.12
Porosity	0.55
Diffusivity of hydrogen, dg (m <sup>2</sup> /s)	$4.6 \times 10^{-12}$
Permeability, k (m <sup>2</sup> )	$10^{-8}$
Energy for Activation, Ea (J/mol)	21179.5
Constants (Ca)	59.187
hydride bed - Initial temperature, T <sub>0</sub> (K)	293
Hydrogen inlet pressure, P <sub>in</sub> (Bar)	8.0–15.0
Cooling media temperature, T <sub>f</sub> (K)	293–323
Coefficient of overall heat transfer, h (W/m <sup>2</sup> K)	500–1500
Bed thickness, b (mm)	10–27.5
Cooling tube diameter, d <sub>2</sub> (mm)	5–20
Ratio of container radius to pitch (r <sub>1</sub> /s)	3–7 (corresponding to N =31.163)

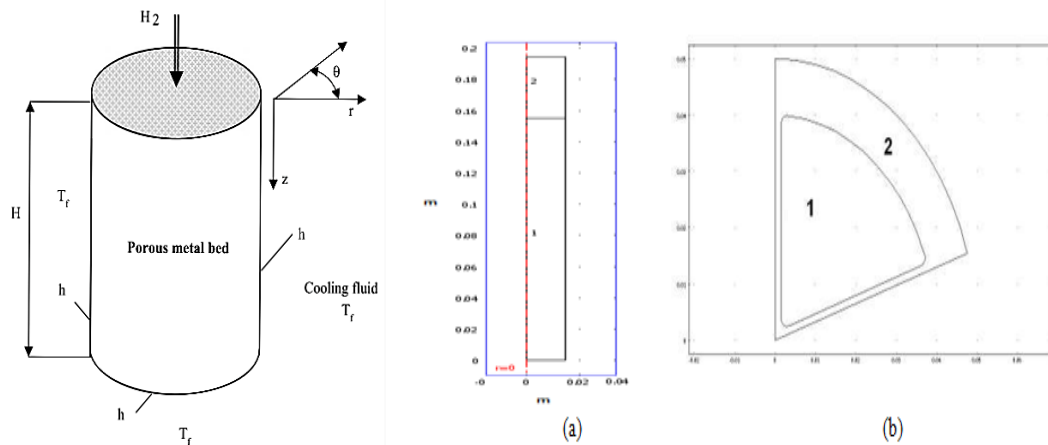


Figure 2.19. MHT modeling's [74], and [62]. (a) Geometry used in modeling MHT-1 and (b) MHT-2.

The MHTs (Figure 2.19) are simulated for 2-D metal hydride formation in the COMSOL Multiphysics software. MHT is built using a cylindrical-shaped structure that swaps heat through its external walls (bottom and sides). A free space is left for metal hydride expansion after the absorption process (approximately 20% of the total volume). Aldas et al. [74]. The model was applied to two different cylindrical geometries with/without metal fins. Figure 2.19a shows the geometry used in

modeling MHT-1 (sub-domain 1: porous media, sub-domain 2: free space) and Figure 19b shows the geometry used in modeling MHT-2 (sub-domain 1: porous media, sub-domain 2: steel wall). Baldissin et al. [62]. The parameters used in the model computations are shown in Table 2.9.

Table 2.9. The parametric values used in modeling [62].

Parameter	LaNi <sub>5</sub>
Initial temperature – absorption ( $T_0$ )	294 K
Initial temperature – desorption ( $T_0$ )	300 K
Initial pressure – absorption ( $P_0$ )	19 bar
Initial pressure – desorption ( $P_0$ )	2 bar
Initial hydride density ( $\rho_0$ )	8300 kg/m <sup>3</sup>
Density of saturated hydride ( $\rho_{ss}$ )	8354 kg/m <sup>3</sup>
Molecular weight of hydride ( $M_s$ )	426·10 <sup>-3</sup> kg/mol
Gas molecular weight ( $M_g$ )	2·10 <sup>-3</sup> kg/mol
Hydride specific heat ( $C_{p_s}$ )	355 J/kgK
Specific heat of gas ( $C_{p_g}$ )	14890 J/kgK
Hydride porosity ( $\epsilon$ )	0.5
Reaction enthalpy( $\Delta H$ )	-32600 J/mol
Reaction entropy( $\Delta S$ )	-104.5 J/mol K
Kinetic constant – absorption ( $C_a$ )	59.187 s <sup>-1</sup>
Kinetic constant – desorption ( $C_d$ )	9.57 s <sup>-1</sup>
Activation energy for absorption ( $E_a$ )	21179.6 J/mol
Activation energy for desorption ( $E_d$ )	16420 J/mol

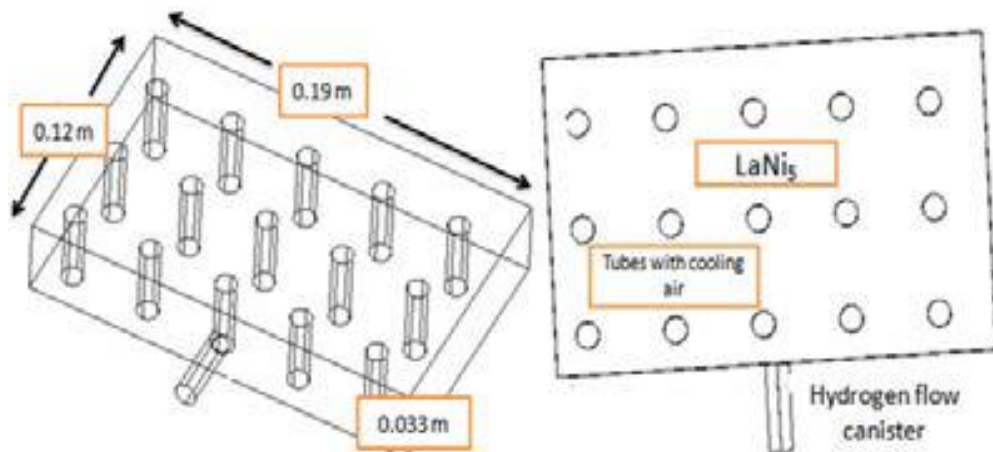


Figure 2.20. MHT geometry used in simulation [61].

Gkanas et al. [61] used the MHTs as shown in Figure 2.20, which are simulated as 3-D metal hydrides in COMSOL Multiphysics software. The model consists of three sub-domains: the perforated rectangular MHT (sub-domain 1), the cooling tubes (sub-domain 2), and the hydrogen channel (sub-domain 3). The model parameters have been shown in Table 2.10.

Table 2.10. The parametric values used in modeling [61].

Parameter	LaNi <sub>5</sub>
Density of LaNi <sub>5</sub> ( $\rho_s$ )	8300 (kg/m <sup>3</sup> )
Saturation hydride density ( $\rho_{ss}$ )	8354 (kg/m <sup>3</sup> )
Density of Hydrogen ( $\rho_g$ )	0.0838 (kg/m <sup>3</sup> )
Hydride molecular weight ( $M_s$ )	432.45 (grams per mol)
LaNi <sub>5</sub> specific heat ( $C_{ps}$ )	355 (J/kgK)
Hydrogen - Specific heat ( $C_{pg}$ )	14,890 (J/kgK)
Reaction enthalpy( $\Delta H$ )	30000 (J mol)
Reaction entropy( $\Delta S$ )	104.7 (J/mol K)
Porosity	0.5
Coefficient of heat transfer ( $h$ )	400 (W/m <sup>2</sup> K)
Hydride conductivity ( $\lambda$ )	1.32 (W/mK)

Kyoung et al. [58] used the MHT (Figure 2.21), which is simulated for 3-D metal hydride formation in computational fluid dynamics (CFD). The MHT is built using a mesh configuration of a 3-D cylindrical shape. The thermo-physical properties and operating conditions used in computations have been mentioned in Table 2.11.

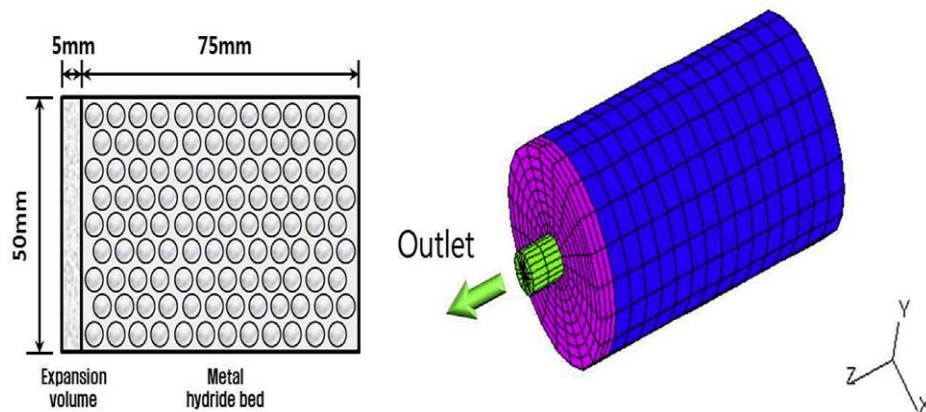


Figure 2.21. Computational domain and geometric details of MHT [58].

Table 2.11. The thermal-physical properties and operating conditions used in computations [58].

Parameter	LaNi <sub>5</sub>
Saturated metal density, ( $\rho_s$ )	5369 (kg/m <sup>3</sup> )
Hydrogen-free metal density, ( $\rho_g$ )	0.5300 (kg/m <sup>3</sup> )
LaNi <sub>5</sub> specific heat (C <sub>ps</sub> )	0.419 (kJ/molK)
Specific heat of Hydrogen (C <sub>pg</sub> )	14.890 (J/kgK)
Thermal conductivity of LaNi <sub>5</sub> (k <sub>s</sub> )	1.04 (W/mK)
Hydrogen - thermal conductivity (k <sub>g</sub> )	0.167 (W/mK)
Porosity of the metal	0.63
Reference pressure, (P <sub>ref</sub> )	10 (bar)
Metal permeability (k)	10 <sup>-8</sup> m <sup>2</sup>
Activation energy, (E <sub>d</sub> )	23.879.6 (J/mol)
Desorption rate constant, (C <sub>d</sub> )	9.57 s <sup>-1</sup>
Initial temperature of hydride bed, (T <sub>0</sub> )	20 (°C)
Inlet pressure of hydrogen (P <sub>in</sub> )	85 mbar
Heating temperature, (T <sub>h</sub> )	20 (°C)
Coefficient of heat transfer (h)	1652 (W/m <sup>2</sup> K <sup>1</sup> )

In the Table 2.12 shows the summary of numerical investigations on the MHTs in literature

Table 2.12. Summary of numerical studies on MHTs.

Investigator/Date	Geometry Used	Parameters Study	Observations
Mellouli [12] 2010	MHTs (Fig. 9)	The 2-D mathematical model is utilized using Fortran 90 to investigate the performance of MHST configurations and the influence of the fin geometry on hydriding process.	The storage time can be improved by 66% out of the time that 90% storage takes when circular fins are applied to enhance heat transfer in comparison with the situation, in which, fins aren't used; therefore, good fin geometry is significant.
	MHTs (Fig. 10).	The 2D mathematical modeling has been utilized using CVFEM for finding the effect of the proposed configurations and the results were compared with reported literature.	1- The thermal conductance is a key factor that transfers heat between the cooling fluid and the hydride material. 2- 80% improvement was recorded in storage time with finned concentric heat exchanger tube.

Table 2.12. (continued)

Investigator/Date	Geometry Used	Parameters Study	Observations
			3- Good agreement for experimental and numerical results was observed.
Mellouli [28] 2009	MHTs (Fig. 12).	The 2-D mathematical model is utilized using Fortran 90 to investigate the performance of MHST configurations and the impact of using aluminum foam.	1- Total 60% improvement was observed in the required time for 90% storage when aluminum foam was used. 2- Better performance of MHST can be achieved by combining metal foam with concentric heat exchanger tube.
Jemni [15,26] 1995	MHT (Fig. 11)	The 2-D mathematical model is utilized using MFD for investigating the geometrical impact of the tank geometry under several operating conditions on the process of absorption/desorption of hydrogen.	1- The successful heat removal design reduces the hydrogen storing time by means of good choice of operating conditions such as inlet/outlet pressure and cooling/heating temperature. 2- The tank performance improved by increasing the solid thermal conductivity and convection.
Wang [66] 2012	MHT (Fig. 13).	The 3-D mathematical model is utilized using Ansys Fluent for investigating the effect of thermal conductivity, tank geometry, and heat transfer of the stored hydrogen mass.	1- The aspect ratio of the tank (radius/height) has been observed in case of lower thermal conductivity and higher removal of heat. 2- MHT can perform better using an active cooling system as compared to the natural convection when a substance is used for enhancing thermal conductivity.
Freni [57] 2008	MHT (Fig. 14).	The 3-D mathematical model is utilized using COMSOL to recognize the important factors, which lead to improve the MHST performance.	Hydrogen supply pressure, thermal conductivity, and permeability are the key factors to optimize the MHST performance.
Freni [67] 2009	MHTs (Fig. 15).	The 3-D mathematical model is utilized using COMSOL to investigate the performance of three MHST configurations.	1- The configuration with concentric tubes and additional cooling jacket that leads to the shortest charge time.

Table 2.12. (continued)

Investigator/Date	Geometry Used	Parameters Study	Observations
			2- The metal hydride permeability and conductivity are the key factors to optimize the MHST performance.
Chung [65] 2009	MHT (Fig. 16).	The 2D mathematical modeling was utilized on COMSOL for evaluating the influence of the convection and expansion volumes.	The reaction rates reduced by the expansion volume. Heat convection performs a significant role once the expansion volume is included.
Kaplan [73] 2003	MHT (Fig. 17).	The 2D mathematical model is utilized with CVFEM to evaluate heat/mass transfer mechanisms.	The storage capacity is influenced by fluid flow and the results are very close to the reference values .
Sakti [63] 2007	MHT (Fig. 17).	The 2D mathematical model is utilized with FEMLAB to evaluate heat/mass transfer mechanisms.	The model successfully presents the hydriding behavior, which is similar to the one, which is available in the literature.
Mohan [40] 2007	MHT (Fig. 18).	The 2D mathematical modeling was utilized on COMSOL to evaluate influences of heat exchanger tubes with filters and several operating conditions, for example, heat transfer coefficient, pressure, and temperature.	The heat exchanger tube diameter with high MHST ratio and thickness of bed are major geometric parameters and offer good operating conditions.
Baldissin [62] 2009	MHTs (Fig. 19).	The 2-D mathematical model has been utilized with COMSOL to investigate the performance of MHST configurations.	Two tank geometries were examined and it was found that geometrical fins resulted in less temperature without fins (24°C rather than 30°C).
Gkanas [61] 2013	MHTs (Fig. 20).	The 3D mathematical modeling has been utilized applying COMSOL to investigate the MHST configurations.	The ambient air can be perforated on a metal hydride tank, which increased the absorption/desorption systems.
Kyoung [58] 2015	MHT (Fig. 21).	The 3-D mathematical model is utilized with the help of CFD to investigate hydrogen desorption kinetics.	1- A good agreement was found between the calculated result and values reported in the literature.

Table 2.12. (continued)

Investigator/Date	Geometry Used	Parameters Study	Observations
			2- The simulation offered a basic kind of heat/mass transfer desorption phenomena, and it also proposes a good MHT design, which is necessary for quick discharging performance.

### 2.1.3. MHT Design for Effective Heat Management

The proper design of MHT leads to a better hydrogen storage capacity. MHT, which has a better management of cooling design, confirms the shortest storing time [6,12, 15,26,28–31,33,36,40,53,54,57,58,61–63,65,66,67,69–71,73,]. In AB<sub>5</sub>-H<sub>2</sub> system, MHTs have been widely studied in different geometries and shapes in terms of hydrogen absorption/desorption, both experimentally and numerically in the literature. The sensitivity of several parameters have been studied and reported, including the MHT geometric design, configurations and/or the operating conditions are associated with hydriding process.

#### 2.1.3.1. Influence of MHTs geometry and configuration

Heat transfer mechanism in hydriding reaction is strongly influenced by MHT geometries and configurations. The summary of experimental and numerical studies on MHT design in literature is shown in tables 2.1 and 2.12. In general, the literature studies confirmed that the high temperature created in the first stage of absorption is evident for exothermic reaction. Commonly, additional hydride is formed closer to the tank walls, as a result of cooling system. Since there is an argument in the literature that the hydrogen storage process requires heat transfer management, therefore, managing MHT heat transfer is needed to improve hydriding process. Accordingly, the next review showed various MHT designs taken from the previous studies. Jemni et al. [56] experimentally and theoretically inspected kinetic and thermal attributes of the hydriding method. Simulations show good agreement with

experimental outcomes and recognize that the model can be sufficiently used for hydriding. Askri et al. [31] showed reasonable agreement between the numerical and experimental results according to their findings and the reference values given in the literature (Jemni [56]). Optimization results also indicated that almost 80% development on storing time with finned concentric heat exchanger tube. Laurencelle et al. [19] confirmed the better MHT performance by using aluminum foam. Mellouli et al. [28] presented better performance of MHT that could be achieved by combining the concentric heat exchanger tube and the metal foam. Consequently, time efficiency 60% increased while storing 90% hydrogen. The results of simulation agree with the values reported in the literature by Laurencelle et al. [19]. Kaplan et al. [73] highlighted the fluid flow impact on capacity to store hydrogen and the results confirm the previous findings by Jemni [56]. Baldissin et al. [62] proved that the configuration with fins had lesser temperature in comparison with when no fins were added (24°C rather than 30°C). Gkanas et al. [61] claimed that ambient air is present in the tubes, which improves the performance of metal hydride tank and the processes such as absorption/desorption when a traditional rectangular MHT is used. Chung et al. [36] presented a novel design to clarify heat transfer mechanism in MHTs with/without adding a heat pipe. According to results, a finned heat pipe is a useful addition for enhancing capacity to store hydrogen. More than half time reduced in case of absorption process, and 44% of the time increased at 1L/min hydrogen desorption at 10bars atmospheric hydrogen supply pressure. Wang et al. [66] demonstrated the impact of the tank aspect ratio on heat removal and thermal conductivity. They believed that MHT performs better when an active cooling system is used rather than relying on natural convection as it actively increases the thermal conductivity. Dhaou et al. [70] experimentally investigated the absorption/desorption storing time of two MHTs, with and without cooper fins. The results depicted 75% increase in the storage capacity even in a shorter storage time, and this happened because of using a finned, spiraled, and coiled heat exchange system.

In literature, heat exchangers are considered as useful technical heat management devices as a part of the MHT design. In particular, employing finned spiral tubes embedded inside MHTs can result in important progress [12,28–30,68]. Kikkinides



et al. [32,68] recognized better MHT performance that is possible by using an internal cooling tube, which resulted in 60% efficiency with respect to storing time applying the similar design with exterior cooling that shows approximately 82% improvement. Mellouli et al. [12] mentioned that heat exchanger fin geometry is a useful method to increase heat transmission from the hydride. The optimized results showed 66% improvement in storage time when circular fins were used, which means that good fins are also important besides the geometric shape of the tank. Askri et al. [31] analyzed time versus temperature change in a hydride bed using two different fin sizes. Obviously, higher temperature was noted closer to the fins, which is the evidence that the heat transfer enhanced specifically when the fin diameter was increased. The optimized results show 80% progress in storage time when a finned and concentric heat exchanger tube was used. The results obtained out of the literature show that the stored hydrogen mass improved in case of increase in the heat transfer applying various vessel designs, and when additions were done, including water coolers, and finned devices, heat pipes, ambient air blowers, concentric cooling tubes, and spiral/circular heat exchanger tubes.

#### **2.1.3.2. Influence of cooling rates with operating conditions**

As mentioned before, the reaction speed of hydrogen storage in MHTs is dependent on rate of heat removal from hydrogen storage because during the absorption process, the heat addition rate rises. Consequently, various cooling/heating configurations in literature have been utilized to extract/add heat from/to the system. Jemin et al. [56] observed that the reduction of hydrogen storing time took place in absorption/desorption processes by means of decreasing/increasing cooling fluid temperatures, respectively. Wang et al. [66] highlighted the role of cooling system for the hydriding process. Better MHT performance can be assured when active cooling is applied. Such configuration can offer up to four times improvement in heat transfer mechanism as compared to natural cooling. Jiao et al. [60] verified that upgrading the MHT performance is possible through the natural cooling that counters the heat transfer coefficient and the increasing surrounding temperature. Souahlia et al. [53] conducted an experiment to test the effect of hydrogen supply pressure on two different MHTs. They showed that the lower cooling temperature cools more

effectively in case of AB<sub>5</sub> alloy and speeds up the kinetics of the exothermic reaction. Dhaou et al. [69] have confirmed that in case of substantial temperature differences between the cooling fluid and the metal hydride leads to cool more effectively, which leads to hydride formation, and speeds up the kinetic exothermic reaction. Souahlia et al. [71] confirmed that the proper choice of the operating conditions including cooling/heating fluid temperature can improve the hydrogen storage capacity. Mellouli et al. [29] recognized the role of cooling/heating configurations on the absorption/desorption processes. For the absorption process, the heat removal takes place and the cooling leads to better storing capacity and the high value of heat transfer coefficient that reduces the storage time. Desorption rate is enhanced by the heat that is applied using a heating system. Gkanas et al. [61] confirmed that the air cooling perforated the MHT and enhanced the absorption/desorption processes. Chung et al. [36] proved that the absorption/desorption processes improvement can be achieved by employing heat pipes. Kaplan et al. [33] observed that the forced convection by cooling fluid provides maximum effective heat transfer coefficient, which cools the hydride formation and speeds up the kinetic exothermic reaction. Jemin et al. [15,26] and Chung et al. [65] confirmed that the heat transfer by convection cannot be ignored in the presence of expansion volume.

### **2.1.3.3. Influence of hydrogen inlet pressure**

Hydrogen inlet pressure is an important factor for MHT design that affects the absorption kinetics [40,53,55,57,67,69–71]. The high value of hydrogen inlet pressure leads to increase mass transfer mechanism in the hydriding process. Dhaou et al. [69] experimentally investigated the effect of hydrogen inlet pressure in an AB<sub>5</sub> MHT system, and they found better MHT performance by means of increasing the storage ability and reducing storage time. Souahlia et al. [53] confirmed that the inlet pressure enhances the mass transfer mechanism and absorption kinetics, which improves the hydrogen charging rate. Souahlia et al. [55] pointed out that increasing inlet pressure results in increasing the hydrogen storage mass, which means that 10grams hydrogen storage took 23 min at 4 bar, while it only takes 90s at 11 bar hydrogen inlet pressure. Freni et al. [57] confirmed that the absorption kinetics

improved when the hydrogen inlet pressure increased. Souahlia et al. [71] and Mellouli et al. [29] mentioned that the hydrogen inlet pressure can improve the hydrogen storage capacity, since it enhances the absorption kinetics. Souahlia et al. [55] and Kaplan et al. [72] found that the variations in the hydride formation equilibrium pressure and the hydrogen pressure supply in the presence of a designed cooling configuration lead to good MHT performance

#### **2.1.3.4. Influence of permeability and thermal conductivity**

Metal hydride conductivity and permeability are key-parameters for chemical hydrogen storage [26,28,56,57,62,64,66,67]. Jemni et al. [26,56] respectively and Wang et al. [66], recognized a better MHT performance as a result of increasing the solid thermal conductivity by adding enhance conductivity materials such as; aluminum foam. Mellouli et al. [28], presented 60% upgrading in the time required for 90% storage by use aluminum foam. Freni et al. [57], explained the relationship between gas permeability and mass transport. Low permeability leads to low gas velocity which guide to increasing saturation time. The system confirmed a decrease of MHST performance below a permeability of  $K=1e^{-13} \text{ m}^2$ . Freni et al. [67], confirm higher than ( $K>1e^{-12} \text{ m}^2$ ) permeability establish mass transfer limitations decreases of MHT performance.

## CHAPTER 3

### HYDROGEN STORAGE WITHIN HYDRIDE IN SOLID FORM

#### 3.1. HYDRIDES ALLOYS FOR HYDROGEN STORAGE

Since hydrogen is abundant, and it has the highest per unit energy; so, it has a future. Besides, it doesn't pollute the environment because hydrogen burns to form water vapors:



Hydrogen usually does not react with other chemicals at room temperature due to extremely strong bonds between the atoms in the molecule; so, it requires substantial energy for decomposing hydrogen molecules into reactive atoms. Hydrogen is extremely volatile in the form of a frozen liquid or compressed gas, and there is a risk of explosion, so special treatment is required. Table 3.1 shows the physical properties of hydrogen.

Table 3.1. Physical properties of hydrogen.

Properties	Value
Color	Colorless
State of matter	Gas
Density (at 0 °C)	0.0899 kg/m <sup>3</sup>
Melting point	-259.14 °C
Boiling point	-252.87 °C
Specific heat	14.304 J/kg K
Evaporation heat	0.447 MJ/kg
Ignition limits (% vol.)	4.1–74.0
Flame speed	2.91 m/s
Diffusion coefficient	0.61 m <sup>2</sup> /s

Several hydrogen storage options are available, which means that it is the energy of the future:

- Compressed storage of gas at 35 MPa-70 MPa
- Cooling and liquefying up to very low temperatures – 252.8 °C, and
- Solid storage in physically carbon nanotubes and hydrides.

As a result of the studies, it is clear that hydride form is the best available hydrogen storage method because it assures suitable working environments and performs at low pressures (Figure 3.1).

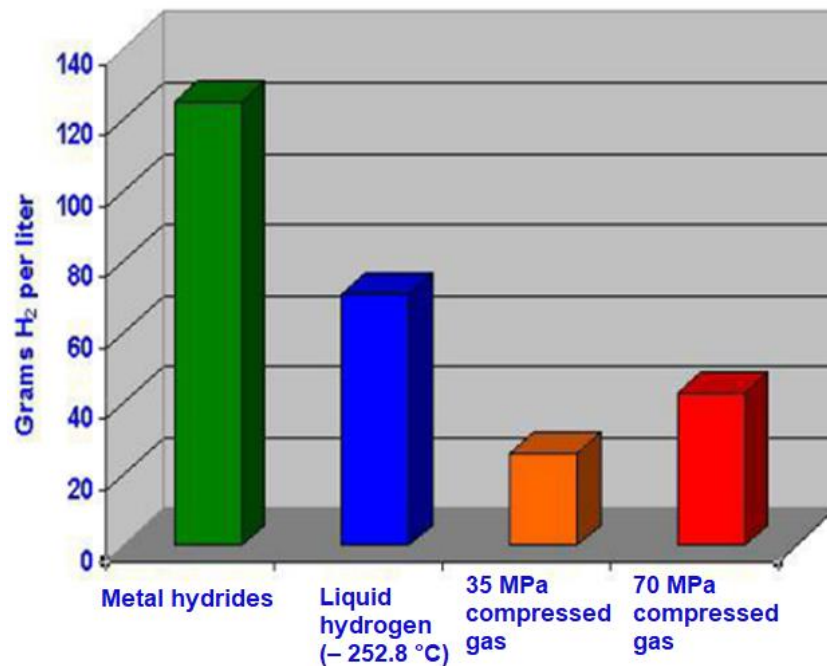


Figure 3.1. Amount of hydrogen stored in different storage methods.

Some compounds or alloys that produce after the reactions with hydrogen are called hydride. Hydrides are compounds that absorb hydrogen at a certain temperature and release the hydrogen when heated. As can be seen from the above graph, the most hydrogen can be stored with the same volume of hydride materials.

### 3.2. METAL HYDRIDES STORAGE OF HYDROGEN

Several alloys and metals reversibly react with hydrogen, which results in metal hydride formation, which can be expressed by the equation given below:



In this equation, **Me** represents a metallic or inter-metallic compound, while **MeH<sub>x</sub>** shows the hydride formation, and **x** represents the hydrogen-metal ratio. Here, **Q** means generated heat in the reaction. Eq. 3.2 shows exothermic absorption/forward reaction and endothermic desorption/backward reaction. The metal alloy used for hydrogen storage is converted into the powder form, as shown in Figure 3.2. The metal hydrides powder is put in a tank that generally has a cylindrical pressure vessel, which has application in reversible hydrogen storage; so, the alloy has to go through activation at high pressure and temperature based on the type of alloy used. This process increases the hydrogen storage capacity, and makes it maximum [75].



Figure 3.2. Metal Hydrides.

Employment of metal hydrides in energy conversion applications began to gain importance with the oil crisis in 1978. Since then, studies have been progressing towards the use of metal hydride energy technology to run cooling and heating systems on metal hydrides, especially with restrictions on the use of hydrocarbon-containing fossil fuels, and after development of metal hydride materials because they have great hydrogen storage potential including Mg<sub>2</sub>Ni and LaNi<sub>5</sub>.

### **3.3. METAL HYDRIDE MATERIAL SELECTION**

Reversible metal hydride alloys are inter-metallic compounds capable of absorbing significant amounts of hydrogen in the metal hydride form. During absorption, hydrogen atoms are dispersed and trapped in the spaces between the metal cages. In this process, molecules, which are different from the adsorption process in the metal hydride material structure, are absorbed, and make a strong bond. The most important reasons why metal hydrides are preferred in Hydrogen storage are that they can be subjected to charge/discharge processes without structural failure, eliminating the need for high-pressure vessels; therefore, high hydrogen storage rate per storage mass is assured [76].

The current section deals with metal hydride alloy families, which have been summarized to create clarity about choosing an alloy in the later part of this thesis. Hydrogen is usually bonded in interstitial positions in the alloy arrangement. The optimization of inter-metallic compounds was accomplished by material scientists who combined metals, which can absorb hydrogen (referred to as A which is rare elements: La, Mg, Ca, Ti, and Zr); however, metals can't absorb hydrogen on their own (referred to as B, which are weak hydriding elements: Fe, Co, Ni, and Mn). Common metal hydride alloy families have been described as AB, AB<sub>2</sub>, and AB<sub>5</sub> inter-metallic materials [75].

#### **3.3.1. AB Inter-metallic Compounds**

This inter-metallic compound family is referred to TiFe alloy and its replacement modifications are possible such as Ni or Mn to replace Fe. The PCT (Pressure-Composition-Temperature) can be adjusted to be familiar with the replacement of Ti and Fe elements. Hydrogen storing capacity is competitive with other families of inter-metallic compounds. They tend to have two plateaus; they have excellent cyclic stabilities at lower plateau but higher upper plateau. The upper plateau and the sensitivity to the impurities of hydrogen gas reduced the used of AB alloys [75,77].

### **3.3.2. AB<sub>2</sub> Inter-metallic Compounds**

The AB<sub>2</sub> family has wide-range versatility due to large numbers of different elements, which can substitute A and B in the alloy structures. For this reason, the AB<sub>2</sub> family is providing high degree of fine adjustment in PCT properties. The A-elements are referred to rare elements (Zr, Hf and Ti) showing different atomic numbers (57-71). The B-elements are weak hydriding elements (such as V, Cr, Mn, and Fe) having atomic numbers (23-26) [75,77].

The PCT properties for AB<sub>2</sub> can be adjusted over the range that is typically used for storage applications (1-10 atm, and 0-100 °C). The sensitivity to the impurities of hydrogen gas is showed more than AB<sub>5</sub>. Hydrogen's stored capacity has the same range with the other families of inter-metallic compounds with the exception of high temperatures and pressures, while AB<sub>2</sub> shows higher capacity as compared to AB<sub>5</sub>. Such AB<sub>2</sub> alloys have some overriding advantages as compared to AB<sub>5</sub> in terms of cost; however, the AB<sub>2</sub> production is more difficult than the AB<sub>5</sub> alloys [75,77].

### **3.3.3. AB<sub>5</sub> Inter-metallic Compounds**

Like the AB<sub>2</sub>, the AB<sub>5</sub> family has wide range versatility due to large numbers of different elements, which can substitute A and B in the alloy structures. For this reason, the AB<sub>5</sub> family is providing high degree of fine adjustment in the PCT properties. The A-elements have at least one lanthanide with atomic numbers 57-71. The B-elements are weak hydriding elements, including Al, Co, Mn, Cu, Fe, Sn, Ti, and Si [75,77].

The PCT properties for AB<sub>5</sub> can be adjusted over the range that is typically used for storage applications. Hydrogen storing capacity doesn't exceed 1.3% for reversible capacity. It seems to be costlier than the other families of inter-metallic compounds.



### 3.4 HYDRIDING REACTION AND IMPORTANT PARAMETERS

Hydriding is an exothermic reaction; therefore, when the hydrides are heated, stored hydrogen releases, this process is called de-hydriding reaction. Metal hydrides operate at low pressures such as 10-55bar, so they are safe and have high storage capacities. Hydrogen storage characteristics of some metal hydride materials are given in Table 3.2 [78]. Although some hydride alloys have high hydrogen storage properties, their use is limited due to their high recovery energy. Hydride alloys such as  $\text{LaNi}_5$  recover Hydrogen they store at low temperatures. Another problem is the low stored hydrogen mass.

The heat generated in the hydriding reaction must be effectively removed by means of a heat exchanger, and this reaction must be carried out under conditions, which allow the hydrogen to be successfully charged into high-pressure metal hydride. On the other hand, the storage system must be capable to cool down and meet the hydrogen gas required by the fuel cell.

Table 3.2. Hydrogen storage characteristics of some metal hydride materials [78].

Alloy	H <sub>2</sub> Storage Capacity %	Hydriding Pressure (Bar)	Hydriding Temperature (°C)	Reaction heat (kJ/mol)
$\text{MgH}_2$	7.6	1.0	290	-74.5
$\text{Fe}_{0.8}\text{Ni}_{0.2}\text{TiH}_6$	5.5	1.0	80	-
$\text{Mg}_2\text{NiH}_4$	3.6	1.0	250	-64.5
$\text{Ti}_{0.9}\text{Zr}_{0.1}\text{Mn}_{0.19}\text{V}_{0.2}\text{Cr}_{0.4}\text{H}_{3.2}$	2.1	9.0	20	-29.3
$\text{Ti}_{0.96}\text{Zr}_{0.02}\text{V}_{0.45}\text{F}_{0.10}\text{Cr}_{0.05}\text{Mn}_{1.5}\text{H}_{3.4}$	2.1	10.0	24	-
$\text{TiFeH}_{1.9}$	1.8	10.0	50	-23.0
$\text{TiFe}_{0.85}\text{Mn}_{0.15}\text{H}_{1.9}$	1.8	5.0	40	-
$\text{TiMn}_{1.5}\text{H}_{2.47}$	1.8	7.0	20	-28.5
$\text{Ti}_{0.8}\text{Zr}_{0.2}\text{Cr}_{0.8}\text{Mn}_{1.2}\text{H}_{3.6}$	1.8	5.0	20	-28.9
$\text{Ti}_{0.8}\text{Zr}_{0.2}\text{Mn}_{1.8}\text{M}_{0.2}\text{H}_{3.0}$	1.7	-	20	-7.0
$\text{MmNi}_{4.5}\text{Mn}_{0.5}\text{H}_{6.6}$	1.5	-	50	-4.2
$\text{LaNi}_5\text{H}_{6.7}$	1.4	-	50	-7.2

Recently, MHTs which can store high capacity of hydrogen in small volumes and provide the possibility to work at high pressures, have received great attention; therefore the scientists have focused their work on rare metal alloys. Several studies

were conducted on hydrogen storage in alloy tanks. The hydrogen storage in metal hydride reactors commonly takes place but some metals such as Mg, La, Na and Li stand out because of their impressive properties.

### **3.4.1. Equilibrium Pressure**

Thermodynamically, equilibrium pressure is the most important factor in the hydriding/de-hydriding processes in metal hydride systems. The thermodynamic behavior of metal hydrides is shown through isothermal pressure composition (P-C) hysteresis (Figure 3.3) [77]. Figure 3.3 illustrates how hysteresis is mathematically defined the hydrogen storage capacity, and plateau slope. This figure represents the equilibrium pressure (values along y-axis) which shows absorption/desorption processes at different levels of hydrogen concentration (along x-axis) at a specific and constant temperature. The upper line shows the absorption reaction, and the lower line shows the desorption reaction.

When the upper curve showed left to right change; it means hydrogen absorption in the metal hydride alloy. Figure 3.3 indicates that hydrogen (absorption/desorption) capacity has a reversible range with small change in pressure, which is referred to the plateau at the flat section of the curves but major changes in pressure make storage difficult [75]. The alloys, which have the flat plateau slope, are helpful to use hydrogen storage; therefore, the pressure variation during charging/discharging processes should be kept at minimum. Hysteresis implies the equilibrium pressure differences between absorption-desorption processes. The maximum capacity (Figure 3.3) implies the metal hydride capacity to store hydrogen at a specific operating pressure.

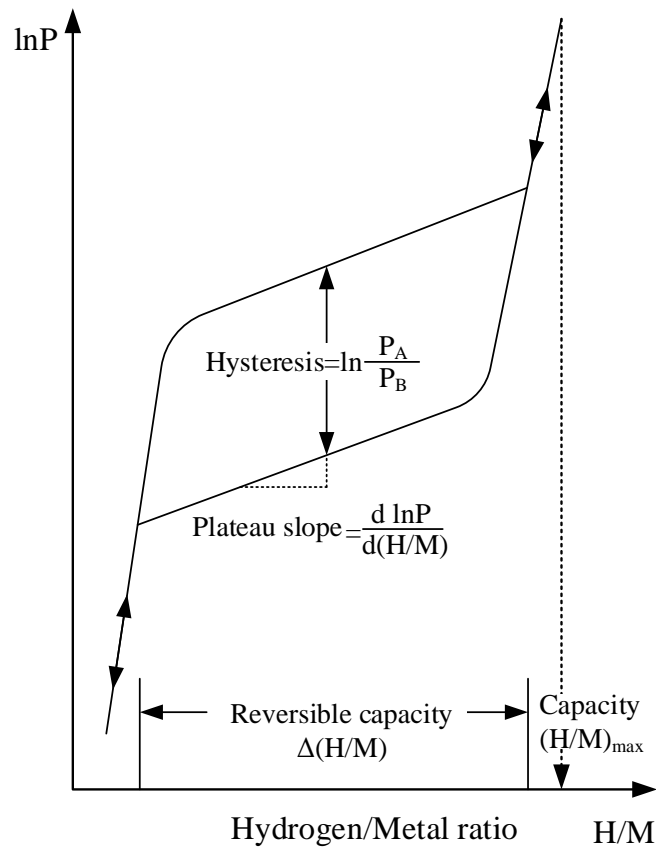


Figure 3.3. Schematic isothermal pressure-composition hysteresis loop [77].

Figure 3.3 shows the shapes that symbolize different temperatures, and they are applied to a single alloy at elevated pressures and temperatures. On the other hand, low temperatures result in low pressures, and besides, equilibrium pressure is directly proportional to the temperature, which can be mathematically expressed. Temperature control is a method that controls both absorption and desorption processes [75].

At a given hydride temperature, hydriding takes place at a system pressure more than the equilibrium pressure. Similarly, de-hydriding takes place when the pressure is lower than the equilibrium pressure but the equilibrium pressure is not the same for the hydriding and de-hydriding reactions. The equilibrium pressure of each of the hydriding and de-hydriding reactions is functionally dependent on the metal hydride temperature, entropy, and enthalpy of a reaction. It also depends on a metal hydride's kinetic properties.

Thermodynamics dictates that the equilibrium pressure in the system for the isothermal reaction process can be correlated with temperature by means of the Van't Hoff equation [77]:

$$\ln P_{eq} = \frac{\Delta H}{RT} - \frac{\Delta S}{R} \quad (3.3)$$

Here P stands for equilibrium pressure, while  $\Delta H$ ,  $\Delta S$  respectively represent changes in enthalpy and entropy. Here, T stands for the temperature while R represents the gas constant.

The heating and cooling systems' performances of metal hydride-based systems depend largely on the selected metal hydride material properties (for example, high formation enthalpy of metal hydrides to be used in these systems, high hydrogen absorbing capacity, low specific heat, fast reaction kinetics, high thermal conductivity, low hysteresis, preferable equilibrium pressures, minimum degradation, low cost after cycle operation, and simple activation process. Generally, the internal reaction kinetics of metal hydrides is relatively rapid. In the case of absorption, when the hydrogen charge above the equilibrium pressure, the reaction bed may overheat, or in case of desorption, when the hydrogen releases, the reaction pressure may fall below the equilibrium pressure, thereby causing the reactions to remain incomplete.

#### **3.4.2. Particle Distribution of Metal Hydride and Activation**

Another parameter that affects hydrogen storage in hydride reactors is the alloy grain size. Hydrogen can be stored in lattice defects and inter-atomic spaces. As the grain size decreases, the amount of Hydrogen that can be stored increases, but crystal cracking and the corrosion resistance of the alloy become problems.

First metal hydrides require activation, and then they are capable of absorbing hydrogen. During activation, the hydride is broken down into smaller particles, which increases its surface area; therefore, the absorbed regions for hydrogen atoms are also increased. Activation is repeated to expose the process, in which, the metal

hydride powders have high and low pressures and temperature in vacuum. First, 5.0 grade hydrogen is used to pressure metal hydride powder at 20 MPa gas pressure. In the meanwhile, a hydride is added to a pressurized tank, which is kept in the nitrogen bath for 4 hours at -195 °C. This is followed by heating the hydride at a temperature raised to 0.1 Pa and 100 °C. Thus, it releases a large quantity of hydrogen. Then the hydride is cooled at the ambient temperature, which accomplishes the 1<sup>st</sup> activation cycle. Then, it is repeated for three times that fully activates the hydride.

The inactivated or oxidized metal hydride particle sizes are 100µm, which is too large to absorb hydrogen. For this purpose, under repeated cycles of heating under vacuum and cooling at high pressure, the metal hydride is broken down into fine dust particles of small order sizes as 5 µm to obtain the hydride that can react with hydrogen. When the activation process is completed, the metal hydride can react with any oxidizer or air. Since the hydride contains a temporary metal, its might have up to 1000°C ignition temperature.

When the hydride formation takes place, the metal hydride undergoes voluminous expansion, for instance, the AB<sub>5</sub> has 20% greater expansion rate by volume [79]. Still, this effect at the microscopic level may not cause stress damage at the macro level. Experimental studies have shown that the actual stress seriously occurs with packing density, channel depth, absorbed quantity of hydrogen, and number of cycles [80,81]. When the studies carried out in this context were considered, it was concluded that the pulverization/condensation mechanism is widely accepted [81,82]. Initially, metal hydride powders become finer (pulverization) during a small number of hydriding/de-hydriding cycles. The fine particles then tend to fall down by gravity and fill the gaps in the bottom. This increases the packet density. When this process is repeated, self-condensation or compacting occurs.

The reaction rate for a given metal hydride material is related to the heat transfer parameters. The metal hydrides' thermal properties also depend on metal hydride temperature, hydrogen pressure, metal hydride particle size, absorbed hydrogen concentration, and porosity. Heat transfer is determined by hydride powder-cold zone wall contact resistance. It largely depends on material properties of the powder,

including the package density, particle size, and wall properties, which can be determined by considering geometry, material type, and surface roughness.

The fine metal hydride particles tend to move out with Hydrogen. The particle distribution has a small negative effect on the metal hydride reactor's performance. A fine filter or sieve of approximately  $1\mu\text{m}$  can be considered as a simple solution to protect the fine particles. The metal hydride powder bed shows a specific thermal conductivity and a typical grain size in the order of  $1\text{ W/mK}$  and  $1\mu\text{m}$ , which are very low. It has been shown to block valves by manifolds in the most severe cases [83,84]; therefore, the thermal properties can be increased, which raises the thermal conductivity of the bed. This happens when very highly porous Al foam or other Al or Cu structure is used.

Chung et al, experimentally worked on the MHT's rate of hydrogen charging and discharging using heat pipes for improving heat transfers [36]. In this study, 295 g  $\text{LaNi}_5$  was used in the tanks. The metal hydride powders were passed through 100 and 200 mesh sieves to ensure particle sizes between 75 and 150  $\mu\text{m}$ .

In metal hydride beds, hydrogen storage creates a complicated issue because it involves flow of a compressible gas from a porous medium with specific reaction kinetics and heat transfers. When charging takes place, the hydrogen gas is pressured in a porous metallic bed that absorbs its heat release during an exothermic reaction [85].

## CHAPTER 4

### EXPERIMENTAL WORK

#### 4.1. EXPERIMENTAL SETUP, DESIGN, AND PROCEDURE

Some of the machinery, equipment and consumables materials were used in Karabuk University Energy Systems Engineering Department laboratories within the scope of the project work are listed below:

- Metal hydride Storage Tanks (MHTs) were used to storage Hydrogen: three configurations of metal hydride reactors were designed and manufactured.
- Heat Pipes were fabricated and manufactured in laboratory in order to use for removal and extract out the huge heat producing in exothermic reaction from the reactor during absorption process.
- Mechanical Grinder Machine.
- LaNi<sub>5</sub> Alloy used as storage media.
- Temperature Scanner and Data Collecting System.
- Temperature Thermocouple Probes.
- Manometers and regulators.
- Control valves: Used for control purposes in gas tubes.
- Hydrogen gas installation and stainless steel tubes with a diameter  $\Phi^{1/4}$ . Hydrogen installation used to transport hydrogen between the hydrogen cylinder and test systems.
- Vacuum pump.
- Ceramic resistance heater.

All MHTs heat pipes and circulated fins are fabricated and manufactured in the energy systems department lab, Karabuk University. The hydrogen leak problem was recognized in all tanks at the treated parts during activation operation processes by

using hydrogen sensor and/or tester instrument. The leak caused variation of the activation process for all tanks. Prefabricated all the MHTs were done by using thermal glue, thermal isolated material and welding process in order to reach full activation process at all the tanks.

#### **4.1.1. Metal Hydride Tank Design**

In this thesis, we determined the reactor geometry and its impact on charging/discharging hydrogen; three configurations of MHTs were designed and manufactured, as shown in figures 4.1 and 4.2. They were made using an alloy (St-52) with internal and external dimensions 29 mm and 35 mm, respectively, and the inner height was 60 mm. Tank 1 was manufactured without using any heat pipe in order to make a comparison (Figure 4.1a). In the lab, a couple of heat pipes were manufactured combining copper and methanol. The external diameter and the heat pipe thicknesses were 6 and 1 mm, respectively but the length was 250 mm. The axis of tank 2 was where the first heat pipe was placed, as Figure 4.1b indicates. An aluminum alloy 3003 sleeve (4.5% Cu, 0.6% Mn, and 1.5% Mg) that formed thickness and inner diameter 1 mm and 6 mm, and that was linked to 30 fins, which had circular shapes and they were made using aluminum. The fins' diameter was 20 mm and thickness was 1 mm. There was 3 mm space among the adjacent fins. Around the second pipe, a sleeve was positioned on a section that was on the outer side of the tank. On the tank 3 axis, a finned heat pipe was placed, as Figure 4.1c shows. The mentioned heat pipes were sealed and linked to the MHTs.

Three thermocouple probes ( $P_1$ ,  $P_2$ , and  $P_3$ ) were used to monitor inner temperature of the hydride beds in each of the three tanks. They were placed in the tank only 5 mm away from the internal wall. The first probe ( $P_1$ ) was located at the bottom, the second one ( $P_2$ ) was located at 18 mm above the bottom, while the third probe ( $P_3$ ) was located at 24 mm from the top as Figure 1 indicates. Just  $P_2$  was an exception because it was placed at the center of the tank 1 at a similar height as other reactors had. It is shown in Figure 4.1a. On a steel sheath, all the thermocouple probes were mounted. It had 1 mm diameter that was linked to the tank wall and sealed. In addition,  $P_4$  was another thermocouple probe that has been linked to the external wall



of each tank that was 18 mm high. It helped measuring the temperature of the external surface. Another metal foil tape attached the MHTs to the probe. Two additional thermocouple probes  $P_5$  and  $P_6$  were linked to the internal bottom surface as well as to the heat pipe. In the external section of the tank, a metal foil tape was used to note the heat pipe's external surface temperature that is shown in figures 4.1b and c [85].

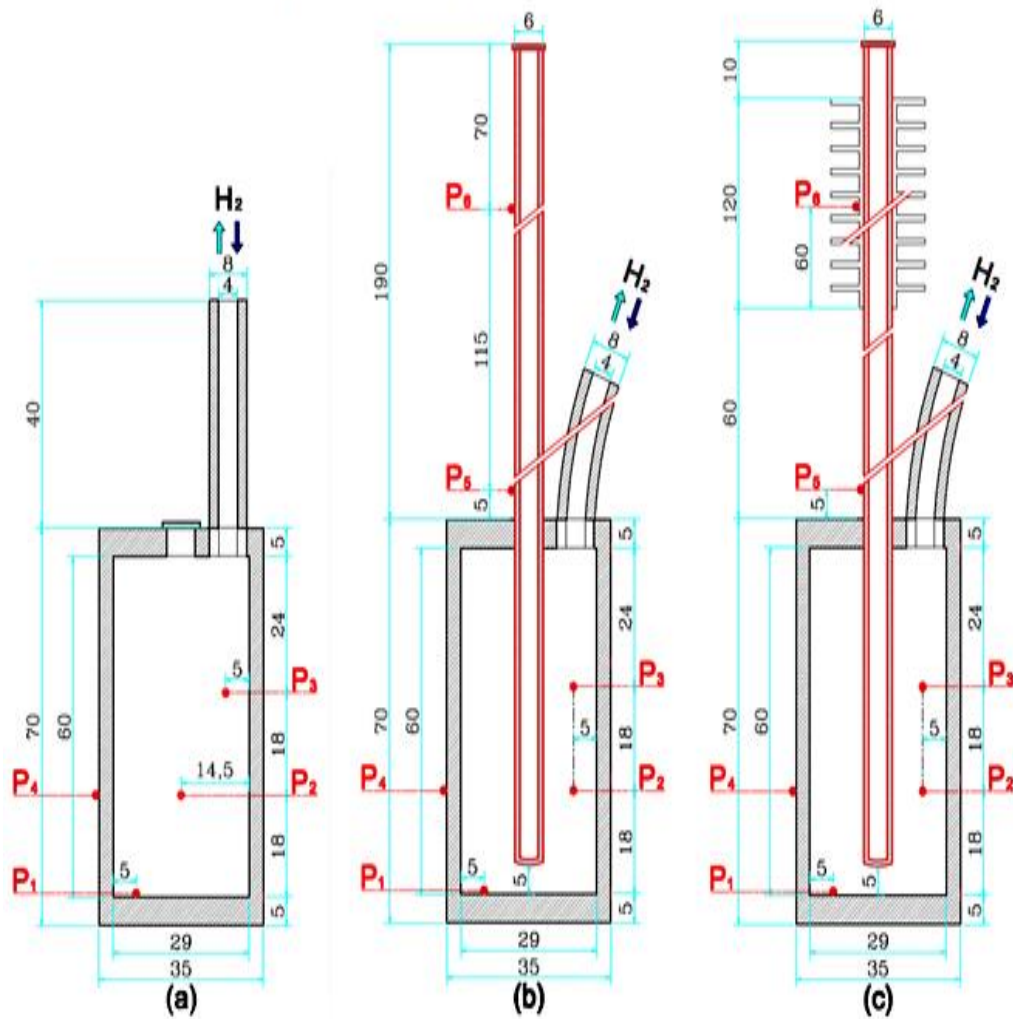


Figure 4.1. Schematic diagram of MHTs a) w/o heat pipe b) with heat pipe c) with finned heat pipe [85].



Figure 4.2. Photograph of three metal hydride tank configurations.

#### 4.1.2. Machinery and Equipment Used in Experimental Study

According to findings, the total heat extraction from the vessel in the absorption process was 59,000 J when hydride formation was 15,400 J per gram hydrogen, and the storage capacity was 1.3wt% for hydrogen [36,47,85]. When the hydrogen charge takes 20 minutes, the total extracted heat from the reactor (absorption process) will be 50 W. Under such design conditions, we need a heat pipe with more than 50 W heat rate capacities. For meeting such requirements, a copper-menthol heat pipe was used with 45% menthol filling ratio [86]. The required numbers of heat pipes for this study were fabricated and manufactured at the Energy Systems Department Lab, Karabuk University. The outer thickness and diameter of the heat pipe were respectively 1 mm and 6 mm, while its length was 250 mm as Figure 4.3 shows. The characteristics of heat pipe include thermal resistance ( $R$ ) that exists between the evaporating sites and the heat pipe at the heat transfer rate ( $Q$ ). The menthol thermal resistance was found to be 0.51, 0.52 and 0.63 °C/W at vertical, 45° inclined, and

horizontal orientation, respectively, as Figure 4.4 indicates. It can be interpreted by saying that using methanol (working fluid) lowers the surface tension as compared to water by one-third. Menthol has higher saturation pressure, which affects the spatial dynamic pressure perturbations to minimize gravity and its impact on the vapor-slug system [85].

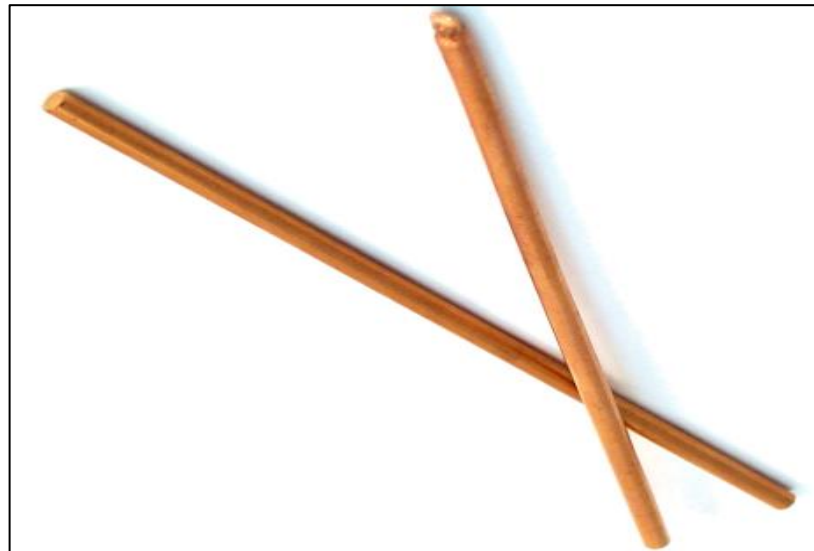


Figure 4.3. Laboratory Manufactured Heat Pipe.

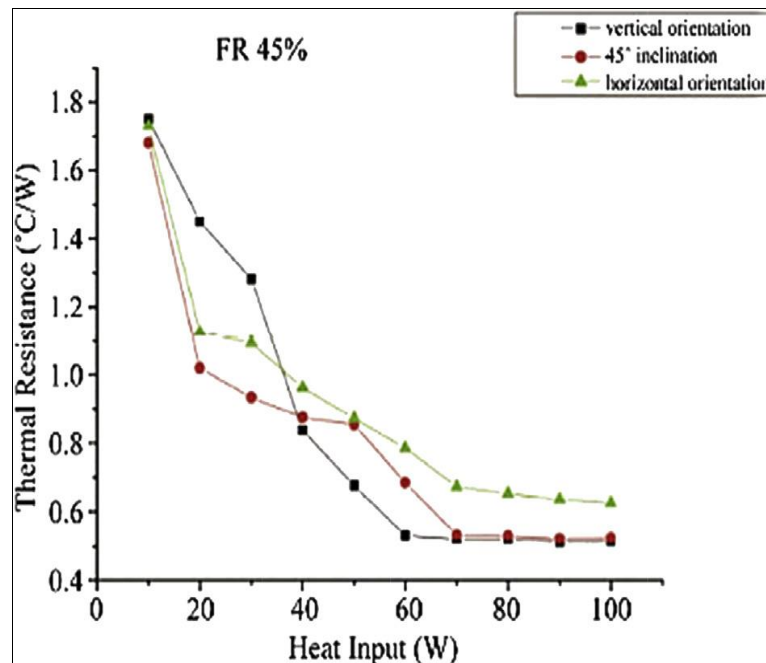


Figure 4.4. Characteristics of the heat pipe [86].

A data collection system (German Pico thermocouple data logger TC-08) and temperature scanner were applied for measuring and recording temperature values by means of thermocouples placed at different coordinates' channels of the hydrogen storage reactor (Figure 4.5).



Figure 4.5. Data Collection System (Pico thermocouple data logger TC-08).

We used thermocouple probes (Type K, Beijing Sheng RuiKe Automation Equipment Co., Ltd, China) for measuring the distribution of temperature in the hydriding process (Figure 4.6).



Figure 4.6. K-type thermocouples.

We used a mechanical grinder (Planetary Mono Mill PULVERISETTE 6 classic line, FRITSCH, Germany) for grinding the metal hydride material according to the required size (Figure 4.7).



Figure 4.7. Photo of the Mechanical Grinder Machine.

LaNi<sub>5</sub> alloy was used as a storage media for the hydrogen storage process (Figure 4.8).



Figure 4.8. LaNi<sub>5</sub> alloy.

Manometers and regulators (200 Bar / 15 Bar): used to adjust the hydrogen charge pressure to the desired values. Control valves: used for control purposes in gas installation. Stainless steel tubes with a diameter  $\Phi 1/4$ . Hydrogen installation used to transport hydrogen between the hydrogen cylinder and test systems (Figure 4.9).

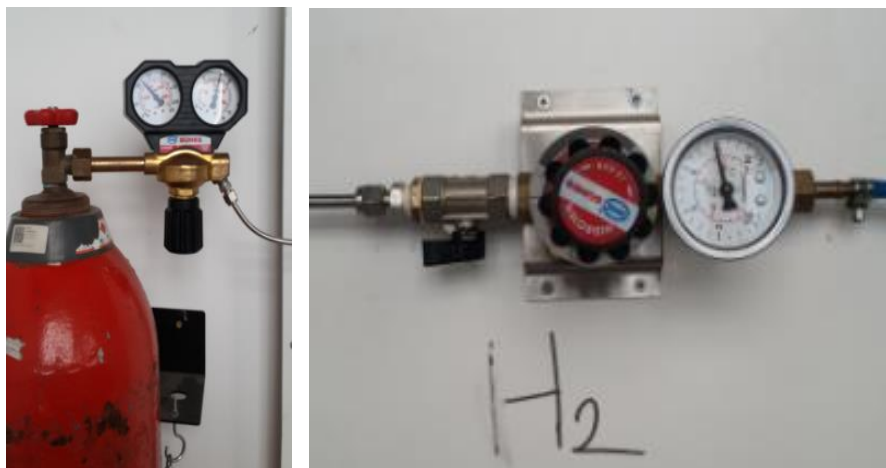


Figure 4.9. Hydrogen charge pressure (10 Bar) where the absorption process takes place.

Vacuum pump (Value - VE135 N, China) was used for removing the moisture and the air inside the reactor before initiating the experiment (Figure 4.10).



Figure 4.10. Vacuum pump.

We used a specific ceramic resistance heater (RASAK ISI 230 V, 1200 W, made in Turkey) to evaporate the moisture but the air stayed in the reactor (Figure 4.11).



Figure 4.11. Ceramic resistance heater.

We also used a weight balance machine (Danlab, EWseries, EW600-2M, accuracy 0.01) for measuring hydrogen storage mass (Figure 4.12).



Figure 4.12. Analytical weight balance machine.

In addition, we also used a laptop computer to analyze and display the results.

### 4.1.3. Experimental Set-up

Figure 4.14 showed the schematic image of the experimental tools. The experimental setup is arranged so as to determine reaction speed, hydrogen storage quantity, and absorbing features of a metal hydride  $\text{LaNi}_5 - \text{H}_2$  system. In the assembly; a design tank, a mechanical grinder machine with steel balls for producing metal hydride particles, a ceramic resistance heater to evaporate moisture and remove air from the tank, a vacuum pump for moisture and air removal from the reactor before experimentation, temperature thermocouples for measuring hydriding temperature distribution, pressure manometer for controlling hydrogen inlet pressure, an adjustment regulator to adjust the pressure of hydrogen, a laptop system for analysis and showing experimental results, data collecting system, a tank containing hydrogen with 99.999% purity. In experimental studies, three tank configurations (as mentioned above) pertaining to tank design were used for each experiment.

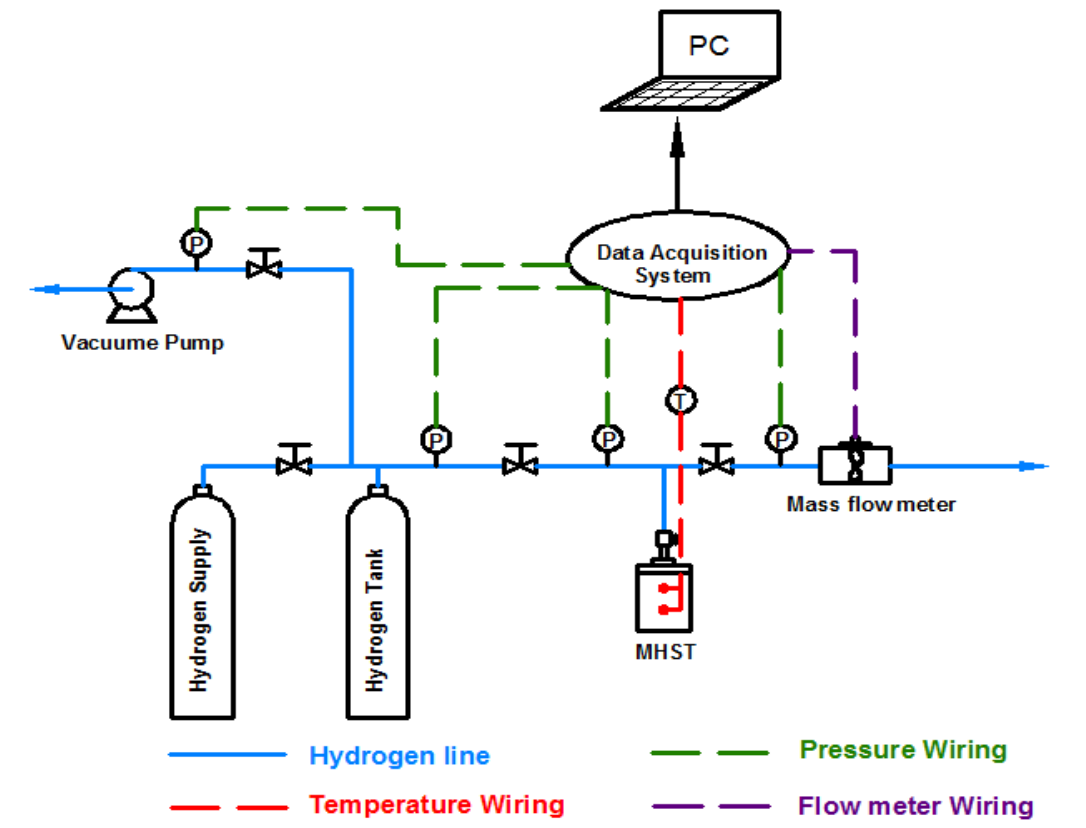


Figure 4.13. Schematic diagram of the experimental setup.



#### 4.1.4 Experimental Procedure

First, the LaNi<sub>5</sub> alloy was grinded for two hours at 600 rpm in a mechanical grinder for powder production with 10-50 μm size. 120 g LaNi<sub>5</sub> in powdered form was then 60 vol% filled in every reactor. The leftover 35 vol% space was kept free, and only 5% was occupied by the inner heat pipe. Then, the reactor was adjusted at the required level of ceramic resistance with the help of a vacuum pump at only 0.01 bar pressure, which was connected to the hydrogen tank adjusting the pressure at 8 bars for activation process. After that, the tank heated within the temperature range of 350-450 °C, and low-pressure vacuuming was continued for 25 min. During activation, charging and discharging processes were repeatedly conducted for over 20 cycles. It was continued until reach the maximum hydrogen storage capacity (1.3wt%). After the metal hydride activation, the reactor was cooled down at room temperature, and then, the experiment of hydrogen charging was conducted for 5000s. In the MHTs, the temperature was monitored by using thermo-couple probes. Then, sensitive scales and temperature scanner were linked to the laptop using the data cables. At different inlet pressures (2-15 bars), hydrogen charging pressure was controlled using a pressure regulator. In each tank, all the mentioned actions were performed, starting with the tank that had no heat pipe. When the absorption started, inner temperature of the reactor first increased since the reaction was exothermic. It progressively decreased with reducing reaction kinetics. For studying the hydrogen input pressure and its effect on the internal temperature, we conducted the hydrogen absorption experiment maintaining different pressures (from 2 to 15 bar). In this case, the natural convection coefficient remained 8 W/m<sup>2</sup>K while the ambient temperature was 20 °C. After conducting experiments on the tank with no heat pipe, we repeated the same experiment with the tank that had a heat pipe and repeated the experiment with the tank that had a finned heat pipe keeping the experimental conditions similar. Thermal imaging camera photos for the three designed tanks were taken during each experiment in order to compare the thermal temperature of each reactor to the temperature recorded in experimental work.

It was given that the K-type thermocouples had accuracy levels ±0.5 °C. The MHTs were equipped with a cylindrical container for exchanging heat from side and bottom

surfaces. Every one of the mentioned tanks contained 120 g LaNi<sub>5</sub> powder, which was used as a storage medium comprising 60 vol% of the reactor and it was hydrogen-charged. The metal hydride has expansionary tendencies; so some free space was left for possible expansion of metal hydride when the hydrogen absorption is carried out. For this study, the powder size was 10-50 μm. A filter (0.5 μm graded tubular filter) was attached to the inlet and outlet tubes for preventing the spillage of metal powder when the discharging process is carried out.

#### 4.1.5. Uncertainty Analysis

It is a necessary engineering process, which is part of almost all the critical engineering projects. The fidelity issue is countered by uncertainty analysis in different experimental phases; starting from planning to reporting phase. The range of different errors is termed as uncertainty that has a probability and range. Moreover, uncertainty can also be assessed through standard deviation [54]. When errors are minimized, so that the leftover errors are random, at that point, it is possible to conduct statistical analysis. If N shows quantity measurement x, the individual readings' mean  $x_m$  can be expressed as follows:

$$x_m = \frac{\sum_{i=1}^N x_i}{N} \quad (4.1)$$

Here,  $x_m$  stands for the arithmetic mean of measurements. We calculated uncertainty using sensitivity and standard deviation using the equations given below:

$$S = \sqrt{\frac{1}{N} \sum_{i=1}^N (x_i - x_m)^2} \quad (4.2)$$

$$a = \frac{1}{\sqrt{N}} \quad (4.3)$$

$$U = \sqrt{\sum_{i=1}^R a_i^2 \cdot S_i^2} \quad (4.4)$$

Here  $a$  stands for sensitivity,  $S$  represents standard deviation, and  $U$  means uncertainty. In this case, standard deviation helps estimating the average uncertainty levels linked with  $N$  measurements. Table 1 gives the details of the uncertainty analysis. Both stored hydrogen and the temperature exhibit good stability for different configurations under different values of pressure.

Table 4.1. Uncertainty analysis of absorbed hydrogen and temperature with/without heat pipe at varying charging pressures [85].

Pressure (bar)	MHT <sub>1</sub> (with finned heat pipe)		MHT <sub>2</sub> (with heat pipe)		MHT <sub>3</sub> (without heat pipe and fin)	
	Temperature (°C)	Stored H <sub>2</sub> (g)	Temperature (°C)	Stored H <sub>2</sub> (g)	Temperature (°C)	Stored H <sub>2</sub> (g)
2	±0.143	±0.0734	±0.093	±0.0753	±0.079	±0.1096
4	±0.183	±0.0671	±0.096	±0.0709	±0.089	±0.1035
6	±0.208	±0.0625	±0.128	±0.0650	±0.132	±0.0984
8	±0.206	±0.0573	±0.125	±0.0592	±0.136	±0.0920
10	±0.222	±0.0542	±0.148	±0.0560	±0.146	±0.0846
15	±0.192	±0.0537	±0.160	±0.0549	±0.172	±0.0812

## CHAPTER 5

### SIMULATION OF THE HYDRIDING PROCESS

#### 5.1. DEVELOPMENT OF MATHEMATICAL MODEL

Figure 5.1 shows the typical MHTs geometries discussed in the simulation studies. The current study discusses the performance of MHT keeping in view its major aspects such as time and storage capacity for three different sample MHTs. We used  $\text{LaNi}_5$  powder as a media for storage. a) Tank with no heat pipe, b) tank equipped with a heat pipe, c) tank equipped with a finned heat pipe.

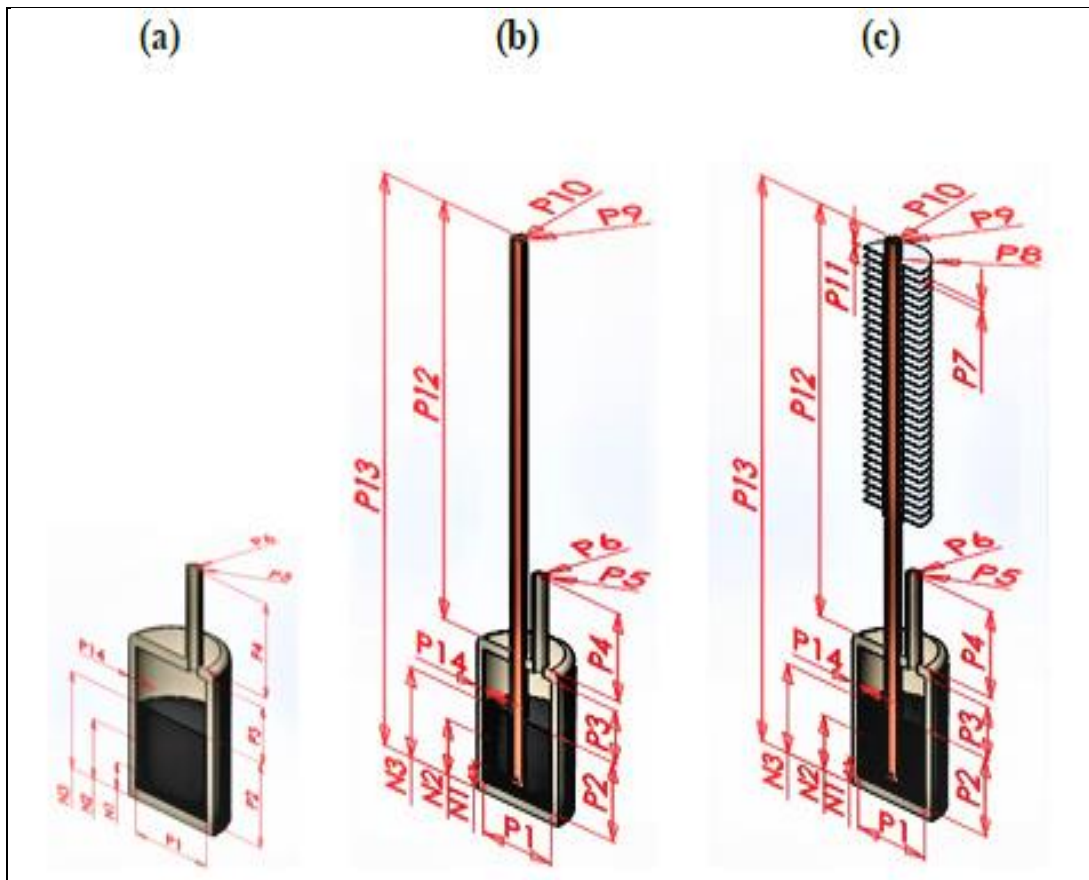


Figure 5.1. Geometries of the MHTs used in modeling and simulation: a) MHT using natural convection, b) MHT equipped with a heat pipe in the center, c) MHT with finned heat pipe.

Hydrogen is charged from the inlet tube during the storage operation at a certain pressure and is absorbed by metal hydride atoms and meshes associated with a chemical reaction, while the heat released is discharged from the system through the heat pipe and cooling fins. If the heat generated during the reaction is not removed from the system, the temperature will rise and all the reactors performance will decrease and may cause structural deterioration. Therefore, accurate and stable cooling of the system is of great importance. Since the reaction conditions will vary according to the metal hydride material to be used, optimum wing geometry will vary.

During the absorption, the metal hydride reacts with the hydrogen charged in the tank to form a porous media. Process, Hydrogen reacts with metal hydride by filling into the gaps in this porous structure. The metal hydride releases heat in order to be able to combine with hydrogen during the reaction and this heat is removed from the system by the heat pipe and fins and transferred to the coolant media.

## 5.2. CHEMICAL REACTIONS FOR METAL HYDRIDE POWDER

Several alloys and pure metals reversibly react with hydrogen. It forms metal hydrides, so the following reaction takes place:



In this equation,  $MeH_x$  is a hydride,  $Me$  stand for a metal/inter-metallic compound,  $x$  means hydrogen-metal ratio, and  $Q$  represents generated heat. The hydrogen-LaNi<sub>5</sub> reaction is given below:



When the absorbed hydrogen mass is deduced with respect to volume and time ( $m_{abs}$ ) and  $Q$  is the heat released, we can develop the mathematical model applying COMSOL Multiphysics™ for evaluating the mass transfer and the transient heat

using a tank consisting of cylindrical metal hydride. This kind of model can predict the time-variations and the hydrogen mass, which can be stored because it is proportional to effective thermal conductivity of the hydride aspect ratio of the cylindrical tank, and thermal boundary conditions.

The hydrogen release and absorption modeling pertaining to a metal hydride require complex modeling approach. In order to approach the real situation and associate the model with experimental data, it is necessary to evaluate and solve multiple physical equations [15,16,26]. Besides, the relations of these equations with each other should be correctly modeled and their compatibility with the solver algorithm should be considered. The main approaches that should be applied are:

- Modeling of free flow of hydrogen by Navier-Stokes momentum equations,
- Solving the flow of hydrogen in the porous structure by Darcy equation,
- Modeling of chemical reaction and heat generated,
- Conventional and conductive heat transfer models between the reactor and the cooler.

Since the nature of mass transfer and coupled heat are complex, it is possible to consider basic assumptions for the hydriding process to obtain governing equations, which are as follows:

- The shape of the storage tank is cylindrical with length  $Z$  and radius  $R$ . It is filled with a metal hydride powder to a certain level, and it absorbs hydrogen at a certain temperature and pressure.
- From the thermodynamic perspective, hydrogen is an ideal gas.
- There is local-thermal and gas-solid equilibrium.
- There is negligible dissipation.
- The metal hydride has uniform and homogenous permeability and porosity.
- Van't Hoff equation employed to calculate equilibrium gas pressure, neglecting hysteresis and plateau inclination of the real pressure/concentration isotherms.

- Constant thermo-physical properties exist during the hydriding/dehydriding process.
- There is negligible radiation heat transfer.
- There is negligible advection transport.

Based on the given assumptions, we solved the equations of heat diffusion, mass balance, and mass absorption for a specific hydride - LaNi<sub>5</sub>. The model for hydrogen storage has been used as a basic typical mathematical model for cylindrical reactors shown below [87–90]:

### 5.3 GOVERNING EQUATIONS FOR FLOW AND HEAT TRANSFER

Initialize  $T_m$ ,  $T_g$ ,  $\rho_s$ , and  $X$  at the cylindrical tanks (metal hydride was filled in the tank).

For Absorption; Concentration  $x$  is minimum, let's say 0.1. Density ( $\rho_s$ ) of solid (Metal) in kg/m<sup>3</sup>,  $T_m$  and  $T_g$  are metal and gas temperatures in C° during time interval  $t=0$  second (taking atmospheric temp).

For Desorption; Concentration  $x$  is maximum, let's say 0.9. Density of the solid is saturated density (Metal density + Hydrogen density).  $T_m$  stands for metal temperature while  $T_g$  means gas temperature at time  $t = 0$ .

Using Van't Hoff equation, calculate the equilibrium pressures ( $P_{eq}$ ) at the corresponding tanks of the time ( $t$ ) = 0.

$$P_{eq} = 10^5 \exp \left[ \frac{\Delta H}{R_u T} - \frac{\Delta S}{R_u} + (\phi \mp \phi_0) \tan \left[ \pi \left( \frac{x}{x_f} - \frac{1}{2} \right) \right] \mp \frac{\beta}{2} \right] \quad (5.3)$$

Where,  $\Delta H$  (enthalpy) and  $\Delta S$  (entropy) of reaction,  $R_u$  (a universal gas constant).  $\phi$ ,  $\phi_0$  and  $\beta$  are the slope and hysteresis factors (Obtained from experimental data).

Find the mass of hydrogen transfer by using the following kinetic expression for both absorption and desorption [65],

For absorption process:

$$m = C_a \exp\left(\frac{-E_a}{R_u T}\right) \ln\left(\frac{P_s}{P_{eq}}\right) (\rho_{ss} - \rho_s) \quad (5.4)$$

For desorption process:

$$m = C_d \exp\left(\frac{-E_d}{R_u T}\right) \ln\left(\frac{P_{eq} - P_d}{P_{eq}}\right) \rho_s \quad (5.5)$$

Where,  $m$  (mass of hydrogen absorbed/desorbed in a given time per unit volume ( $\text{kg/s} \cdot \text{m}^3$ )),  $C_a$ ,  $C_d$  and  $E_a$ ,  $E_d$  (reaction rate constants and activation energies during absorption and desorption processes (Calculate from Arrhenius Eq.)).  $P_s$  and  $P_d$  = (supply and delivery pressure (bar)).

The absorption of hydrogen takes place when the equilibrium pressure becomes equal to the supply pressure. First, the absorption rate is substantially high because of larger driving force ( $P_s/P_{eq}$ ). Similarly, desorption happens when the equilibrium pressure becomes equal to the delivery pressure.

Substituted ( $m$ ) in the Energy equation to find the temperature in the tank; the hydrogen (gas) and hydride powder (solid) are in thermal equilibrium as per assumptions,

$$(\rho C_p)_e \frac{\partial T}{\partial t} + (\rho C_p)_g \vec{u} \cdot \nabla T = \lambda_e \nabla^2 T - m \left[ \frac{\Delta H}{M_g} - T(C_{p_g} - C_{p_m}) \right] \quad (5.6)$$

If we just consider heat conduction in gas and solid phases, the expressions for thermal conductivity and effective specific heat will be as given below:

$$(\rho C_p)_e = (\varepsilon \rho C_p)_g + ((1 - \varepsilon) \rho C_p)_m \quad (5.7)$$

$$\lambda_e = \varepsilon \lambda_g + (1 - \varepsilon) \lambda_m \quad (5.8)$$



Where,  $C_p$  (specific heat) and  $\lambda_g$  (thermal conductivity) and  $\varepsilon$  denote hydride porosity.

Hydride mass balance in the tank,

$$(1 - \varepsilon) \cdot \frac{\partial(\rho_s)}{\partial t} = m \quad (5.9)$$

Hydrogen mass balance in the tank,

$$\varepsilon \frac{\partial(\rho_g)}{\partial t} + \nabla(\rho_g \vec{u}_g) = m \quad (5.10)$$

Density of hydrogen gas is calculated using the *perfect gas law*:

$$\rho_g = \frac{P_g \cdot M_{H_2}}{R_u T} \quad (5.11)$$

From Momentum equation, the velocity in the porous bed is obtained by using Darcy's law,

$$\vec{u}_g = -\frac{K}{\mu_g} \nabla P_g \quad (5.12)$$

Here,  $K$  represents solid permeability while  $\mu_g$  represents dynamic gas viscosity. The Kozeny Caman's equation is used to calculate the solid permeability.

$$K = \frac{dp^2 \varepsilon^3}{180 \cdot (1 - \varepsilon^2)} \quad (5.13)$$

Substitute the equations (9),  $\rho_g$  and (10),  $u_g$  in the hydrogen mass balance equation,

$$\left(\frac{\varepsilon M_g}{R_u T}\right) \frac{\partial P_g}{\partial t} + \left(\frac{\varepsilon M_g P_g}{R_u}\right) \frac{\partial}{\partial t} \left(\frac{1}{T}\right) - \frac{K}{\nu_g r} \frac{\partial}{\partial r} \left(r \frac{\partial P_g}{\partial r}\right) - \frac{K}{\nu_g} \frac{\partial}{\partial z} \left(\frac{\partial P_g}{\partial z}\right) = m \quad (5.14)$$

Update the concentration and density of solid using the above parameters for the first time step at tank A.

### 5.3.1. Initial and Boundary Conditions

In the beginning, solid and gas had the same temperatures. On the other hand, the hydride density and pressure were considered as constants.

$$T_s = T_g = T_0$$

$$P_g = P_0$$

$$\rho_s = \rho_0$$

The storage tank's outer boundary is considered as adiabatic.

$$\frac{\partial T(r_0)}{\partial r} = 0$$

According to the assumptions, a porous filter just lets hydrogen transfer to happen. No heat transfer took place from the porous filter; so the pressure of the gas is constant during the process; so it equals the hydrogen supply pressure; so:

$$\frac{\partial T(r_i)}{\partial r} = 0$$

$$P_g(r_i, t) = P_s$$

Therefore:

$$\rho_{m,A}(z, r) = \rho_{ss}^*; \quad T_{m,A}(z, r) = T_{g,A}(z, r) = T_H; \quad X_A(z, r) = X_{\max,A}$$

Left and right side of the boundary conditions;

$$\frac{\partial T}{\partial r}(z, r, t)_{z=0} = 0;$$

$$\frac{\partial T}{\partial r}(z, r, t)_{z=Z} = 0$$

Bottom boundary:

$$P_g(z, r_i, t) = P_g \quad \frac{\partial T}{\partial z}(z, r, t)_{z=0} = 0$$

Top boundary (mixed convective condition);

Heat transfer fluid temperature in the axial direction is assumed as constant.

$$-\lambda_e \frac{\partial T}{\partial r}(z, r_o, t) = h (T_{z, r_o, t} - T_c) \quad (5.15)$$

Here,  $h$  is the heat transfer coefficient represented the heat transfer through the walls and  $T_c$  is the cooling fluid temperature.

Update the concentration, density of metal for the next time, and go to the beginning at the initialization state to find the new equilibrium pressure, mass of hydrogen absorption/desorption and tank temperature.

### 5.3.2. Creating a Finite Element Solver Model

COMSOL Multi-physics software was used for solving partial differential equations given in the mathematical model applying the finite element method (Figure 5.2). System parameters, which were defined as fixed in the model, were determined, functions and correlations outside the differential equations were defined as system variables, and measurement probes were defined at some points in order to find the results. At these points, where measurement probes are defined, equilibrium pressure, hydrogen mass change and temperature in different regions of metal hydride can be monitored. Finite element density is also defined as parametric.

Mesh is formed according to the finite element principle of the modeled system. Particularly smooth meshes, which form the mid-volume of the system, and the corresponding meshes are defined. This information is stored parametrically in the modeled system. The continuity of the dimensions of the mesh elements in different regions is very important for the modeling and solution of the system. Figure 5.3 shows the mesh screen, and the Figure 5.4 showed the mesh structure.



Figure 5.2. Software and revision information used in simulation study.

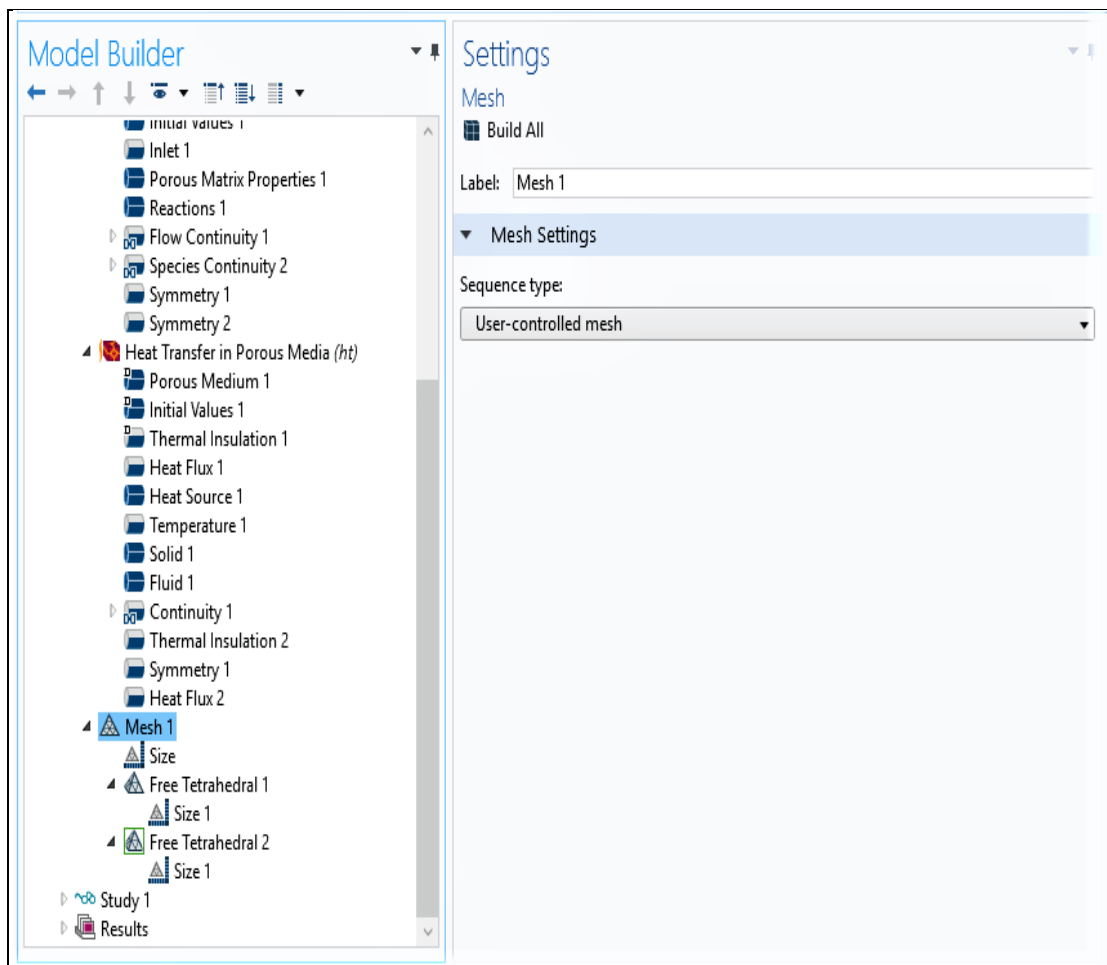


Figure 5.3. Modeling work - Mesh screen.

The modeled hydrogen storage vessel is a steel cylindrical tank with inner and outer diameter dimensions 29 mm and 35 mm, respectively, and the inner height was 60 mm. A three-dimensional ax-symmetric geometric model is shown in Figure 5.4. Six type K thermocouples are distributed along the axial and radial directions to monitor the variations of temperature in the tank, we chose three monitoring points coordinated as  $TC_1$  (5.1 mm),  $TC_2$  (17.9 mm), and (35.8 mm) as shown in Figure 5.1. There are 17268 triangular elements in the model see Figure 5.4.

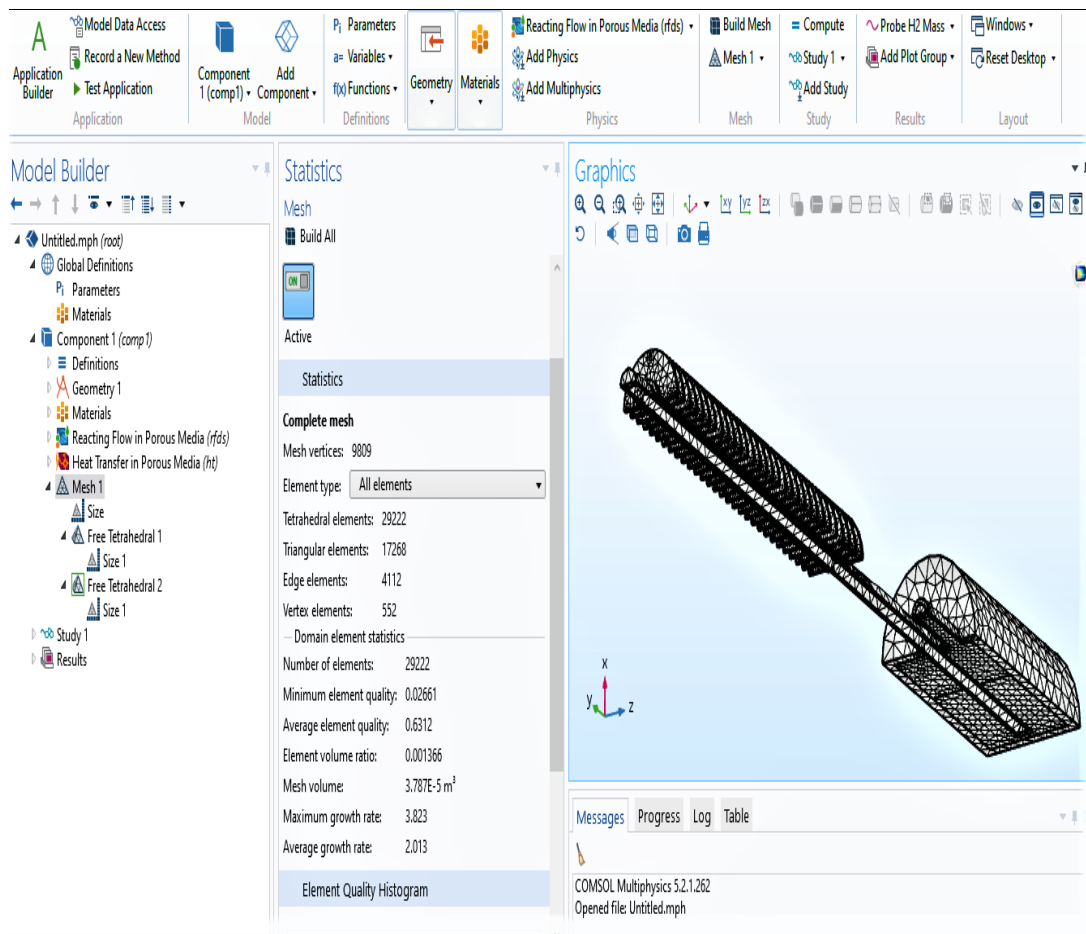


Figure 5.4. Mesh Structure.

Graphs of changes in temperature, and absorbed  $H_2$  amount obtained in the process of absorption for cylindrical volume reactor model over time are given in Figure 5.5 and Figure 5.6 for a finned heat pipe reactor for example. The distances of the three thermocouples ( $TC_1$ ,  $TC_2$ , and  $TC_3$ ) given the temperature change are 5.1 mm, 17.9 mm, and 35.8 mm respectively as shown in Table 5.1.

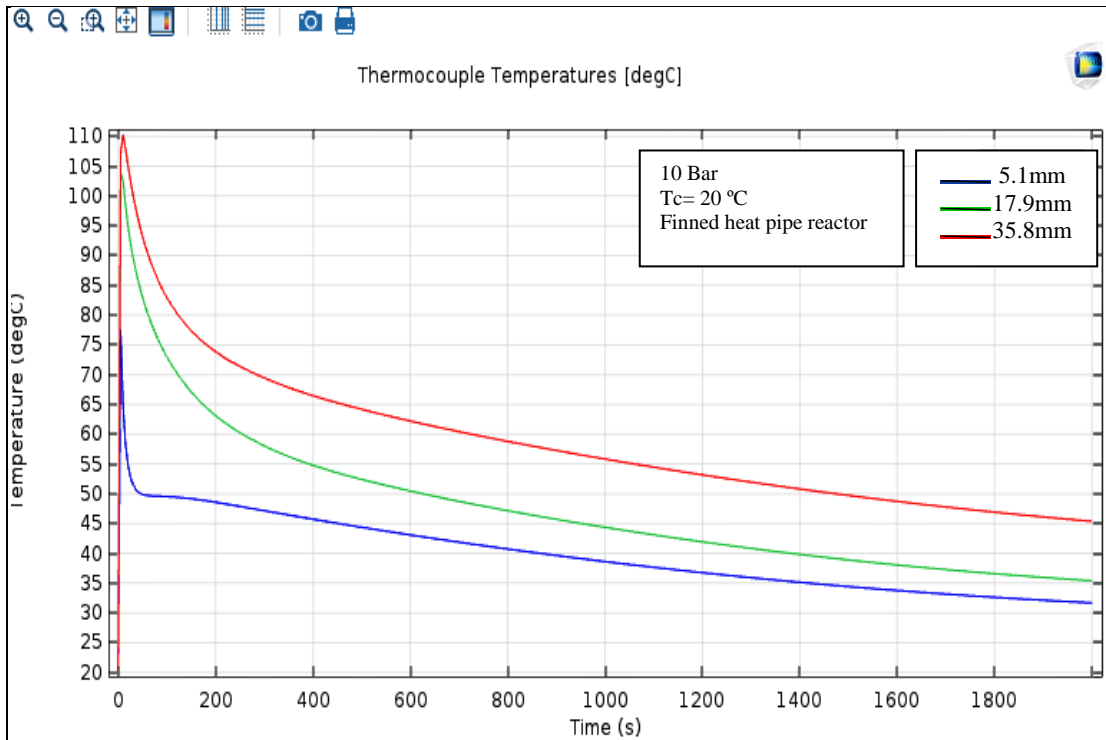


Figure 5.5. Temperature change graph obtained during the absorption process - Three thermocouples placed in different locations.

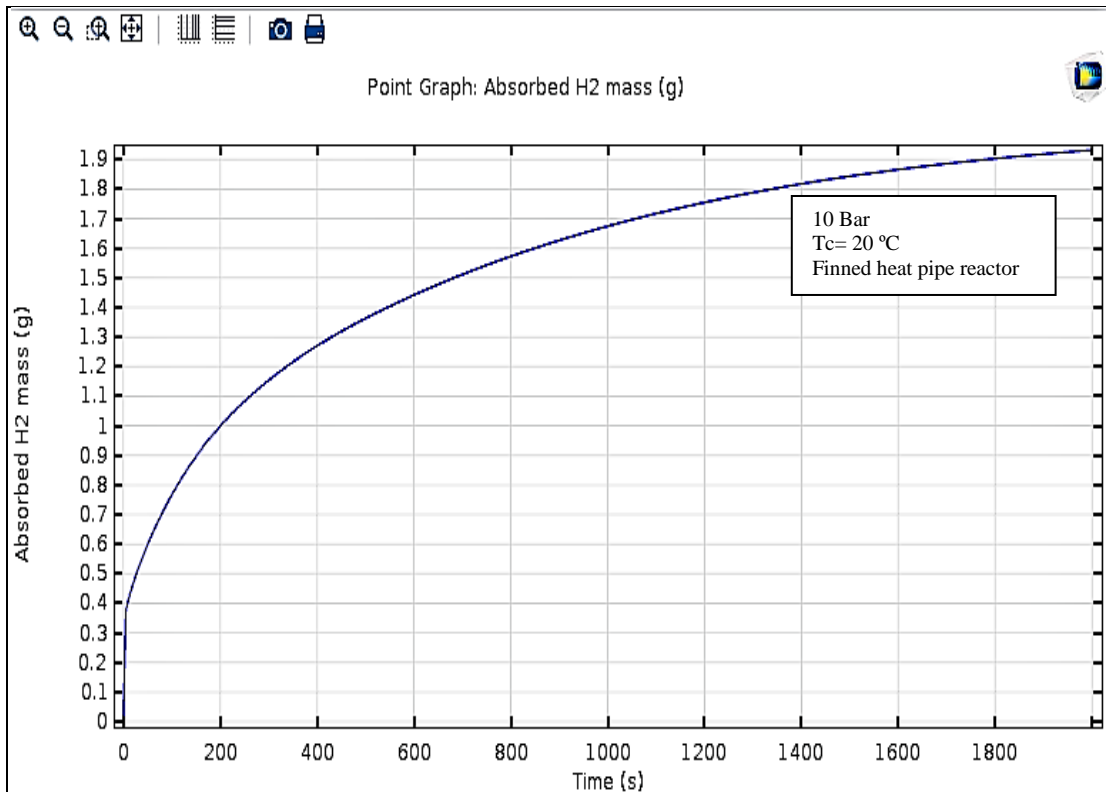


Figure 5.6. H<sub>2</sub> absorbed mass over time.

### 5.3.3. Modeling of MHTs Design for Effective Heat Management

It has been argued in the literature that the successful process of MHT strongly depends on effective heat transfers to and from the hydride beds. Managing MHT heat transition in order to improve the hydriding process is essential. Practically, several approaches to device design have been presented so far [68], including:

#### 5.3.3.1. Modeling of Circular Fins on MHT Outer Surface

The simplest way to model the influence of fins in the heat transition through the tank walls is to conserve the hypothesis of a simple cylindrical geometry and adjust the heat transfer coefficient ( $h$ ) through some semi-empirical term to integrate the influence of fins [35]:

$$h_f = \frac{hA_{tot}}{A_w} \left[ 1 - \frac{N_f A_f}{A_{tot}} (1 - n_f) \right] \quad (5.16)$$

Where  $h_f$  is the heat transfer coefficient with the impact of fins and  $A_w$  stands for the wall surface area without fins,  $A_{tot}$  represents total surface area with fins, and  $A_f$  is the area that the fins cover. Here,  $n_f$  stands for fin efficiency while  $N_f$  shows the number of fins.

#### 5.3.3.2. The Model Equation for Cooling Fluid [31]:

$$\rho_f c_{pf} \frac{\partial T_f}{\partial t} + \rho_f c_{pf} u_f \frac{\partial T_f}{\partial Z} - \lambda_f \frac{\partial^2 T_f}{\partial Z^2} + h_f (T_f - T(r_o, Z)) = 0 \quad (5.17)$$

The main thermal, physical, and geometrical parameters, which are simulated, have been reported in Table 5.1 and 5.2. Table 5.3 is the combination table of different parameter changes, which affect the hydration process.

Table 5.1. Hydrogen storage tank geometry and parametric dimension changes used in analyzes.

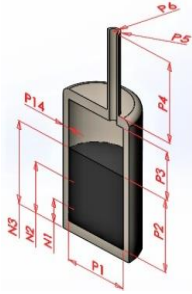
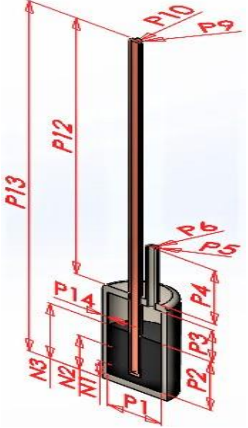
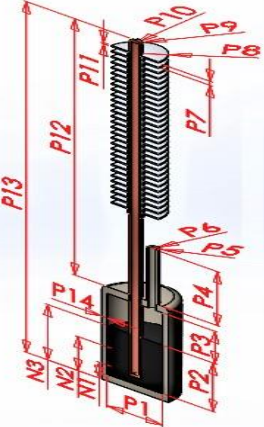
Geometric Features	Parameter	Value	Description	
 <p>Reactor without heat pipe (R1)</p>	Reactor diameter P1	29 mm	Variables in the range of 5.0 to 35 mm in all three different metal hydride material	
	Tube height with metal hydride P2	36 mm	Constant parameter	
	Tribune free height P3	24 mm	Constant parameter	
	Tube inlet height P4	40 mm	Constant parameter	
	Tube inlet internal diameter P5	4 mm	Constant parameter	
	Tube inlet external diameter P6	6 mm	Constant parameter	
 <p>Reactor with heat pipe (R2)</p>	Aileron step P7	4 mm	Constant parameter	
	Fin diameter P8	20 mm	Constant parameter	
	Heat pipe internal diameter P9	4 mm	Constant parameter	
	Heat pipe external diameter P10	6 mm	Constant parameter	
	Fin width P11	4 mm	Constant parameter	
	Heat pipe section outside the reactor P12	190 mm	Constant parameter	
	Total heat pipe length P13	250 mm	Constant parameter	
	 <p>Finned heat pipe reactor (R3)</p>	Reactor wall thickness P14	3 mm	Variables in the range of 1.0 to 7.0 mm in the analyzers of all three different metal hydride materials
		Aperture angle	0 deg	In analyses of all three different metal hydride materials, 0 and 45 degree variable parameters
		TC1 thermocouple position N1	5.1 mm	Constant parameter
TC2 thermocouple position N2		17.9 mm	Constant parameter	
TC3 thermocouple position N3		35.8 mm	Constant parameter	



Table 5.2. Constantly used parameter values in analyzes.

Parameter	LaNi <sub>5</sub> value
Metal hydride porosity	0.5
Coefficient of diffusion (H <sub>2</sub> ) (m <sup>2</sup> /s)	50x10 <sup>-9</sup>
H <sub>2</sub> initial concentration (g)	0
Storage tank initial pressure Bar	1
Constant of reaction rate for absorption (1/s)	59.188
Constant of reaction rate for desorption (1/s)	9.58
Activation energy - Absorption (J/mol)	21179.7
Activation energy - desorption (J/mol)	15473
Reactive enthalpy (J/mol)	30800
Reactive entropy (J/mol)	104.5
Reaction hysteresis	0.2
Metal hydride saturation density (kg/m <sup>3</sup> )	8394
Thermal conductivity of metal hydride (W/mK)	1.32
Specific heat value of Metal hydride (J/kgK)	419
Storage tank material density (steel) (kg/m <sup>3</sup> )	7800
Storage tank material thermal conductivity (steel) (W/mK)	80
Storage tank material specific heat value (steel) (J/kgK)	2000
H <sub>2</sub> inlet temperature (°C)	20
H <sub>2</sub> system pressure Bar	3
Time (s)	5
Overall simulation time (s)	5000

Table 5.3. Different parameter changes affecting the hydration process.

Features	Parameter	Unit	Explanation
Porous structure matrix properties	Hydride particle size	Mm	The variable parameter in the range of 20 µm - 60 µm
Boundary Conditions	Coolant temperature	°C	Variables in the range of 10-35 °C (283 - 308 K)
	H <sub>2</sub> feed pressure	Bar	Variable parameter in the range of 5 - 35 bars
	Coefficient of convection heat transfer	W(m <sup>2</sup> K)	100 – 2250 (W/m <sup>2</sup> K)
	Storage reactor including fins	--	Variable ranges with and without fins, and no angle
	Inlet reactor radius	mm	Variable ranging in between 4.00 and 8 mm
	Wall thickness of reactor	mm	3 -7 mm for the three MHTs

The current study analyzes the MHTs capacity to store hydrogen through hydrogen absorption test that depends on a few tank design parameters including the size of metal hydride particles, addition of a simple and finned heat pipe, temperature of the coolant, MHT inlet radius, inlet pressure of hydrogen, coefficient of general convective heat transfer, and MHT wall thickness. We entered the specified parameters in COMSOL Multi-physics software (Version 5.2a) for obtaining some large-scale approaches.  $\text{LaNi}_5$  metal hydride was used as a storage media, and all the parameters were calculated based on that. A few parameters, such as internal temperature distribution of the tank, the hydrogen mass storage quantity, the storage time duration, and variations in the equilibrium pressure have been optimized

## CHAPTER 6

### RESULTS AND DISCUSSION

#### 6.1. EXPERIMENTAL RESULTS AND DISCUSSION

As a part of this research, we conducted experiments for evaluating the hydrogen storage performance of three similar tanks (MHTs), out of which, one had no heat pipe, another one was equipped with a heat pipe, and the third one had a heat pipe with fins. Experiments were conducted on the tanks and some results were obtained, which were later analyzed. The current study clearly indicates the hydrogen storage devices' performances mainly in terms of absorption rates and hydrogen storage capacity. As expected, the hydride bed temperature abruptly increased as soon as the process of absorption started, which later reduced to room temperature (18-22 °C) when the test ended. It was noted that during the initial part of the experiment, the temperature sharply increased that shows hydriding, which took place in the overall metal bed. The exothermic hydriding process heats up the metal powder that leads to stop absorption since the absorption pressure increases as a result of temperature enhancement. When the temporary pause occurs, it stops the heat release, which immediately reduces the temperature; therefore, the hydriding is mainly about heat management and removal. The hydride bed should be cooled down to control heat release during an exothermic reaction; so, we evaluated the hydriding process, noted down the time durations, and measured the quantities of absorbed hydrogen. We repeated the hydriding tests under different hydrogen gas pressures (2 to 15 bars) so as to elaborate the effect of simple and finned heat pipe on hydriding for 5000 s duration. We have shown the hydrogen storage rates in Figures 6.1 and 6.2. The capacity to store hydrogen was approximately 1.3 wt% for the configurations shown in Figure 6.1.

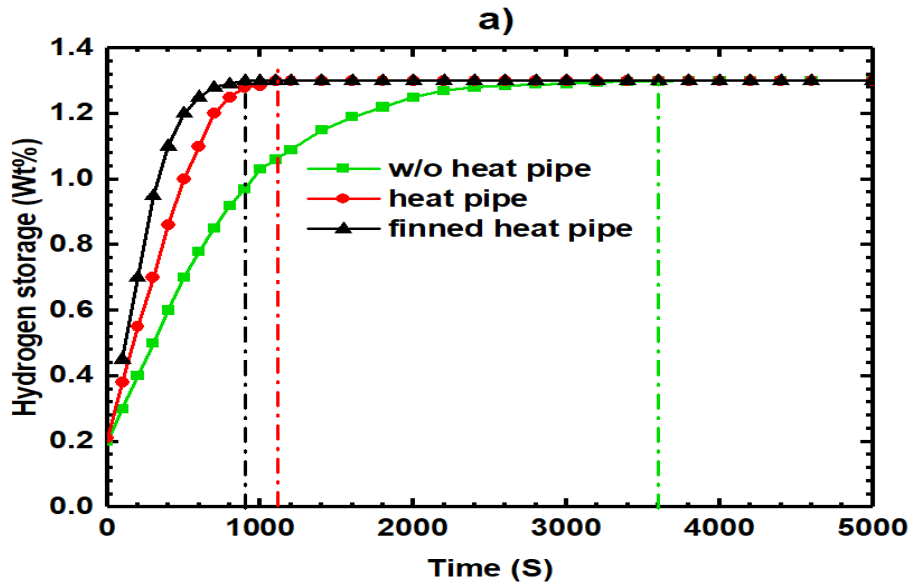


Figure 6.1. Hydrogen storage in the metal hydride at the pressure 10 bar by wt%.

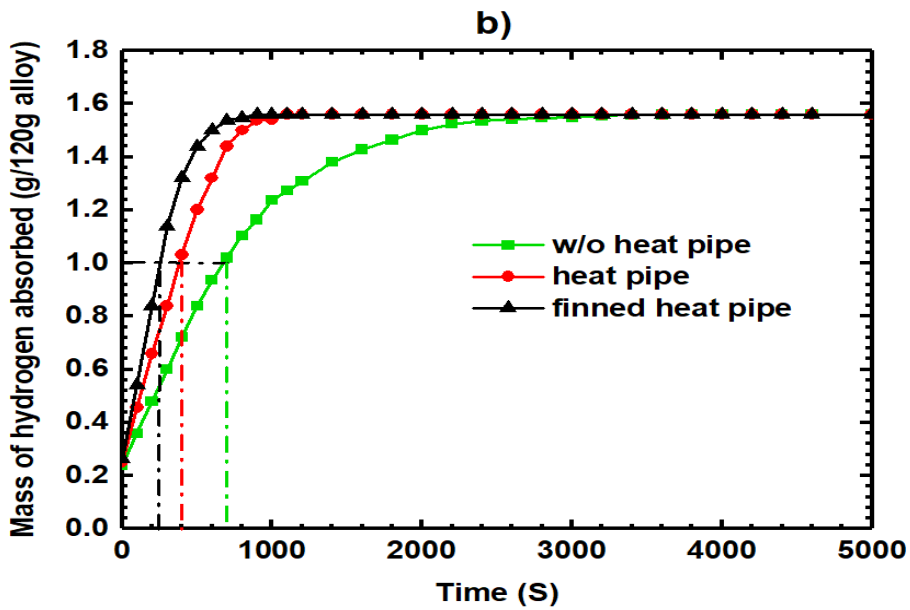


Figure 6.2. Hydrogen storage in the metal hydride (absorption/g alloy) at the pressure 10 bar.

According to Figure 6.2, the storage of hydrogen (g/g) for every gram of alloy during 900 s has been displayed below 10-bar pressure. The tank that had no heat pipe showed storage capacities 0.36, 0.48, 0.6, 0.72, 0.84, 0.94, 1.02, 1.11, and 1.16 g at time intervals 100, 200, 300, 400, 500, 600, 700, 800, and 900 s, respectively. The tank equipped with a heat pipe tank showed storage capacities 0.46, 0.66, 0.84, 1.03,

1.2, 1.32, 1.44, 1.5, and 1.54 g in the above mentioned time intervals from 100 to 900 s, as listed above. When a finned heat pipe was installed on the tank, we recorded storage capacities 0.54 g after 100 s, 0.84 g after 200 s, 1.14 g after 300 s, 1.32 g after 400 s, 1.44 g after 500 s, 1.5 g after 600 s, 1.54 g after 700 s, 1.55 g after 800s, and 1.56 g after 900 s. Earlier, the reactors' weights were calculated when hydrogen wasn't charged. Weighing process was conducted again after hydrogen charging to know the quantity of gas storage (Figure 6.3).



Figure 6.3. Storage tank weights after absorption process is complete.

During and after the experimentation, we noticed significant storage performance when we used finned heat pipe with the MHT. It was noticed that every gram of hydrogen storage took 250 s when a finned heat pipe was used while the time was 400 s when a simple heat pipe was used. When there was no heat pipe, it took 700 s to charge the same amount of hydrogen (Figure 6.2). Moreover, the charging time without heat pipe was 1.3wt% after 1 hour while it was only 1100 s with a heat pipe. When the finned heat pipe was added, the same amount of hydrogen took 900 s for charging (Figure 6.1). It is clear that the time period significantly decreased with both simple heat pipe and fins because they substantially increased the heat transfer. As a result, reduction in the charging time was observed by 75% when the finned heat pipe was used. It reduced 60% when a simple heat pipe was used as compared to the MHT relying on natural convection.

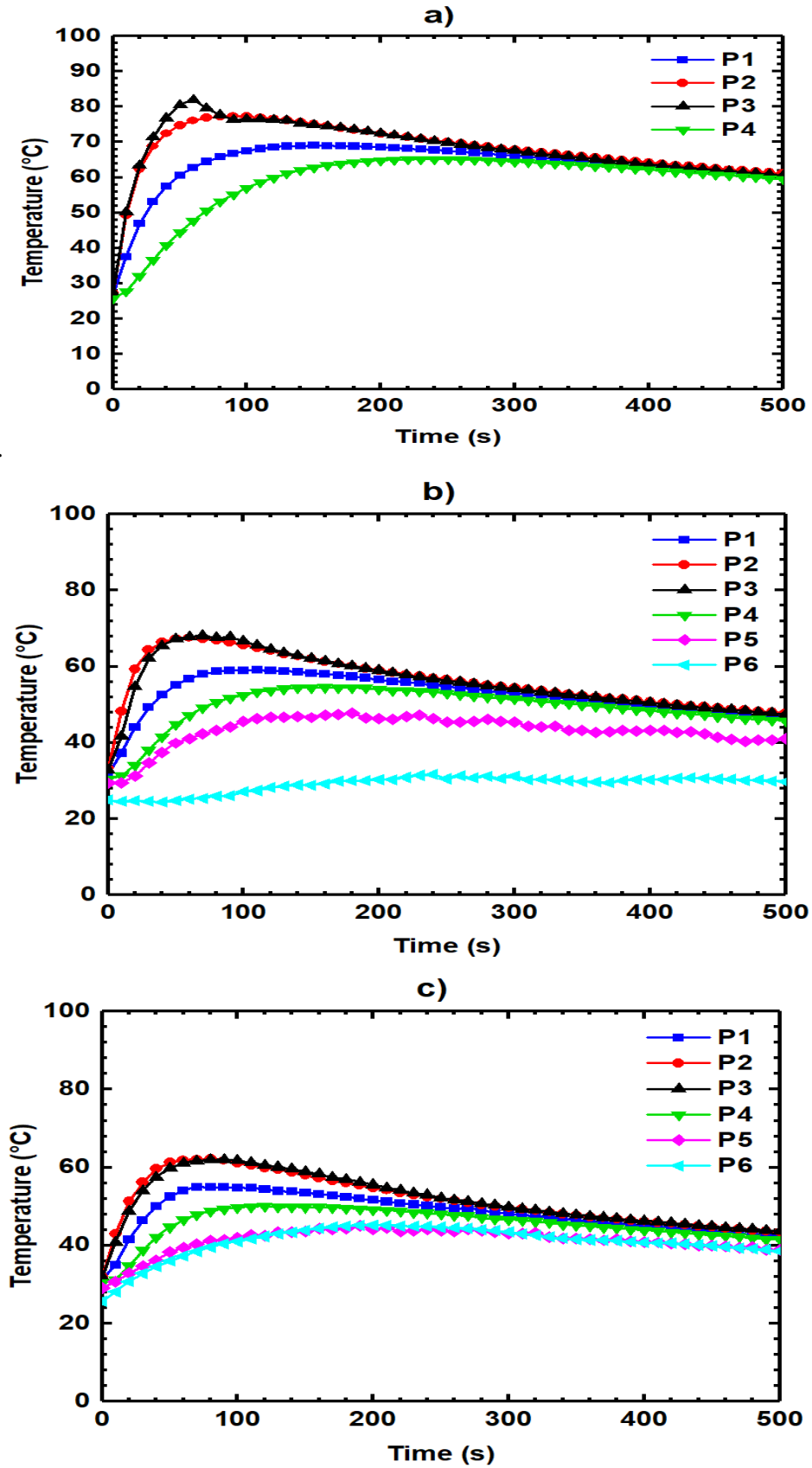


Figure 6.4. Temperature of metal hydride during MHT hydriding at 4 bar pressure in the first 500s: a) without heat pipe b) with a heat pipe c) equipped with a finned heat pipe.

The variations in temperature of a metal hydride at inlet pressure 4 bar for all the MHTs has been shown in Figure 6.4 for the first 500 s. The P<sub>3</sub> temperature probe showed substantially increased temperature than P<sub>2</sub> when the exothermic reaction began in the MHT without any heat pipe, as Figure 6.4a shows. Seconds later, P<sub>2</sub> temperature exceeded the temperature of P<sub>3</sub>. Such differences in temperature show that the rate of absorption was higher in the locations near the tank walls and the hydrogen inlet; so, the temperature maximized and later it slowly moved towards the center of the reactor. P<sub>4</sub> was a probe that measured the surface temperatures in case of all the MHTs because it immediately undergoes a temperature drop to room temperature (18-22 °C) when the heat releases. Both P<sub>2</sub> and P<sub>3</sub> were used in the MHTs with heat pipes. Figures 6.4b and 6.4c show their performances. They have a reaction that is equidistant from the wall of the MHT but closer to the hydrogen inlet. On all the MHTs, Probe P<sub>1</sub> measured a lower temperature as compared to P<sub>2</sub> and P<sub>3</sub> since the P<sub>1</sub> probe is closer to the bottom of the tank and cooling is controlled in the bottom with the help of convection. Repeated observations show that the limitation of heat transfer is substantial in thick beds [11], because increase in thickness reduces the pressure closer to the cold wall, which happens as a result of resistance against the hydrogen flow. The reduction in the local absorption takes place when the hydride bed shows reduced driving force. The pressure drops and results in decreasing the reactionary driving force. The maximum absorption rate shifts towards the frontal part of the bed that increases the length of the conduction path. When the permeability becomes low, it results in reduced velocity of the gas, which acts as a significant resistance. In case of increase in the absorption rate, it doesn't make permeability a limiting factor. The performance of the system reduces below the permeability level ( $K > 1e^{-12} \text{ m}^2$ ) [67,91]. The hydrogen inlet and the areas close to it bear the peak temperature. It is shown in the figure that P<sub>3</sub> showed higher temperature when  $z=36 \text{ mm}$  in all the configurations. In addition, Figure 6.4 indicates the released heat when the charging process was quickly removed, and the exothermic reaction resulted in 62 °C temperature for the reactor with a finned pipe reactor, while it was 67 °C when the tank had a heat pipe. The MHT that had no heat pipe had 81 °C temperatures.

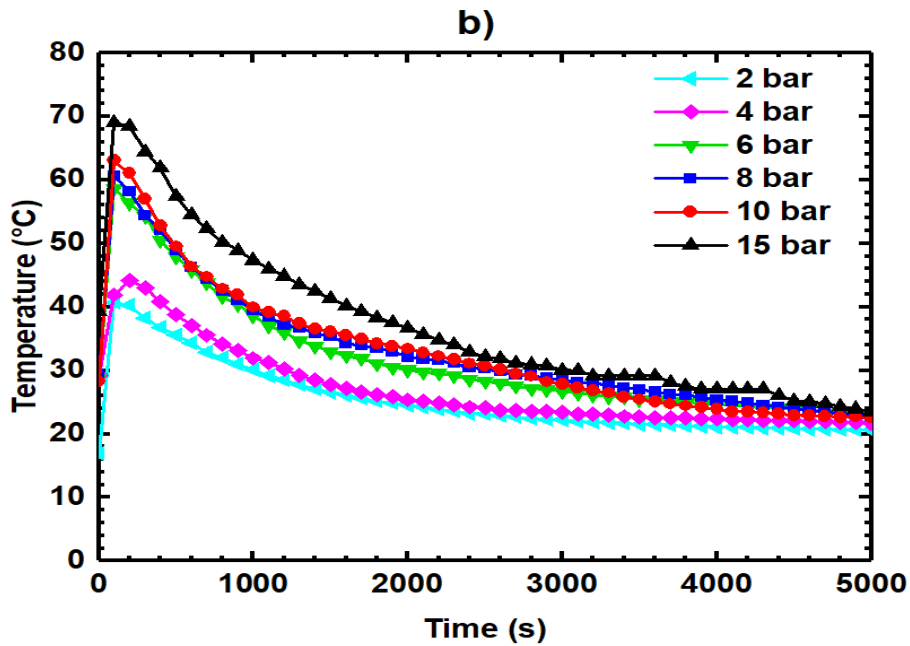
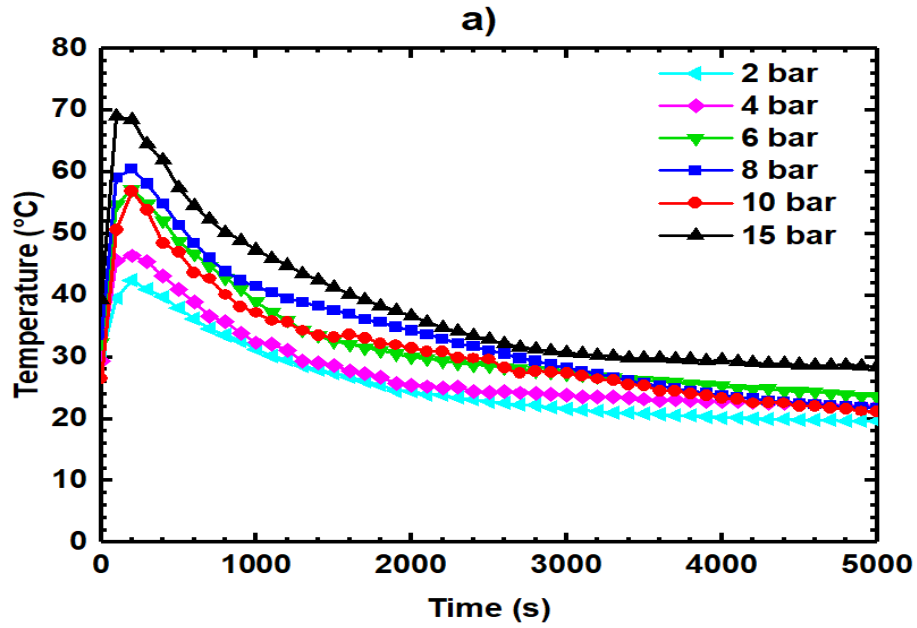


Figure 6.5. Comparison between the heat pipe temperature profiles under several hydrogen supply pressures in the MHTs: a) heat pipe, b) finned heat pipe configuration.

$P_5$  and  $P_6$  probes measure the heat pipe and fin temperature, as Figure 6.5 indicates. Obviously, the heat pipe releases more heat in case of increase in the hydrogen supply pressure. In case the storage tank has a finned heat pipe, which has comparatively lower temperature than the MHT with a simple heat pipe; it showed remarkably lower temperature as compared to the tank that had no heat pipe. As a



result, the heat pipe enhances heat transfer while the fins expose more area that lowers equilibrium hydrogen absorption pressures, which increases the speed of hydriding.

The temperature distribution in the MHTs provides information to explain how we can improve hydriding. The mass transfer reaction increases with the hydrogen supply pressure; so, improved initial hydrogen pressure increases the speed of absorption reaction when we use  $\text{LaNi}_5$ . Figure 6.6 clearly indicates that absorbed hydrogen mass increases along with the rise in inlet pressure from 2 to 15 bars. The hydrogen mass percentage remained constant. Contrary to that, no significant difference was found between the absorption of hydrogen mass from 10 to 15 bars; so, it is sufficient evidence that at low pressure, hydrogen gas gets absorbed in the metal hydrides.

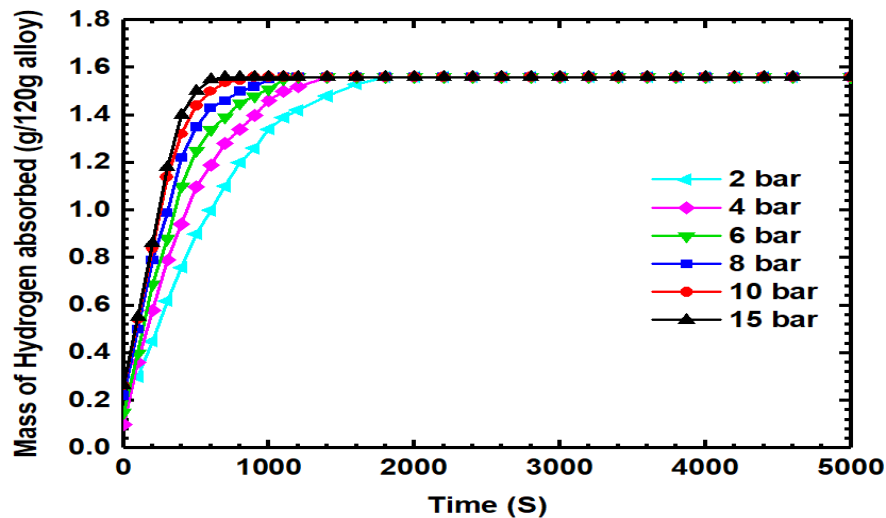


Figure 6.6. Initial hydrogen supply pressure and its effect on the hydrogen storage for MHT that is equipped with a finned heat pipe.

Figure 6.7 shows the MHT temperatures at different hydrogen supply pressure levels (2-15 bars), it is clearly seen under the given conditions, higher inlet pressure increases the hydrogen absorption and the inner temperature; so, the inlet pressure variations are substantial to absorb hydrogen. Obviously, the MHT temperature increases with increasing hydrogen inlet pressure, and that happens when the kinetic reaction enhances, and the exothermic reaction occurs between the metal hydride and

hydrogen. We recorded the highest temperature at 15 bars pressure for every MHT 96 °C (MHT with heat pipe), 121 °C (MHT with no heat pipe), and 88 °C (MHT with a finned heat pipe).

Figure 6.8 compares between the MHTs temperature profiles in the hydriding process at different hydrogen pressures: 4, 10 and 15 bars. Obviously, the device temperature enhances when the pressure rises while the stored hydrogen also increases as a consequence. The use of finned heat pipe in a configuration shows less temperature and the quickest charging time, which confirm better heat removal. It happens because of enhanced heat transfer that takes place through fins and the heat pipe. In the same way, the kinetics of hydrogen absorption improves when both heat pipe and fins are used. Table 6.1 shows the variations pertaining to the reaction temperature, and stored hydrogen mass in many device designs. It is obvious that the outcomes/results of our study have good agreement with majority of the previous experimental researches on the same or relevant topics. This table shows that the hydrogen mass storage increased with improvement in the heat transfer when different vessel designs were used, including fins, air or water cooled devices, heat pipe, combining metal foam with concentric cooling tube, and a circular and/or spiral heat exchanger tube.

Figure 6.9, shows of thermal images at 15-bar hydrogen-charging pressure. For taking these images, we used a high-performance thermal camera (Flir T620 model, auto-focus, no-board 5 MP visual, accuracy calibrated, and temperature range 2000 °C  $\pm$  2%). It is a fact that hydrogen storage depends on MHT temperature distribution and heat management. We have taken these photos after completing the experiments to make comparisons. We sealed the tanks with the help of fitting plugs after removing the thermal probes to avoid hydrogen leakage. For 20 min, the hydrogen gas was charged, and when the exothermic reaction took place, these photos were taken. At that time, the maximum temperature (at 15 bar pressure) was noted from all the MHTs: 97.1 °C (tank with heat pipe), 88.3 °C (finned heat pipe tank), and 121 °C (tank without heat pipe). This indicates highly considerable agreement between the experimental values and the thermal images at 15-bar pressure (Figure 6.7).

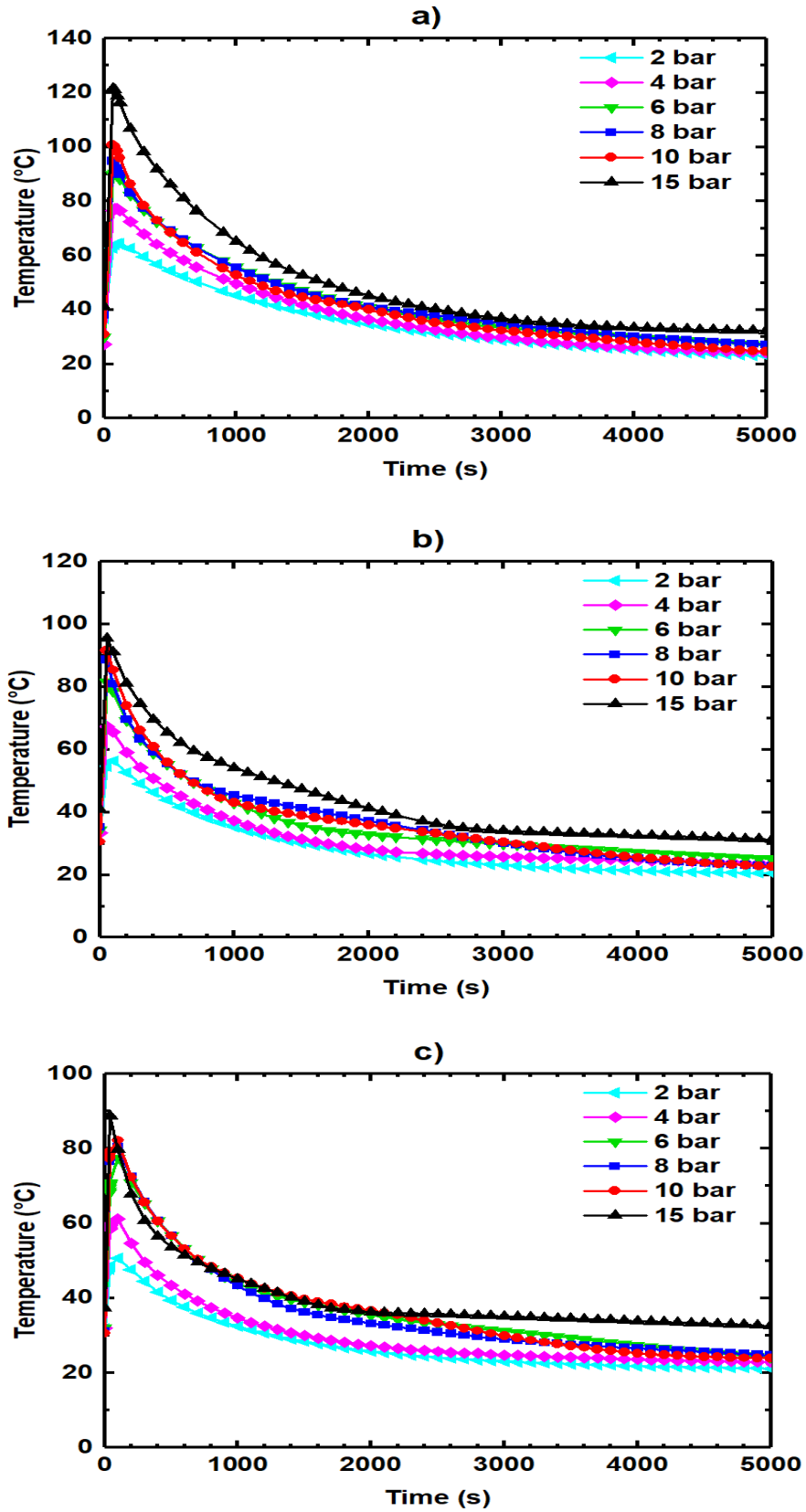


Figure 6.7. The impact of the pressure of the initial hydrogen supply on the hydride temperature, a) without the heat pipe, b) with a heat pipe, c) with a finned heat pipe.

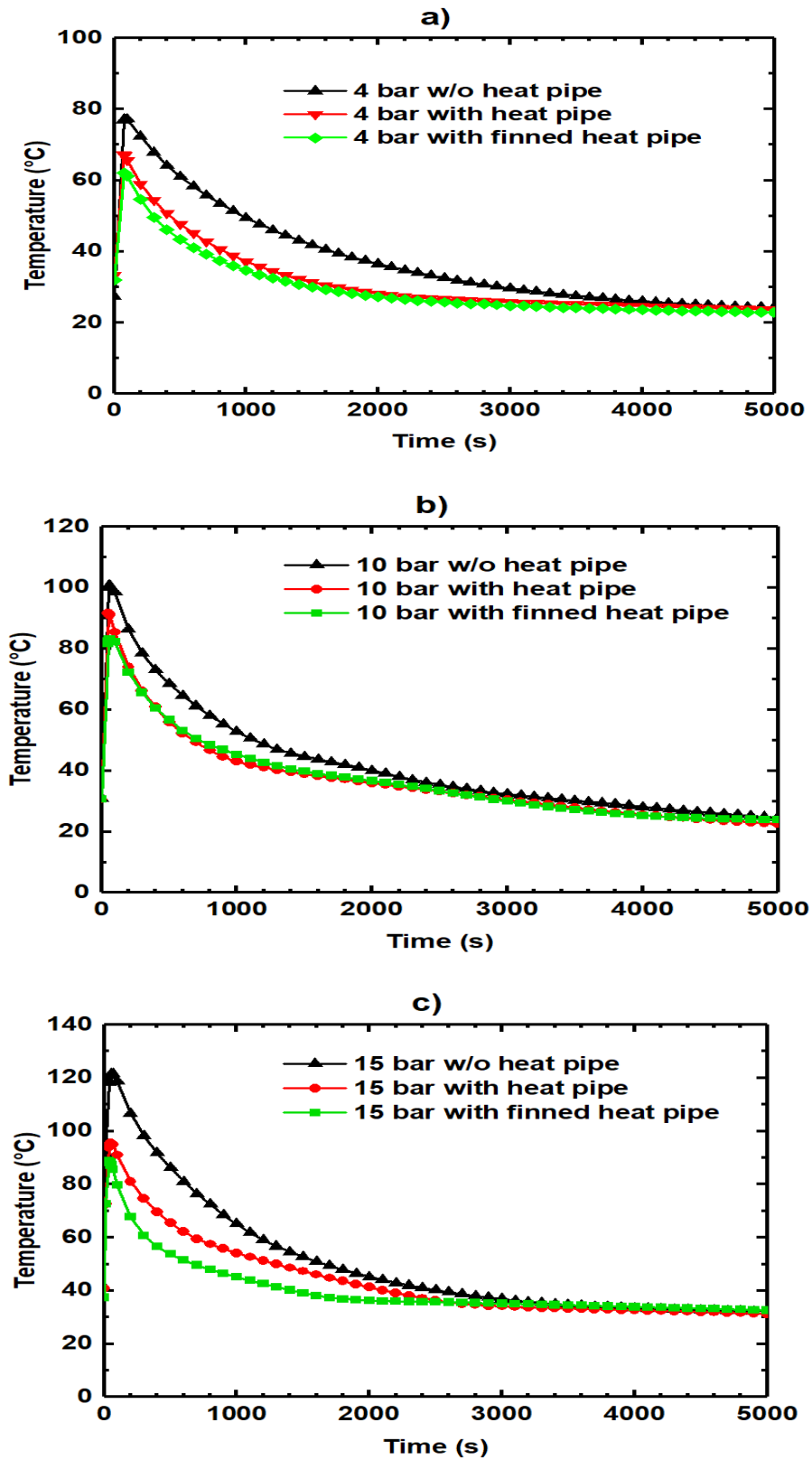


Figure 6.8. Comparison between the temperatures of a metal hydride in the MHT hydriding process without the heat pipe, with a heat pipe and with a finned pipe: a) supply pressure 4 bars, b) supply pressure 10 bars, c) supply pressure 15 bars.

Table 6.1. Comparison between the present results with the results of other similar investigations [85].

Type of MHR	Max. Temp (C°)	Pressure	Hydrogen Capacity (wt %)	Alloys	Reference
Tank without a metal foam	80	10bars	1.3	LaNi <sub>5</sub>	Mellouli [28]
Tank equipped with a metal foam	80		1.3		
Tank with metal foam, and a concentric heat exchanger tubes	59		1.3		
Tank with heat pipes	75		1.3		
Tank without heat pipes	95		1.3		
Water-cooled tanks	33		1.4		
Finned heat exchanger tanks	30		1.4		
Tank with no fins	116		1.07	LaNi <sub>4.75</sub> Al <sub>0.25</sub>	Kayfeci [54]
Tank with fins	113	1.19			
Tank with 7 water-cooling tubes	50	8bars	1.3	LaNi <sub>5</sub>	Freni [67]
Tank with 12 tubes in which cooling water flow	45		1.3		
Tank with 12 tubes in which cooling water flow surrounded by a cooling jacket	37		1.3		
Un-finned tank	58	2bars	-		Kaplan [33]
Finned tank	55		-		
Water cooled tank	32		-		
Tank (2mm diameter) without metal foam	67	6bars	1.3	Laurencelle [19]	
Tank (4mm diameter) without metal foam	67		1.3		
Tank (6mm diameter) without metal foam	69		1.3		
Tank (2cm diameter) without metal foam	72		1.3		
Tank (4cm diameter) without metal foam	79		1.3		
Tank (no heat pipe)	101	10bars	1.3	This study	
Tank with a heat pipe	93		1.3		
Tank with a finned heat pipe	83		1.3		

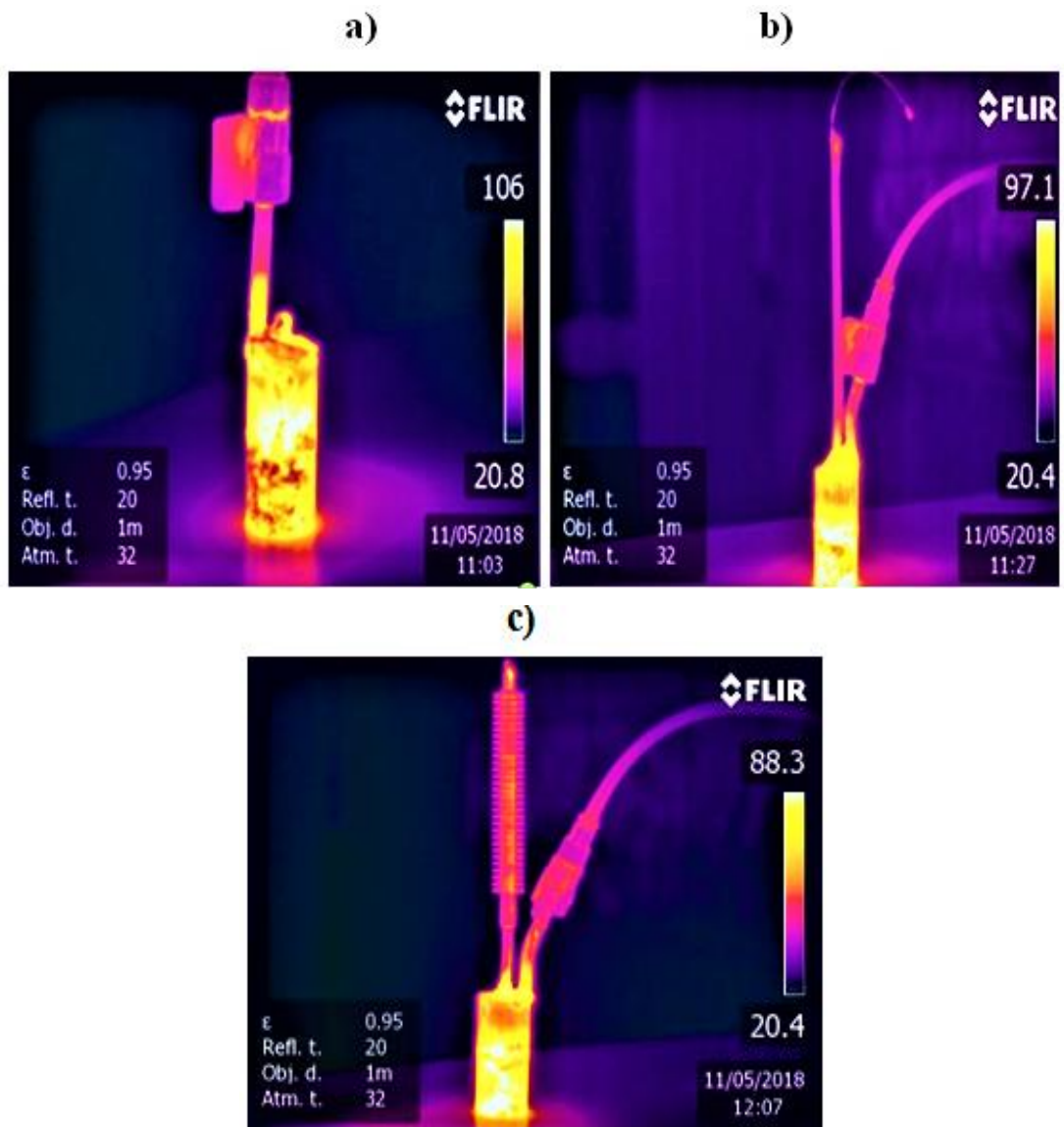


Figure 6.9. Thermal images of three MHTs at 15 bars charging pressure: a) without heat pipe, b) with a simple heat pipe, c) with a finned heat pipe.

## 6.2. SIMULATION RESULTS AND DISCUSSION

In this thesis, we put  $\text{LaNi}_5$  in an MHT for numerical study of hydrogen absorption that has been expressed below:



The generated heat during the hydriding process is extracted with a heat pipe inside the vessel, and the coefficient of heat transfer between the surrounding air and the vessel walls was calculated because it forces the temperature to decrease in the wall region. The cooling level has substantial impact on charging because hydrogen absorption takes place depending on the vessel temperature. Cooler vessels have higher absorption rate and shorter filling time. Both Table 5.1 and 5.2 show important thermal and geometrical parameters, which have been applied in the simulation. Different parameter changes, and/or the operating conditions, which affect the hydration process, are given in Table 5.3.

### 6.2.1. Model Validation

For validation purpose, the used geometries of the MHT configuration are shown in Figure 5.1, and the simulation is performed accordingly. They have cylindrical configurations, and their inner volume is occupied by a finned pipe, while 120g  $\text{LaNi}_5$  powder was 60% filled in the each of the three reactors. The values of the inner temperature were noted at the point, which is at a distance of 35.8 mm from the bottom. We used COMSOL software for solving differential equations. Different parameter changes affecting the hydration process are shown in Table 5.3. They were used in simulation. First, numerical simulations were carried out for comparing the vessel temperature with the reference values when  $\text{LaNi}_5$  was used for hydrogen storage. This comparison has been shown in Figure 4.1 while Figure 4.13 shows the experimental set-up. First a vacuum pump was linked to the storage tank (10 mm Hg) then it was heated until it became 350 °C. Later, it was activated at 10 bar hydrogen pressure. 120 g of  $\text{LaNi}_5$  metal hydride powder was filled, which covered 60% MHT capacity. The metal hydride (MH) particle size was about 20 to 50  $\mu\text{m}$  for this

experiment. The 3D schematic view of geometric configurations and/or the mesh size configuration for each domain of the cylindrical vessel has been shown in Figure 6.10. The elements, Mesh sizes on the domains, the number of elements, minimum and average qualities of them are given in Table 6.2. The measured and predicted capacities of hydrogen have been illustrated in Figure 6.11. Obviously, the numerical results have satisfactory agreement with the experimental data.

Table 6.2. Mesh size on the domains, the number of elements, minimum and average qualities of them.

Mesh on domain	Consisting of elements	Minimum quality	Average quality
Porous	11706	0.2511	0.6782
Free space	11328	0.2191	0.6919
Storage tank well	6424	0.2083	0.6454
Heat pipe	2517	0.1567	0.4691
Fins	14342	0.1404	0.6152

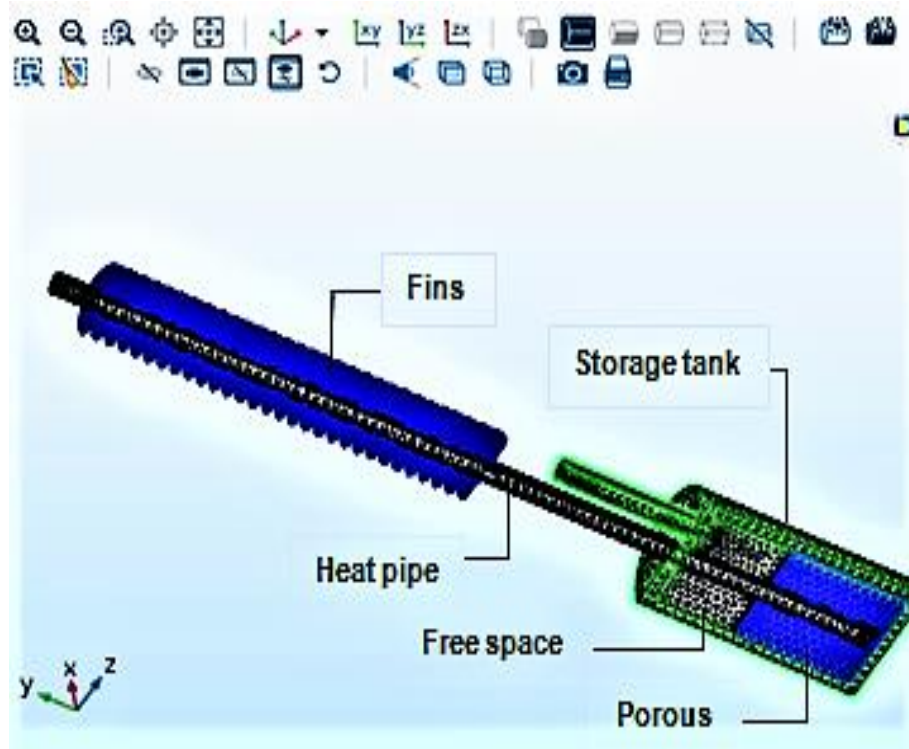


Figure 6.10. Schematic view of the mesh sizes.



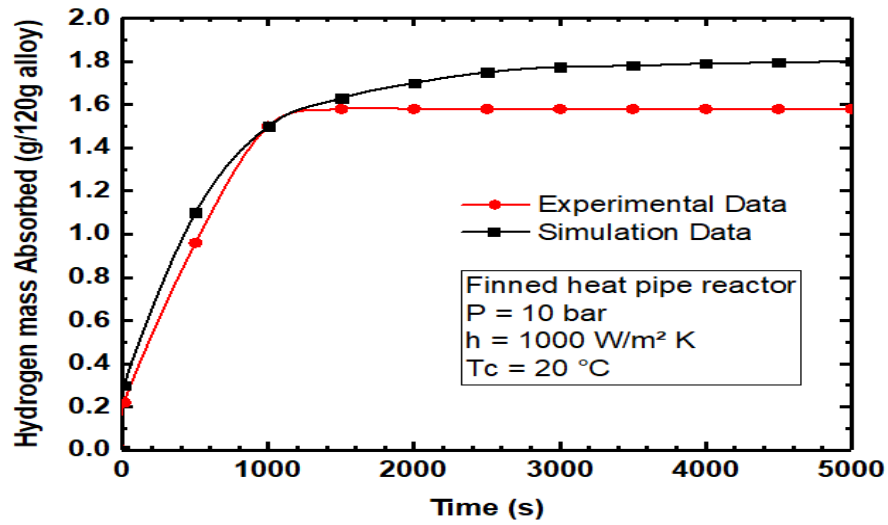


Figure 6.11. Time evolutions of the absorbed hydrogen amount in heat pipe tank configuration under 10 bar hydrogen pressure supply by both experimental and simulation studies.

The temperature history was taken from a point located at 35.8mm from the tank bottom, which is shown with the experimental data (Figure 6.12) for all the three configurations. The peak temperature was recorded in the numerical model, and the experimental work has been shown in Figure 6.12. The 3D-temperature distribution inside the MHR configurations for the numerical model is shown in Figure 6.13. The temperature variations were almost similar for both modeling and experimental findings when both systems operated at the same conditions. It was also observed that the charge time lasted longer in the experiment as compared to the same in the model for the three different configurations. For example; Figure 6.12a shows that without heat pipe reactor at 100 sec. simulation reach maximum temperature 110 °C, while at experimental study reach the same temperature after 200 sec. The maximum temperature for the system when a simple heat pipe used is 97 °C as shown in (Figure 6.12b), while it was 88 °C incase of finned heat pipe reactor as shown in (Figure 6.12c). The evaluation would result in losses in the hoses either in the charging or during vacuuming. The hydrogen storage capacities for the finned heat pipe configuration have been shown in Figure 6.11 in terms of experimental and simulated values, which were very close. Consequently, the obtained results show that the simulation and experimental results reasonably match, which proves that the model has efficiently captured the key experimental trends.

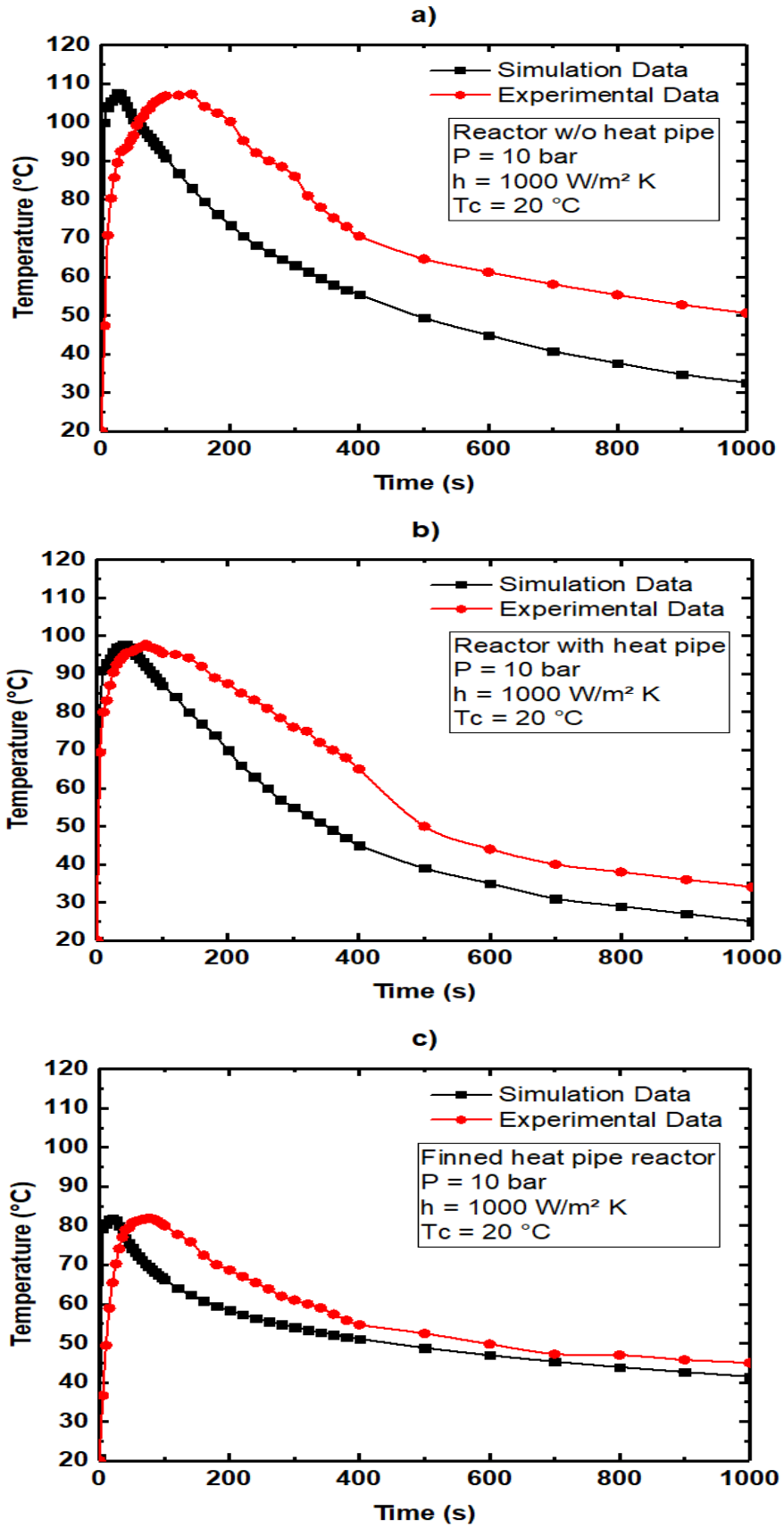


Figure 6.12. The temperature histories at 35.8mm from the bottom. a) with no heat pipe, b) with a heat pipe, and c) with a finned heat pipe.

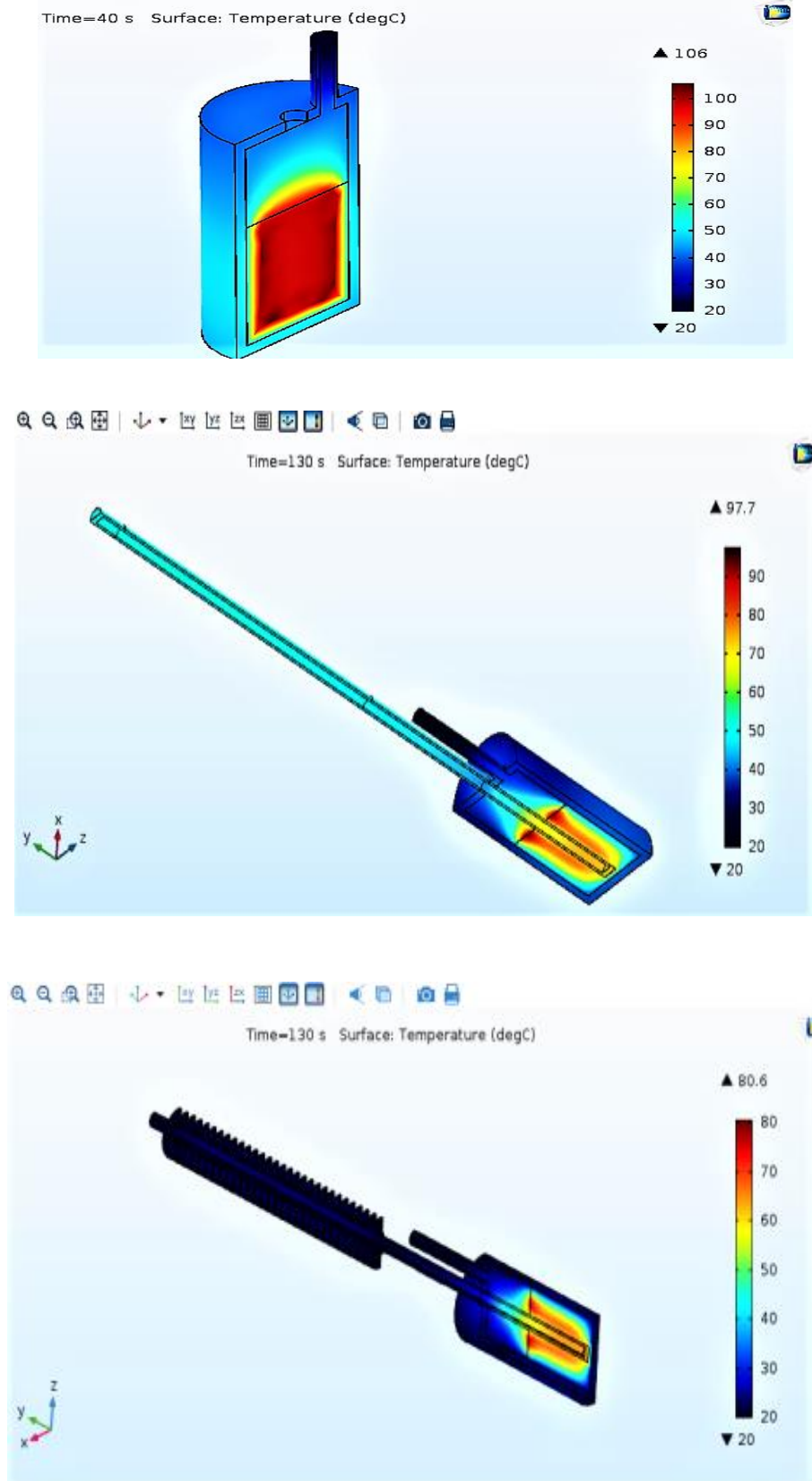


Figure 6.13. 3D-temperature distribution inside the MHR configurations; with and without heat pipe, and with a finned heat pipe;  $P= 10$  bar, and  $h=1500$   $W/m^2K$ .

### 6.2.2. Effect of the Tank Configuration (Fin Parameter)

To compare the considered configurations for certain operating conditions, the metal hydride quantities and other parameters' values have been shown in Table 5.2 while keeping the boundary conditions same.

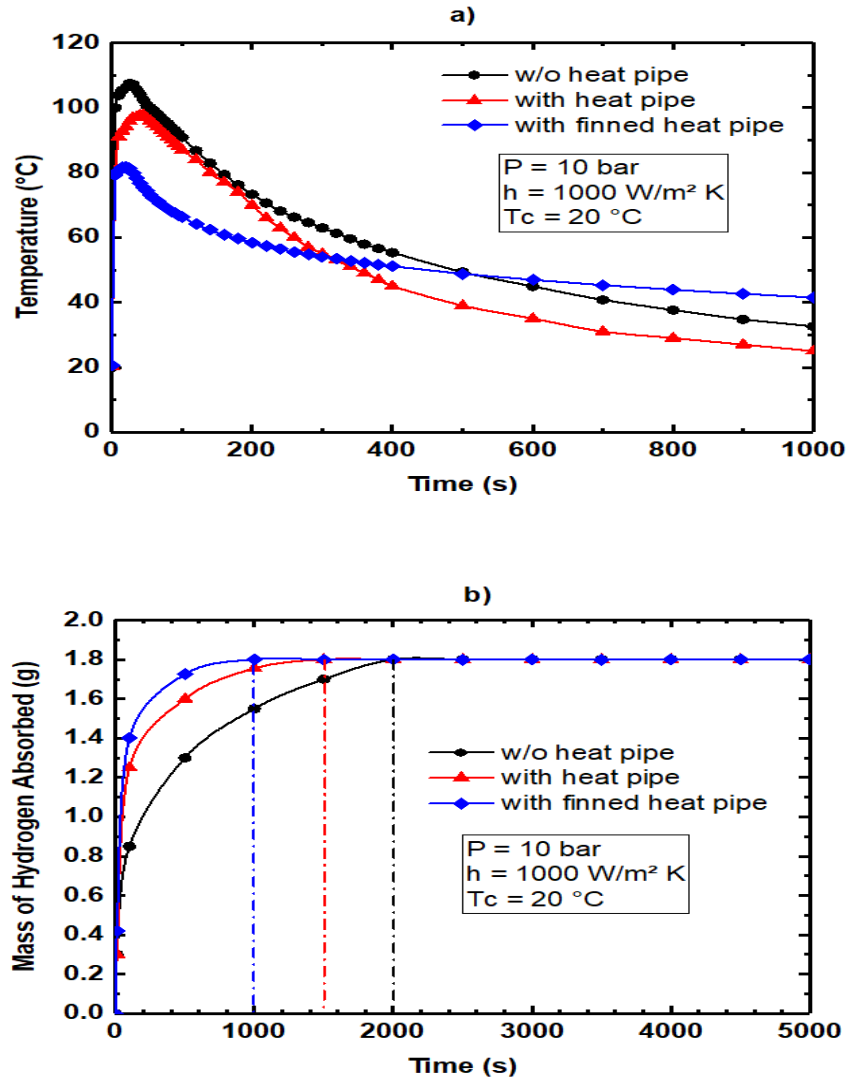


Figure 6.14. a) Temperature-time relationship for MHTs where the storage tank having fins or not as variable. b) Hydrogen mass against time where the storage tank having fins or not as variable.

For evaluating the use of heat pipe and fins, all the operating conditions are based on fixed parameters including 10 bar supply pressure,  $20 \text{ }^\circ\text{C}$  cooling fluid temperature, 3mm vessel thickness, and  $1000 \text{ W/m}^2\text{K}$  coefficient of convective heat transfer. The

mass of hydrogen absorption is presented in Figure 6.14b. It is clear that 1.8g absorption took place in 500 s when a reactor with a finned heat pipe was used while it takes 1000 s to store the same quantity when a reactor with a heat pipe was used, and it was approximately 1500 s when no heat pipe was used, as Figure 6.14b shows. The time period clearly and significantly decreased when the finned and simple heat pipes were used for increasing the process of heat transfer, which reduced the charging time by almost 75% when a finned heat pipe was used. It was 60% reduced when a simple heat pipe was used as compared to the reactor having no heat pipe. These results indicate that the configuration using a heat pipe and fins considerably improves the storage process. When fins were part of the reactor, the system exhibited lower inner temperature and absorbed more hydrogen at a short time as compared to a simple heat pipe (Figure 6.14).

### **6.2.3 Effect of the Hydrogen Inlet Pressure**

For understanding the impact of supply pressure on hydrogen storage and charging time, we performed simulations for every MHR configuration (Figure 5.1). We used  $\text{LaNi}_5$  as storage medium at different pressures (5-35 bars) under similar operating condition; 10 bar supply pressure, 20 °C cooling fluid temperature, 3mm vessel thickness, and 1000  $\text{W/m}^2\text{K}$  coefficient of convective heat transfer. According to Figure 6.15, the inner temperature variation is shown against different time durations while hydrogen inlet pressure was a variable, as Figure 6.15a shows. The variations in the hydrogen mass are shown in Figure 6.15b when the hydrogen inlet pressure was a variable. Figure 6.15 shows the results. When the absorption process begins, the average bed temperature sharply rises and reaches the maximum; later, it declines to the cooling fluid temperature when absorption finishes. The immediate temperature increase happens because of poor heat transfer qualities of the hydride. According to Figure 6.15, the absorption temperature is 20 °C, and higher supply pressures result in higher temperature. The heat is generated when there is higher difference between the hydride's equilibrium pressure and the supply pressure.

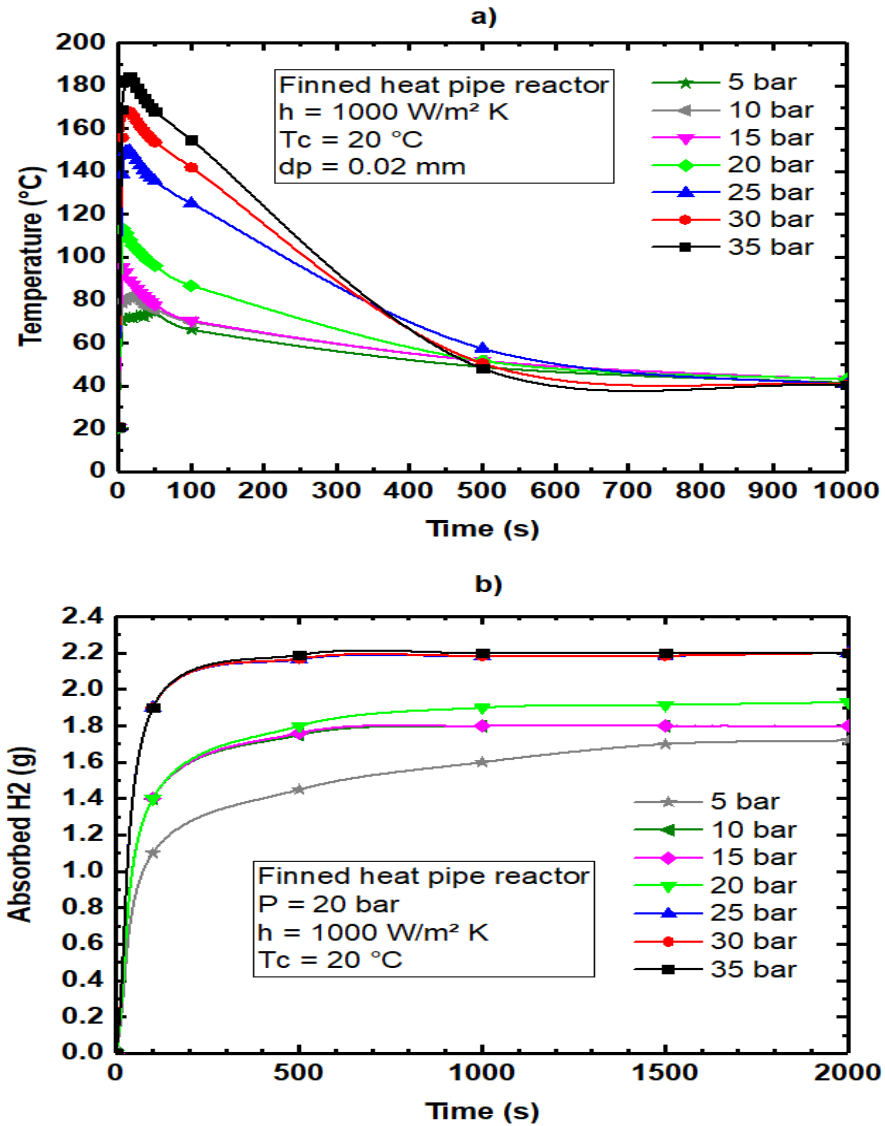


Figure 6.15.a) Temperature history where hydrogen inlet pressure as variable.  
 b) Hydrogen mass vs. time where hydrogen inlet pressure as variable.

Moreover, at high supply pressure, the reaction accomplishes earlier as compared to the reaction at lower supply pressure. The supply pressure effect on the capacity to store hydrogen using  $\text{LaNi}_5$  has been shown in Figure 6.15b. Increasing the hydrogen supply pressure and its storage capacity takes place because of a plateau slope [50,87,89]. Obviously, the inlet pressure rises, which increases the inner temperature, and absorbed hydrogen mass. The variations in the inlet pressure have significant role in the hydriding process, as shown in Figure 6.15.

#### 6.2.4. Effect of the Particle Size

The LaNi<sub>5</sub> metal hydride powder has particle sizes between 20 μm and 60 μm. All the operating conditions were based on fixed parameters including 10 bar supply pressure, 20 °C cooling fluid temperature, 3 mm vessel thickness, and 1000 W/m<sup>2</sup>K coefficient of convective heat transfer. Under the mentioned operating conditions, no big variation was found in the particle sizes (Figure 6.16). The highest possible internal temperature was 86 °C, and the equilibrium temperature was reached within 200s. The maximum hydrogen absorption was almost 1.8 g while 500 s was the minimum time to absorb this hydrogen quantity as Figure 6.16 shows.

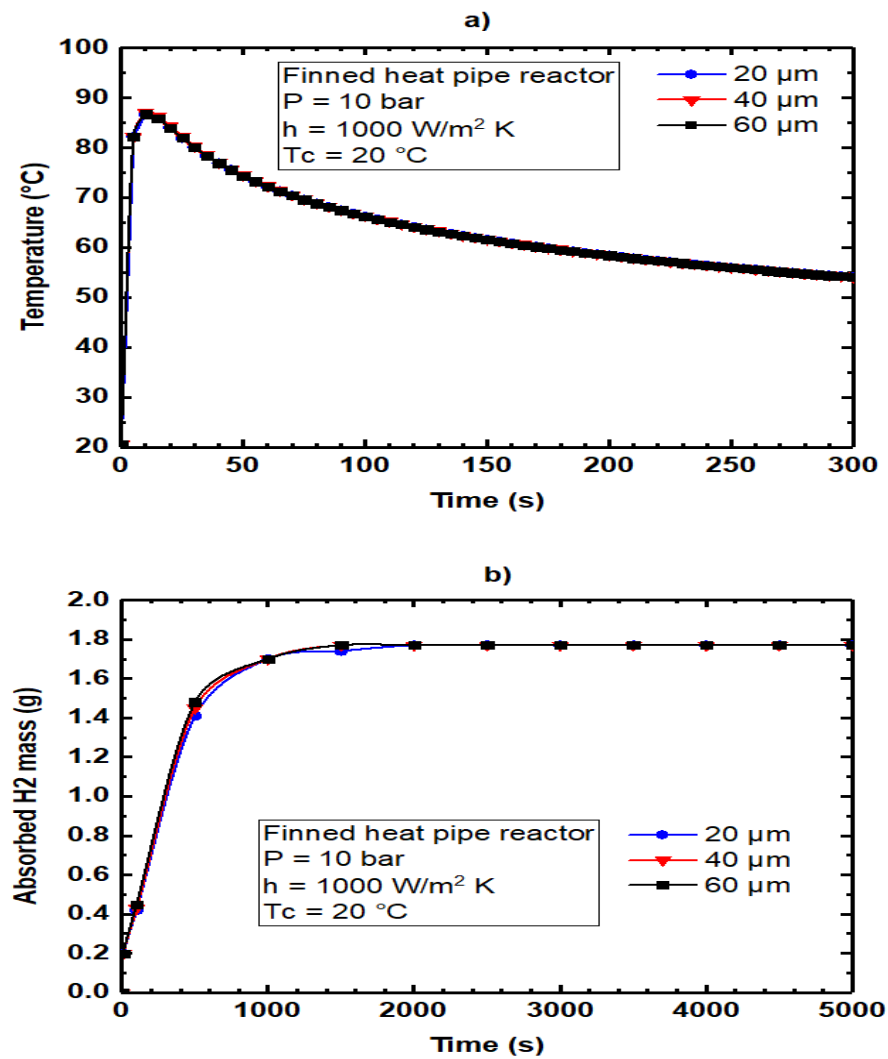


Figure 6.16. a) Temperature history with respect to time where metal hydride powder's particle size is variable, b) Hydrogen mass against time against time where metal hydride powder's particle size as variable.

### 6.2.5. Effect of General Convective Heat Transfer Coefficient

The coefficient of heat transfer ( $h$ ) includes the impact of resistance to convective heat transfer that exists between the cylinder wall and the cooling fluid, and the contact resistance that exists between the hydride and the inner wall of the vessel. When the vessel configuration is known, different “ $h$ ” values are obtainable using a finned heat pipe.

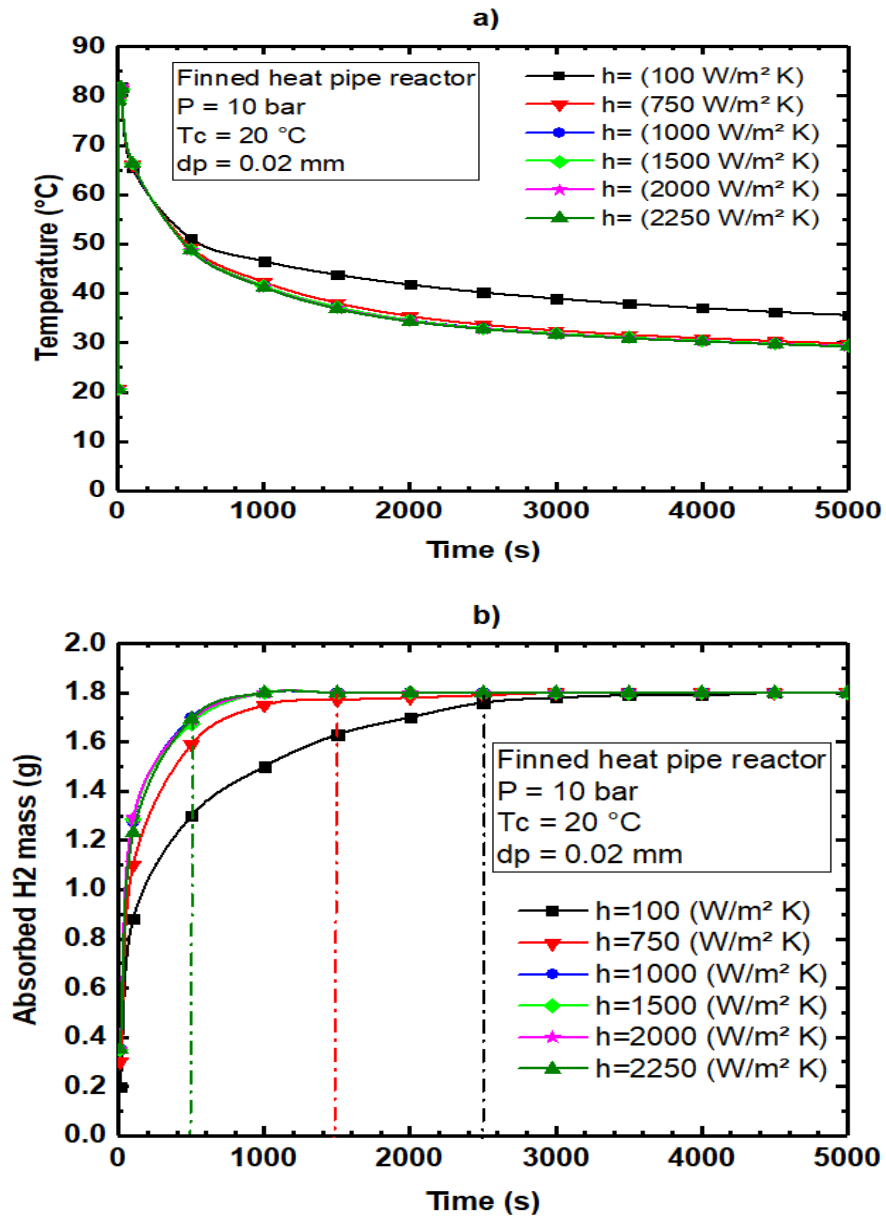


Figure 6.17. a) Temperature history where the convective heat transfer coefficient as variable. b) Hydrogen mass against time where the convective heat transfer coefficient as variable.



For studying its impact on hydrogen absorption, the  $h$  can be within the range 100-2250 W/m<sup>2</sup>K when other operating parameters are constant. If it increases, the hydride bed transfers more heat to the cooling fluid, which results in reducing the temperature of the hydride bed and results in higher hydrogen absorption, as Figure 6.16 shows. The heat transfer coefficient has an impact on heat transfer but it has no effect on the hydrogen storage capacity; however, it significantly reduces the absorption time when  $h$  shows a higher value.

Figure 6.17 shows that the internal heat transfer enhances the heat transfer coefficient above 1000W/m<sup>2</sup>K; however, it has insignificant impact on the absorption time. Thus, for known vessel configuration, an optimum value of  $h$  exists that minimizes the absorption time. Figure 6.17b illustrates the time required to reach 1.8g for different values of  $h$ .

Under the specific operating conditions, no noticeable difference was found in heat transfer coefficient other than an insignificant small value (100 W/m<sup>2</sup>K), and the storage time was comparatively longer, as Figure 6.17b shows. It also shows substantial storage improvement at 1000 W/m<sup>2</sup>K. In case, it took 500 s to reach 1.8 g in the heat transfer coefficient range 1000-2250 W/m<sup>2</sup>K, it requires 1500s at 750 W/m<sup>2</sup>K or 2500 s at 100 W/m<sup>2</sup>K. Certainly, reduction in the time period was observed when the value of heat transfer coefficient was 1000 W/m<sup>2</sup>K or more. As a result, the reduction in the charging time took place by 3 times for  $h$  values above 1000 W/m<sup>2</sup>K, in comparison with using 750 W/m<sup>2</sup>K, and it is 5 times in comparison with using 100 W/m<sup>2</sup>K.

#### **6.2.6. Effect of Temperature of Cooling Fluid**

In order to assure high rate of hydriding, the supply pressure-hydride equilibrium pressure difference should be high during absorption. It is also affected by changes in the cooling temperature, and the absorption temperature should be 10-35 °C while keeping other parameters constant: 10 bar supply pressure, 20 °C cooling fluid temperature, 3mm vessel thickness, and 1000 W/m<sup>2</sup>K coefficient of convective heat transfer. Figure 6.18b clearly indicates that the maximum hydrogen storage capacity

was noted at 283 K. The hydrogen storage improves at low cooling temperature because of the plateau slope, which is found in the metal hydrides' PCT characteristics [92]. When the cooling temperature is lower, the process of cooling down hydride bed is quicker that decreases the duration of hydrogen absorption time, as Figure 6.18b shows.

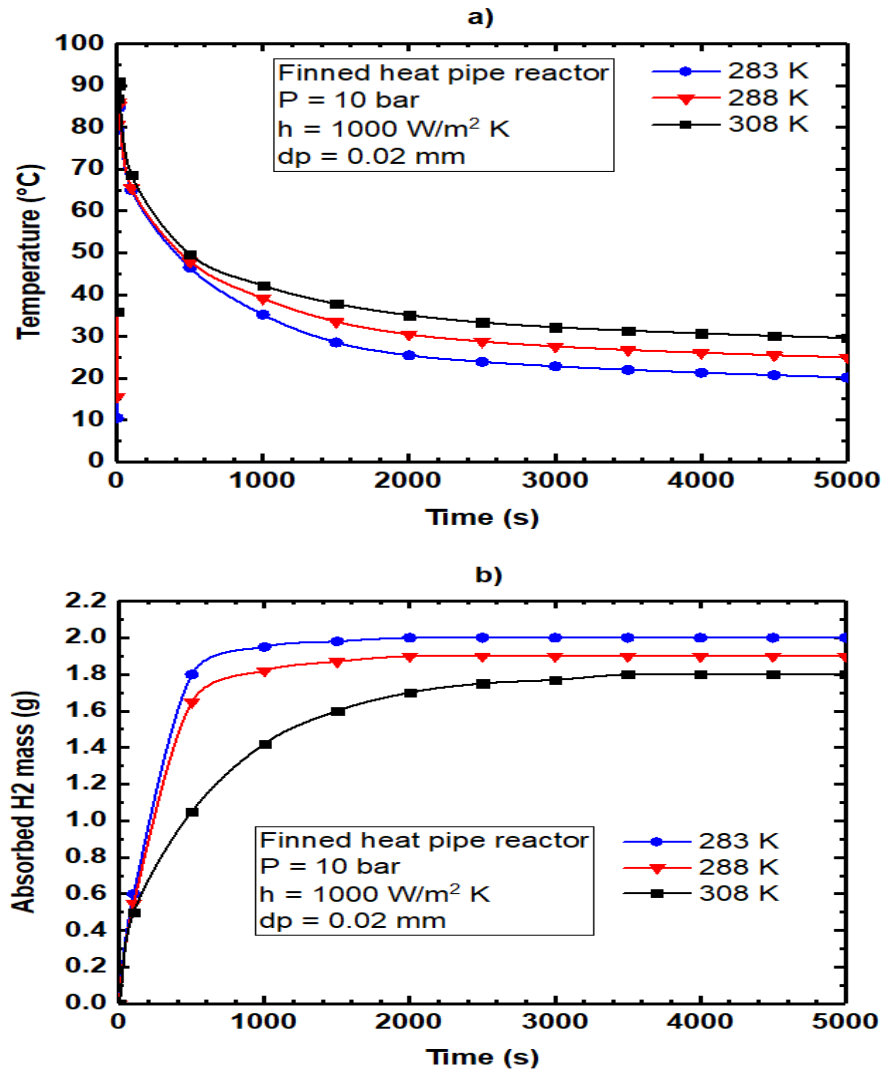


Figure 6.18. a) The temperature histories where cooling temperature as variable, b) Hydrogen mass storage against time where cooling temperature as variable.

Under specific operating conditions, the coolant's properties increase the efficiency of the MHT. The experiments showed a significant improvement in the storage performance and time when the cooling fluid was used at 283 K rather than 308 K. For instance, if the stored hydrogen capacity is 2 g, which requires 500 s times at 283

K, storing 1.6 g will take 2500 s for storage at 308 K, as Figure 6.18b indicates. It is clear that the capacity to store hydrogen increased along with reduction in time consumption, when the cooling fluid temperature around the vessel decreased.

### 6.2.7. Effect of the Wall Thickness of the Storage Tank

The wall thickness of the storage tank is varying in between 3mm and 7mm as variable.

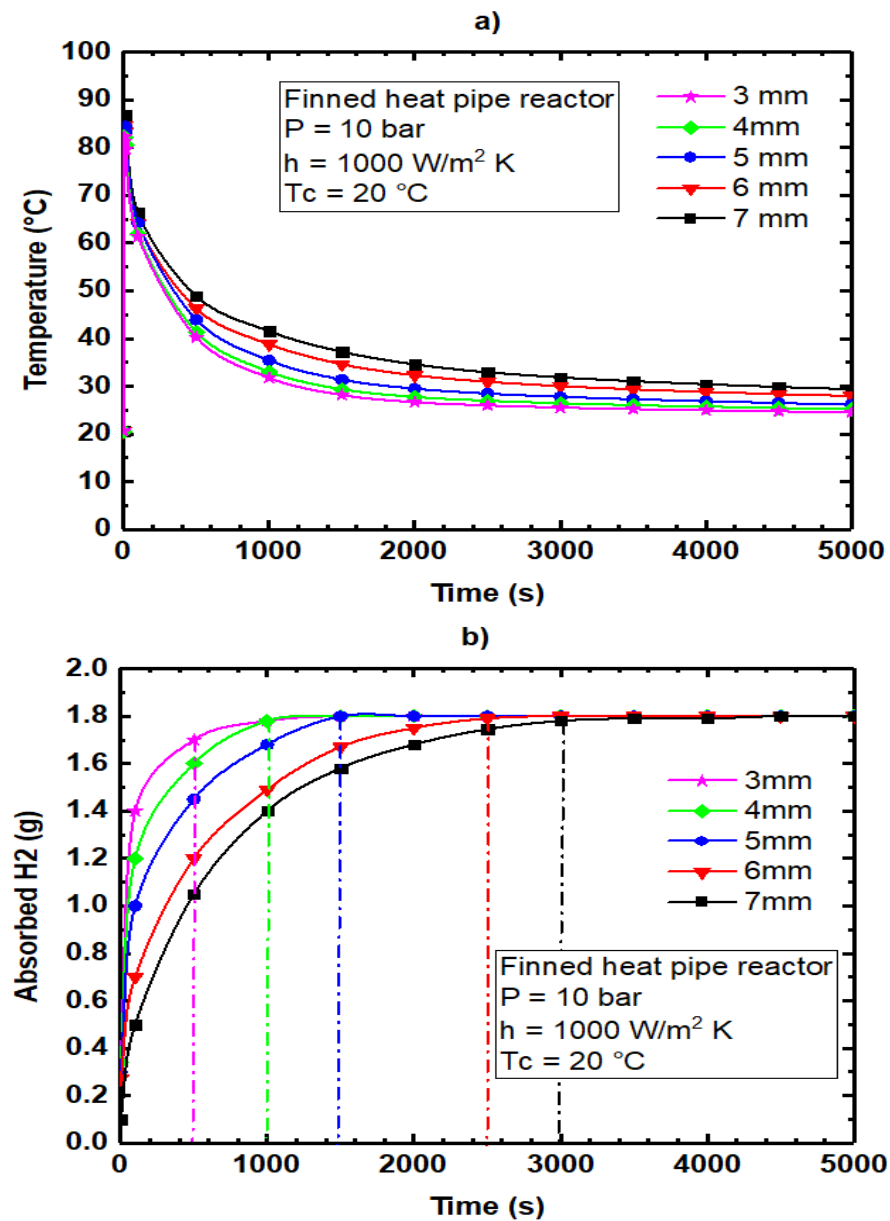


Figure 6.19. a) The temperature histories where the wall thickness as variable. b) Hydrogen storage mass against time where the wall thickness as variable.

This is considered for LaNi<sub>5</sub> metal hydride materials by keeping the other operating parameters as constant; (the general convective heat transfer coefficient as 1000 W/m<sup>2</sup>K, and supply pressure as 10 bars). For the given this operating conditions, it is seen that there is no remarkable difference among the variations of the wall thickness values for the metal hydride materials, as shown in Figure 6.19. The maximum inner temperature value is achieved as 86 °C; on the other hand, the system reaches the equilibrium temperature in about 130 s. The maximum amount of hydrogen to be absorbed is achieved as about 1.8 g for all the considered and/or modeled wall thickness values. The minimum time for absorbing the hydrogen is recorded for the wall thickness of 3mm as about 500 s, whereas the maximum time is for the wall thickness of 7 mm as about 3000 s, as shown in (Figure 6.19b).

#### **6.2.8. Effect of Inlet Radius of Storage Tank**

The variable of inlet radius of the tank is varying in between 4 mm and 8 mm. This is considered for LaNi<sub>5</sub> metal hydride materials by keeping the other operating parameters fixed; (supply pressure as 20 bar, the thickness of the tank as 3 mm, general convective heat transfer coefficient as 1000 W/m<sup>2</sup>K and the cooling water temperature as 20 °C). For these operating conditions, it is clearly seen that the system is affected by the inner radius values which is affect the outputs of the system. As the inner radius increases, the inner temperature values as well as the absorbed hydrogen mass values also increase as shown in Figure 6.20. The maximum amount of hydrogen to be absorbed is recorded as about 2.2 g for the inlet radius of 8 mm. The minimum amount to be absorbed is about 1.8 g for the inlet radius of 4 mm. The minimum time for absorbing the hydrogen is recorded as about 100 s for the inlet radius of 8 mm, whereas the maximum time is about 500 s for the inlet radius of 4 mm (Figure 6.20b). Obviously, the less thickness of the tank you use the more efficiency of the system you have.

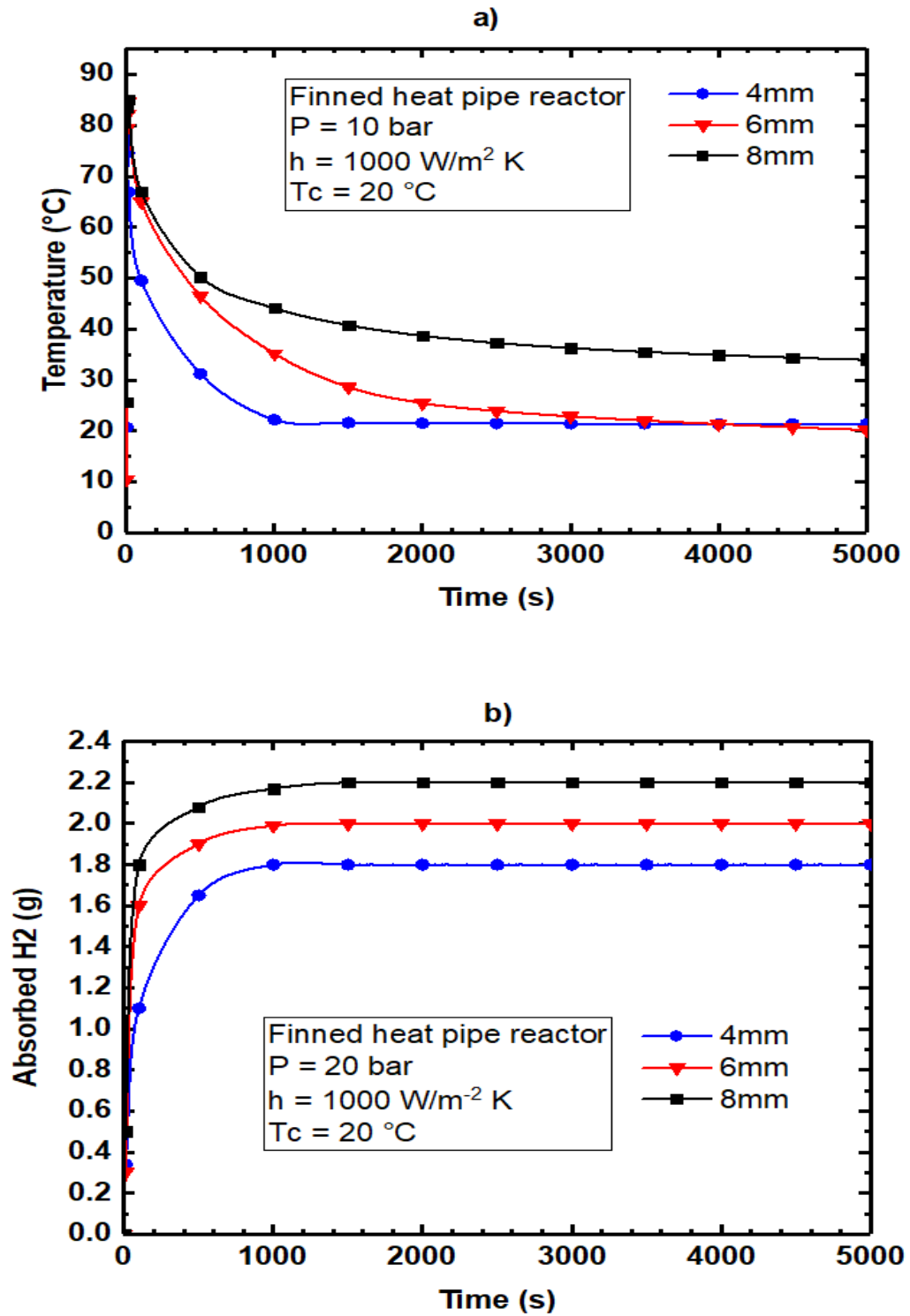


Figure 6.20. a) The temperature histories where the inlet radius of storage tank as variable. b) Hydrogen storage mass against time where the inlet radius of storage tank as variable.

## CHAPTER 7

### CONCLUSION

#### 7.1 SUMMARY AND CONCLUSIONS

In this thesis, we experienced that during the hydrogen absorption in the  $\text{LaNi}_5$  metal hydride results in substantial release of heat energy in a very short time, which happens due to the exothermic reaction, which takes place during the hydrogen absorption process. To assure efficient charging process, this heat release must be minimized. Furthermore, for a better mass transfer, MHT must be properly designed to reduce the charging time and increase the hydrogen absorption.

Based on the above mentioned reasons, three identical MHTs were selected. The first one had no heat pipe, the second one was equipped with a simple heat pipe, and the third one was equipped with a heat pipe that had fins. It was done so as to test different parameters including hydrogen charging volume, charging time, pressure, surrounding temperature, inner radius of the MHT inlet tube, heat transfer coefficient, MHT wall thickness, and thermo-physical properties of  $\text{LaNi}_5$ .

For conducting an appropriate study of the impact of heat pipe and fins, a pilot design of MHTs with  $\text{LaNi}_5$  alloy powder was prepared for hydrogen storage. The investigation also included in-depth analysis of several comparative studies on the subject.

Moreover, the effect of hydrogen charging pressure on the storage time has been experimentally investigated. The obtained results demonstrated that the hydrogen capacity and the absorption rate are directly proportional to the charging pressure at any absorption temperature. The experimental results also showed that the absorption rate highly depends on the removal of heat energy from the system. Accordingly, the

finned heat pipe configuration boosted the hydrogen storage because it increased the heat transfer rate. Also the charging time has been reduced by almost 75% at 10 bar charging pressure as compared to the MHT design without any heat pipe.

A 3D mathematical model of the charging process has been derived and implemented. The derived model has been validated with experimental result. The obtained results show that the simulation and experimental results reasonably match, which proves that the model has efficiently captured the key experimental trends. Moreover, another investigation was carried out to understand the effect of charging variables and cooling levels on the hydrogen charging capacity and time.

The results proved that the MHT design with fins, the hydrogen charging pressure, the temperature in the MHT surroundings, and the inner radius of MHT play very important roles to boost the hydriding process efficiency; whereas, it has been proven that variations in the MHT wall thickness made no remarkable difference. Furthermore, it was found that the MH particle size is not a very significant parameter; however, it has a definitive impact on the overall thermo-physical properties of the MH, which is selected to charge hydrogen.

In conclusion, design of MHTs with a finned heat pipe proved a superior performance over all other configurations in terms of charging time and storage capacity. The time period clearly and significantly decreased when the finned and simple heat pipes were used for increasing the process of heat transfer, which reduced the charging time by almost 75% when a finned heat pipe was used. It was 60% reduced when a simple heat pipe was used as compared to the reactor having no heat pipe. These results indicate that the configuration using a heat pipe and fins considerably improves the storage process. When fins were part of the reactor, the system exhibited lower inner temperature and absorbed more hydrogen at a short time as compared to a simple heat pipe.

## **7.2 FUTURE WORK**

Although this thesis investigates three specific designs to enhance heat removal in a hydride-based hydrogen storage tank, all of the current experimental studies were

limited to a small tank size with small hydrogen storage capacity. A larger tank with different design configurations can be researched in the future. The numerical model in this thesis can be modified easily to accurately predict the performance of the heat removal methods in a large scale tank.

Further studies may investigate the factors affecting the de-hydrating process. The hydride material used in this thesis was  $\text{LaNi}_5$ . Therefore, other types of hydride materials with the required potential can be researched to identify the optimal materials in terms of hydrogen storage capacity and charging time.



## REFERENCES

1. Reilly, J. J. and Wiswall Jr, R. H., "Formation and properties of iron titanium hydride", *Inorganic Chemistry*, 13 (1): 218–222 (1974).
2. Hoffman, K. C., Reilly, J. J., Salzano, F. J., Waide, C. H., Wiswall, R. H., and Winsche, W. E., "Metal hydride storage for mobile and stationary applications", *International Journal Of Hydrogen Energy*, 1 (2): 133–151 (1976).
3. McManus, M. C., "Environmental consequences of the use of batteries in low carbon systems: The impact of battery production", *Applied Energy*, 93: 288–295 (2012).
4. Demirel, Y., "Energy: Production, Conversion, Storage, Conservation, and Coupling", *Springer Science & Business Media*, (2012).
5. Sakintuna, B., Lamari-Darkrim, F., and Hirscher, M., "Metal hydride materials for solid hydrogen storage: a review", *International Journal Of Hydrogen Energy*, 32 (9): 1121–1140 (2007).
6. Demircan, A., Demiralp, M., Kaplan, Y., Mat, M. D., and Veziroglu, T. N., "Experimental and theoretical analysis of hydrogen absorption in LaNi<sub>5</sub>-H<sub>2</sub> reactors", *International Journal Of Hydrogen Energy*, 30 (13): 1437–1446 (2005).
7. Sun, D.-W. and Deng, S.-J., "A theoretical model predicting the effective thermal conductivity in powdered metal hydride beds", *International Journal Of Hydrogen Energy*, 15 (5): 331–336 (1990).
8. Chi, H., Chen, C., Chen, L., An, Y., and Wang, Q., "Hydriding/dehydriding properties of La<sub>2</sub>Mg<sub>16</sub>Ni alloy prepared by mechanical ball milling in benzene and under argon", *International Journal Of Hydrogen Energy*, 29 (7): 737–741 (2004).
9. Lopez-Suarez, A., Rickards, J., and Trejo-Luna, R., "Analysis of hydrogen absorption by Ti and Ti–6Al–4V using the ERDA technique", *International Journal Of Hydrogen Energy*, 28 (10): 1107–1113 (2003).
10. Asakuma, Y., Miyauchi, S., Yamamoto, T., Aoki, H., and Miura, T., "Homogenization method for effective thermal conductivity of metal hydride bed", *International Journal Of Hydrogen Energy*, 29 (2): 209–216 (2004).
11. Choi, H. and Mills, A. F., "Heat and mass transfer in metal hydride beds for

- heat pump applications", *International Journal Of Heat And Mass Transfer*, 33 (6): 1281–1288 (1990).
12. Mellouli, S., Askri, F., Dhaou, H., Jemni, A., and Nasrallah, S. Ben, "Numerical simulation of heat and mass transfer in metal hydride hydrogen storage tanks for fuel cell vehicles", *International Journal Of Hydrogen Energy*, 35 (4): 1693–1705 (2010).
  13. Goodell, P. D. and Rudman, P. S., "Hydriding and dehydriding rates of the LaNi<sub>5</sub>-H system", *Journal Of The Less Common Metals*, 89 (1): 117–125 (1983).
  14. Cao, D.-L., Cheng, H.-H., Ma, L., Chen, D.-M., Lü, M.-Q., and Yang, K., "Effects of Al Partial Substitution for Ni on Properties of LaNi (subscript 5-x) Al (subscript x)", *Transactions Of Nonferrous Metals Society Of China*, 17 (s1B): s967–s971 (2007).
  15. Jemni, A. and Nasrallah, S. Ben, "Study of two-dimensional heat and mass transfer during absorption in a metal-hydrogen reactor", *International Journal Of Hydrogen Energy*, 20 (1): 43–52 (1995).
  16. Mayer, U., Groll, M., and Supper, W., "Heat and mass transfer in metal hydride reaction beds: experimental and theoretical results", *Journal Of The Less Common Metals*, 131 (1–2): 235–244 (1987).
  17. Gopal, M. R. and Murthy, S. S., "Prediction of heat and mass transfer in annular cylindrical metal hydride beds", *International Journal Of Hydrogen Energy*, 17 (10): 795–805 (1992).
  18. Gopal, M. R. and Murthy, S. S., "Studies on heat and mass transfer in metal hydride beds", *International Journal Of Hydrogen Energy*, 20 (11): 911–917 (1995).
  19. Laurencelle, F. and Goyette, J., "Simulation of heat transfer in a metal hydride reactor with aluminium foam", *International Journal Of Hydrogen Energy*, 32 (14): 2957–2964 (2007).
  20. Nasrallah, S. Ben and Jemni, A., "Heat and mass transfer models in metal-hydrogen reactor", *International Journal Of Hydrogen Energy*, 22 (1): 67–76 (1997).
  21. Mat, M. D. and Kaplan, Y., "Numerical study of hydrogen absorption in an Lm– Ni 5 hydride reactor", *International Journal Of Hydrogen Energy*, 26 (9): 957–963 (2001).
  22. Dogan, A., Kaplan, Y., and Veziroglu, T. N., "Numerical investigation of heat and mass transfer in a metal hydride bed", *Applied Mathematics And Computation*, 150 (1): 169–180 (2004).

23. Askri, F., Jemni, A., and Nasrallah, S. Ben, "Study of two-dimensional and dynamic heat and mass transfer in a metal–hydrogen reactor", *International Journal Of Hydrogen Energy*, 28 (5): 537–557 (2003).
24. Askri, F., Jemni, A., and Nasrallah, S. Ben, "Prediction of transient heat and mass transfer in a closed metal–hydrogen reactor", *International Journal Of Hydrogen Energy*, 29 (2): 195–208 (2004).
25. Ben Nasrallah S, J. A., "Heat and mass transfer model in metal-hydrogen reactor", *Int. J. Hydrogen Energy*, 20: 197–203 (1994).
26. Jemni, A. and Nasrallah, S. Ben, "Study of two-dimensional heat and mass transfer during desorption in a metal-hydrogen reactor", *International Journal Of Hydrogen Energy*, 20 (11): 881–891 (1995).
27. Levesque, S., Ciureanu, M., Roberge, R., and Motyka, T., "Hydrogen storage for fuel cell systems with stationary applications—I. Transient measurement technique for packed bed evaluation", *International Journal Of Hydrogen Energy*, 25 (11): 1095–1105 (2000).
28. Mellouli, S., Dhaou, H., Askri, F., Jemni, A., and Nasrallah, S. Ben, "Hydrogen storage in metal hydride tanks equipped with metal foam heat exchanger", *International Journal Of Hydrogen Energy*, 34 (23): 9393–9401 (2009).
29. Mellouli, S., Askri, F., Dhaou, H., Jemni, A., and Nasrallah, S. Ben, "A novel design of a heat exchanger for a metal-hydrogen reactor", *International Journal Of Hydrogen Energy*, 32 (15): 3501–3507 (2007).
30. Mellouli, S., Askri, F., Dhaou, H., Jemni, A., and Nasrallah, S. Ben, "Numerical study of heat exchanger effects on charge/discharge times of metal–hydrogen storage vessel", *International Journal Of Hydrogen Energy*, 34 (7): 3005–3017 (2009).
31. Askri, F., Salah, M. Ben, Jemni, A., and Nasrallah, S. Ben, "Optimization of hydrogen storage in metal-hydride tanks", *International Journal Of Hydrogen Energy*, 34 (2): 897–905 (2009).
32. Kikkinides, E. S., Georgiadis, M. C., and Stubos, A. K., "On the optimization of hydrogen storage in metal hydride beds", *International Journal Of Hydrogen Energy*, 31 (6): 737–751 (2006).
33. Kaplan, Y., "Effect of design parameters on enhancement of hydrogen charging in metal hydride reactors", *International Journal Of Hydrogen Energy*, 34 (5): 2288–2294 (2009).
34. Veerajju, C. and Gopal, M. R., "Heat and mass transfer studies on elliptical metal hydride tubes and tube banks", *International Journal Of Hydrogen Energy*, 34 (10): 4340–4350 (2009).

35. MacDonald, B. D. and Rowe, A. M., "Impacts of external heat transfer enhancements on metal hydride storage tanks", *International Journal Of Hydrogen Energy*, 31 (12): 1721–1731 (2006).
36. Chung, C. A., Yang, S.-W., Yang, C.-Y., Hsu, C.-W., and Chiu, P.-Y., "Experimental study on the hydrogen charge and discharge rates of metal hydride tanks using heat pipes to enhance heat transfer", *Applied Energy*, 103: 581–587 (2013).
37. Lin, C.-K., Huang, S.-M., and Jhang, Y.-H., "Effects of cyclic hydriding–dehydriding reactions of Mg 2 Ni alloy on the expansion deformation of a metal hydride storage vessel", *Journal Of Alloys And Compounds*, 509 (25): 7162–7167 (2011).
38. Reay DA, K. P. A., "Heat Pipes", *Butterworth-Heinemann*, Oxford, (2006).
39. Pant KK, G. R. B., "Hydrogen Storage in Metal Hydrides", *Taylor & Francis Group*, 381 (2009).
40. Mohan, G., Maiya, M. P., and Murthy, S. S., "Performance simulation of metal hydride hydrogen storage device with embedded filters and heat exchanger tubes", *International Journal Of Hydrogen Energy*, 32 (18): 4978–4987 (2007).
41. Nagel, M., Komazaki, Y., and Suda, S., "Effective thermal conductivity of a metal hydride bed augmented with a copper wire matrix", *Journal Of The Less Common Metals*, 120 (1): 35–43 (1986).
42. Kim, K. J., Lloyd, G. M., Feldman, K. T., and Razani, A., "Thermal analysis of the Ca 0.4 Mm 0.6 Ni 5 metal–hydride reactor", *Applied Thermal Engineering*, 18 (12): 1325–1336 (1998).
43. Kim, K. J., Feldman, K. T., Lloyd, G., Razani, A., and Shanahan, K. L., "Performance of high power metal hydride reactors", *International Journal Of Hydrogen Energy*, 23 (5): 355–362 (1998).
44. Kim, K. J., Montoya, B., Razani, A., and Lee, K.-H., "Metal hydride compacts of improved thermal conductivity", *International Journal Of Hydrogen Energy*, 26 (6): 609–613 (2001).
45. Chaise, A., De Rango, P., Marty, P., Fruchart, D., Miraglia, S., Olives, R., and Garrier, S., "Enhancement of hydrogen sorption in magnesium hydride using expanded natural graphite", *International Journal Of Hydrogen Energy*, 34 (20): 8589–8596 (2009).
46. Botzung, M., Chaudourne, S., Gillia, O., Perret, C., Latroche, M., Percheron-Guegan, A., and Marty, P., "Simulation and experimental validation of a hydrogen storage tank with metal hydrides", *International Journal Of Hydrogen Energy*, 33 (1): 98–104 (2008).

47. MacDonald, B. D. and Rowe, A. M., "A thermally coupled metal hydride hydrogen storage and fuel cell system", *Journal Of Power Sources*, 161 (1): 346–355 (2006).
48. Oi, T., Maki, K., and Sakaki, Y., "Heat transfer characteristics of the metal hydride vessel based on the plate-fin type heat exchanger", *Journal Of Power Sources*, 125 (1): 52–61 (2004).
49. Visaria, M. and Mudawar, I., "Experimental investigation and theoretical modeling of dehydrogenating process in high-pressure metal hydride hydrogen storage systems", *International Journal Of Hydrogen Energy*, 37 (7): 5735–5749 (2012).
50. Muthukumar, P., Maiya, M. P., and Murthy, S. S., "Experiments on a metal hydride-based hydrogen storage device", *International Journal Of Hydrogen Energy*, 30 (15): 1569–1581 (2005).
51. Nishimura, K., Inazumi, C., Oguro, K., Uehara, I., Itoh, Y., Fujitani, S., and Yonezu, I., "Simulation and evaluation of a hydrogen storage system using hydrogen storage alloy for a chemical CO<sub>2</sub> fixation and utilization system", *International Journal Of Hydrogen Energy*, 25 (11): 1087–1093 (2000).
52. Fleming, W. H., Khan, J. A., and Rhodes, C. A., "Effective heat transfer in a metal-hydride-based hydrogen separation process", *International Journal Of Hydrogen Energy*, 26 (7): 711–724 (2001).
53. Souahlia, A., Dhaou, H., Askri, F., Sofiene, M., Jemni, A., and Nasrallah, S. Ben, "Experimental and comparative study of metal hydride hydrogen tanks", *International Journal Of Hydrogen Energy*, 36 (20): 12918–12922 (2011).
54. Kayfeci, M., Bedir, F., and KURT, H., "Experimental investigation of the effects of vessel design and hydrogen charge pressure on metal hydride based hydrogen storage parameters", *Journal Of Thermal Science And Technology*, 34 (2): 83–90 (2014).
55. Souahlia, A., Dhaou, H., Mellouli, S., Askri, F., Jemni, A., and Nasrallah, S. Ben, "Experimental study of metal hydride-based hydrogen storage tank at constant supply pressure", *International Journal Of Hydrogen Energy*, 39 (14): 7365–7372 (2014).
56. Jemni, A., Nasrallah, S. Ben, and Lamloumi, J., "Experimental and theoretical study of a metal–hydrogen reactor", *International Journal Of Hydrogen Energy*, 24 (7): 631–644 (1999).
57. Freni, A. and Cipiti, F., "3D dynamic simulation of a metal hydride–based hydrogen storage tank", *Excerpt From The Proceedings Of The COMSOL Conference, Hannover*, (2008).
58. Kyoung, S., Ferekh, S., Gwak, G., Jo, A., and Ju, H., "Three-dimensional

- modeling and simulation of hydrogen desorption in metal hydride hydrogen storage vessels", *International Journal Of Hydrogen Energy*, 40 (41): 14322–14330 (2015).
59. Nam, J., Ko, J., and Ju, H., "Three-dimensional modeling and simulation of hydrogen absorption in metal hydride hydrogen storage vessels", *Applied Energy*, 89 (1): 164–175 (2012).
  60. Jiao, K., Li, X., Yin, Y., Zhou, Y., Yu, S., and Du, Q., "Effects of various operating conditions on the hydrogen absorption processes in a metal hydride tank", *Applied Energy*, 94: 257–269 (2012).
  61. Gkanas, E. I., Makridis, S. S., Kikkinides, E. S., and Stubos, A. K., "Perforation Effect on a Rectangular Metal Hydride Tank for the Hydriding and Dehydriding Process by Using COMSOL Multiphysics Software", *ArXiv Preprint ArXiv:1303.4512*, (2013).
  62. Baldissin, D. and Lombardo, D., "Thermofluidynamic Modeling of Hydrogen Absorption and Desorption in a LaNi<sub>4</sub>. 8Al. 2 Hydride bed", *Excerpt From The Proceedings Of The COMSOL Conference*, (2009).
  63. Sakti, A., "MODELING A METAL HYDRIDE HYDROGEN STORAGE SYSTEM", (2007).
  64. Bao, Z., Wu, Z., Nyamsi, S. N., Yang, F., and Zhang, Z., "Three-dimensional modeling and sensitivity analysis of multi-tubular metal hydride reactors", *Applied Thermal Engineering*, 52 (1): 97–108 (2013).
  65. Chung, C. A. and Ho, C.-J., "Thermal–fluid behavior of the hydriding and dehydriding processes in a metal hydride hydrogen storage canister", *International Journal Of Hydrogen Energy*, 34 (10): 4351–4364 (2009).
  66. Wang, H., Prasad, A. K., and Advani, S. G., "Hydrogen storage systems based on hydride materials with enhanced thermal conductivity", *International Journal Of Hydrogen Energy*, 37 (1): 290–298 (2012).
  67. Freni, A., Cipiti, F., and Cacciola, G., "Finite element-based simulation of a metal hydride-based hydrogen storage tank", *International Journal Of Hydrogen Energy*, 34 (20): 8574–8582 (2009).
  68. Kikkinides, E. S., "Design and optimization of hydrogen storage units using advanced solid materials: General mathematical framework and recent developments", *Computers & Chemical Engineering*, 35 (9): 1923–1936 (2011).
  69. Dhaou, H., Souahlia, A., Mellouli, S., Askri, F., Jemni, A., and Nasrallah, S. Ben, "Experimental study of a metal hydride vessel based on a finned spiral heat exchanger", *International Journal Of Hydrogen Energy*, 35 (4): 1674–1680 (2010).

70. Dhaou, H., Khedher, N. Ben, Mellouli, S., Souahlia, A., Askri, F., Jemni, A., and Nasrallah, S. Ben, "Improvement of thermal performance of spiral heat exchanger on hydrogen storage by adding copper fins", *International Journal Of Thermal Sciences*, 50 (12): 2536–2542 (2011).
71. Souahlia, A., Dhaou, H., Askri, F., Mellouli, S., Jemni, A., and Nasrallah, S. Ben, "Experimental study and characterization of metal hydride containers", *International Journal Of Hydrogen Energy*, 36 (8): 4952–4957 (2011).
72. Kaplan, Y., "Effect of Design Parameters on Enhancement of Hydrogen Charging in Metal Hydride Reactors", 2288–2294 (2009).
73. Kaplan, Y. and Veziroglu, T. N., "Mathematical modelling of hydrogen storage in a LaNi<sub>5</sub> hydride bed", *International Journal Of Energy Research*, 27 (11): 1027–1038 (2003).
74. Aldas, K., Mat, M. D., and Kaplan, Y., "A three-dimensional mathematical model for absorption in a metal hydride bed", *International Journal Of Hydrogen Energy*, 27 (10): 1049–1056 (2002).
75. MacDonald, B. D., "Mathematical modelling of a metal hydride hydrogen storage system", (2006).
76. Magnetto, D., Mola, S., DaCosta, D. H., Golben, M., and Rosso, M., "A metal hydride mobile air conditioning system", *SAE Technical Paper*, (2006).
77. Sandrock, G., "A panoramic overview of hydrogen storage alloys from a gas reaction point of view", *Journal Of Alloys And Compounds*, 293: 877–888 (1999).
78. Favzi BEDIR, U. E., "Reactor Design and Optimization of Metal Hydride Based Hydrogen Storage Systems and Experimental Investigation", *ISPARTA, TURKEY*, (2016).
79. Nakamura, Y., Sato, K., Fujitani, S., Nishio, K., Oguro, K., and Uehara, I., "Lattice expanding behaviour and degradation of LaNi<sub>5</sub>-based alloys", *Journal Of Alloys And Compounds*, 267 (1–2): 205–210 (1998).
80. Ao, B. Y., Chen, S. X., and Jiang, G. Q., "A study on wall stresses induced by LaNi<sub>5</sub> alloy hydrogen absorption–desorption cycles", *Journal Of Alloys And Compounds*, 390 (1–2): 122–126 (2005).
81. Wang, Q.-D., Wu, J., Chen, C.-P., and Li, Z.-P., "An investigation of the mechanical behaviour of hydrogen storage metal beds on hydriding and dehydriding and several methods of preventing the damage of hydride containers caused by the expansion of hydrogen storage metals", *Journal Of The Less Common Metals*, 131 (1–2): 399–407 (1987).

82. Nasako, K., Ito, Y., Hiro, N., and Osumi, M., "Stress on a reaction vessel by the swelling of a hydrogen absorbing alloy", *Journal Of Alloys And Compounds*, 264 (1–2): 271–276 (1998).
83. Kim, K. J., Lloyd, G., Razani, A., and Feldman Jr, K. T., "Development of LaNi<sub>5</sub>/Cu/Sn metal hydride powder composites", *Powder Technology*, 99 (1): 40–45 (1998).
84. Willers, E. and Groll, M., "The two-stage metal hydride heat transformer", *International Journal Of Hydrogen Energy*, 24 (2–3): 269–276 (1999).
85. Elhamshri, F. A. M. and Kayfeci, M., "Enhancement of hydrogen charging in metal hydride-based storage systems using heat pipe", *International Journal Of Hydrogen Energy*, (2018).
86. Verma, B., Yadav, V. L., and Srivastava, K. K., "Experimental studies on thermal performance of a pulsating heat pipe with methanol/DI water", *Journal Of Electronics Cooling And Thermal Control*, 3 (1): 27–34 (2013).
87. Muthukumar, P., Madhavakrishna, U., and Dewan, A., "Parametric studies on a metal hydride based hydrogen storage device", *International Journal Of Hydrogen Energy*, 32 (18): 4988–4997 (2007).
88. Muthukumar, P. and Ramana, S. V., "Numerical simulation of coupled heat and mass transfer in metal hydride-based hydrogen storage reactor", *Journal Of Alloys And Compounds*, 472 (1): 466–472 (2009).
89. Muthukumar, P., Singhal, A., and Bansal, G. K., "Thermal modeling and performance analysis of industrial-scale metal hydride based hydrogen storage container", *International Journal Of Hydrogen Energy*, 37 (19): 14351–14364 (2012).
90. Muthukumar, P. and Ramana, S. V., "Study of heat and mass transfer in MmNi 4.6 Al 0.4 during desorption of hydrogen", *International Journal Of Hydrogen Energy*, 35 (19): 10811–10818 (2010).
91. Blinov, D. V., Dunikov, D. O., and Kazakov, A. N., "Measuring the gas permeability of a metal hydride bed of the LaNi 5 type alloy", *High Temperature*, 54 (1): 153–156 (2016).
92. Elmas, U., Bedir, F., and Kayfeci, M., "Computational analysis of hydrogen storage capacity using process parameters for three different metal hydride materials", *International Journal Of Hydrogen Energy*, (2018).



## **RESUME**

Fawzi ELHAMSHRI was born in Libya on 12, November 1968. He completed primary and elementary education in Gasr Khair - Libya. In 1992, he graduated from Tripoli University, Faculty of Engineering Chemical Engineering Department, Tripoli - Libya, Bachelors/Higher Diploma. In 2004, he graduated from School of Materials, Corrosion and Protection Center, UMIST University, Manchester, United Kingdom, Masters. ELHAMSHRI worked as a cathodic protection technician in Sirte Oil Company, Corrosion Department Marsa El Brega - Libya in the period of 1996-1998, then as Engineer Specialist in the same company in the period of 1998-2004. From 2005 up-to 2010, he worked as Corrosion Engineer - QC/QA, SOGEPI s.r.l. Company (ITALIAN COMPANY), Mabruk Field – Libya. In 2011 he started to work as Staff member - University lecturer in Al-Mergeb University, Faculty of Engineering Al- Garabulli. In 2014, he got a scholarship to continue his PhD education in Turkey. He started his PhD academic program at Turk Hava Kurumu University, at which he completed the courses and passed the qualification exam. In 2016, He moved to Karabuk University, registered in Department of Energy Systems and started his PhD thesis research.

## **CONTACT INFORMATION**

Address: Karabük University

Graduate School of Natural & Applied Science

E-mail: [fhamshri2003@yahoo.com](mailto:fhamshri2003@yahoo.com); 2016738132506@ogrenci.karabuk.edu.tr